AN INVESTIGATION OF WEAR AND THE PERFORMANCE OF STEELS IN THE GOLD MINING INDUSTRY

by

J. B. HARRIS

A thesis submitted to the Faculty of Engineering, University of Cape Town in fulfilment of the degree of Master of Science in Applied Science (February 1983).

Department of Metallurgy and Materials Science, University of Cape Town

C O N T E N T S

ABSTRACT

This investigation was undertaken as part of an endeavour to design an ideal wear resistant material for particular applications. The research was aimed at the alleviation of wear in the gold mining industry. In order to achieve this objective it was necessary to examine the surfaces of worn materials in order to gain a better understanding of the different wear mechanisms and also to examine the extent and depth of deformation induced by abrasive wear.

Numerous proprietary wear resistant materials and stainless steels presently used in the gold mining industry together with other materials were included in this investigation. The abrasion and corrosion-abrasion wear resistance of two particular proprietary wear resisting materials was determined to be superior to mild steel and attempts were made to explain the good performance of these materials in terms of micro-structural and mechanical properties. Various techniques were used to study the effects of *low* and *high stress* wear of materials which had been tested in both the laboratory and in-situ in the mines. These techniques include scanning and transmission electron microscopy, optical metallography and microhardness studies. It was found that as the nominal load on the abrasive increased, the mode of material became more severe, the depth of deformation increased and the surface hardness increased. Attempts were made to explain these phenomena in terms of microstructural considerations, work hardening capacity, phase transformations and recovery and recrys-tallization. This work has assisted in the specification of the composition and microstructure of steels which should provide improved performance in severe working conditions.

ACKNOWLEDGEMENTS

The author is most grateful to the following people for their kind assistance. Firstly, I am indebted to Professor A. Ball for his kind help and guidance and to Mr J. J. Ward for his encouragement and support.

I am also thankful to Mr N. Dreze and Mr B. Greeves for their respective technical and photographic assistance. Mesdames E. Diamond, H. Böhm and J. Granger are thanked for their assistance in the preparation of the manuscript.

The work described in this thesis was performed as part of a collaborative research agreement between the University of Cape Town and the Research Organization of the Chamber of Mines of South Africa.

1.0 INTRODUCTION

The cost of gold production in South Africa is continually increasing. "Great strides have been made by the industry in its endeavour to improve the working conditions, quality and effective utilisation of its human resources and research is continuing. However, the same cannot be said of its material resources and it is in this field, therefore that major opportunities still await exploitation." Mokken (1) In 1976 Joughin (2) realised the potential for the mechanisation of stoping in gold mines. This has subsequently led to advances in the understanding of rock fracture techniques, rock handling techniques and engineering. Shaker conveyors and reciprocating flight conveyors were selected by the Chamber of Mines (C.O.M.) of South Africa for the purpose of moving broken rock out of the stope face (3). The hard, angular quartzitic gold bearing ore slides over metal surfaces and copious amounts of acidic minewater together with elevated temperature and high humidity give rise to extreme conditions of abrasive-corrosive wear which results in high material replacement costs (4).

Traditionally the high cost attributable to abrasion was accepted as inevitable (5), however it appears that this is not so and that wear in the gold mines can be minimised by wise material selection which can be instituted by a better understanding of the mechanisms due to wear.

Two types of wear of hard rock conveyors have been identified by the Chamber of Mines as (a) *high stress* gouging wear and (b) *low stress* sliding wear. Wear plates of reciprocating flight conveyors undergo typical *high stress* abrasion (5) and are subjected to nominal normal contact stresses equal to the stresses necessary to crush quartzites (300 MPa).

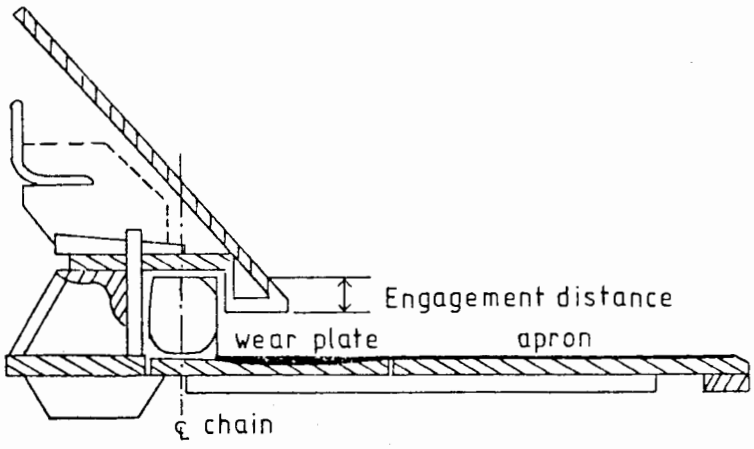

Fig. 1.1 Pattern of wear on a typical line pan. The solid shaded areas indicate the location and extent of the wear.

The wear on the wear plate (Fig. 1.1) is attributed to the trapping of rock between the flight and the pan. During conveying, metal components adjacent to the chain produces high compressive stresses while movement procudes grooving.

Typical *low stress* wear is encountered by the ore pans of shaker conveyors. The nominal contact stresses experienced in a shaker conveyor are small (about 1-10 MPa). In operation the rock is accelerated down dip in contact with the pan which is then pulled up dip, allowing the rock to slide over the pan as static fraction is overcome. Repitition of this cycle results in a nett down dip movement of the rock.

For a given material in a given wear environment, wear resistance can be considered as a product of three functions, viz: wear = f (hardness), F (plastic flow characteristics), ø (corrosion).

The influence of each functional relationship depends on the particular wear environment. In the case of wear of reciprocating flight conveyors, *high stress* abrasion appears to be more dependent on the contribution of the hardness and the plastic flow terms and less dependent on the corrosion factor. The opposite appears to be true for *low stress* wear.

This research was undertaken as part of an overall endeavour to ultimately design an ideal wear resistant material for particular applications and so to alleviate the problem of wear in the gold mining industry. Therefore this research has addressed two objectives, (a) to continue to test and to evaluate materials presently used in the gold mining industry and (b) to examine the surfaces of worn materials in order to gain a better understanding of the different mechanisms by which wear occurs and also to examine the extent and depth of deformation due to wear in the samples tested in the *laboratory* and *underground*. This work is primarily concerned with the abrasive wear of materials and not with the effects of corrosion.

2.0 LITERATURE REVIEW OF ABRASIVE WEAR

2.1 Introduction to abrasive wear

Abrasive wear is a dynamic process in which elastic and plastic microstructural changes are brought about by the strain energy associated with moving abrasive particles. When deformation exceeds the ductility of the material, deterioration and permanent deformation occurs and is observed as wear (5). Abrasive wear is caused by the removal of material from a surface by the mechanical action of the abrasive particles in contact with the surface (6).

Archard and Hirst (7) first made a distinction between *severe* and *mild* wear. In severe wear the crystal structure of the surface layers becomes heavily distorted and deformation may extend to considerable depths. Whereas in the case of mild wear such deformation is confined to the regions very close to the rubbing surface and there is little indication of subsurface damage.

The simplest model for wear of metal by abrasion is the *two-body* case (8) in which rigidly supported hard particles are forced to move across a softer metal surface to form grooves. When free abrasive grit exists between the two rubbing surfaces *three-body* abrasion (9) occurs. Free abrasive grit can originate from an external source or it can be generated internally by adhesive or delaminated wear.

It is well documented that there are three classic broad regimes of abrasive wear processes (5, 6, 9, 10, 11).

(a) *Gouging* abrasion.
(b) *High stress* abrasion (grinding).
(c) *Low stress* abrasion (scratching or erosion).

The severity of wear generally decreases in that order.

(a) Gouging abrasion: This type of wear is most frequently associated with the handling or crushing of coarse ore or rock in which pressure from the hard, sharp corners of the abrasive rock fragments cut into the wearing component with sufficient force to tear our relatively large particles of metal which invariably leads to severe grooving and chip formation.

(b) High stress abrasion: This type of abrasive wear can best be recognised by a metal sandwich situation with the abrasive inbetween. Wear is believed to be caused by a concentrated compressive stress at the point of abrasive contact resulting in a combination of local plastic flow and microcracking. The use of the words *high stress* is intended to imply that the crushing or compressive strength of the abrasive is exceeded.

(c) Low stress abrasion: This type of wear is generated by repeated scratching of the metal surface causing groove formation, associated material displacement and chip generation. The stresses are low and are normally insufficient to cause fragmentation of the abrasive.

It should be noted that these types of abrasive wear can be combined with each other and with impact in many service applications and hence it is therefore difficult to identify specific wear mechanisms which are peculiar to particular wear environments. This work is confined to the study of the so-called *low* and *high stress* abrasive wear.

2.2 Effect of properties of the abrasive

2.2.1 Abrasive type and relative hardness

Early investigations found wear resistance to be independent of abrasive hardness when this hardness was considerably greater than the hardness of the wearing surface (12). However, as the hardness of the worn material approaches that of the abrasive, so wear resistance decreases (13). Moore and King (14) correlated volumetric wear of brittle solids with the ratio of material hardness to abrasive hardness, i.e. $^{H}/_{Ha}$, using flint (Hv 950) and silicon carbide(Hv 2600) abrasives and recorded a rapid decrease in volumetric wear up to an $^{H}/_{Ha}$ value of 0,6 to 0,8. This behaviour and the difference in surface damage after wear, was ascribed to the deterioration of the abrasive and is an important factor determining the wear rates of brittle solids. Gundlach and Parks (15) and Zum Gahr and Eldis (16) investigated the influence of abrasive hardness on the wear resistance of high chromium irons and concluded that the ranking order for as-cast austenitic and heat treated martensitic irons changes with the type and particularly with the hardness of the abrasive. It was particularly noted that when garnet, a soft abrasive, was used martensitic irons performed better than the austenitic irons; however for silicon carbide or alumina, which are hard abrasives, the converse was observed.

2.2.2 Abrasive grit size

Larsen-Badse (17) investigated the abrasive wear of cold-drawn copper on silicon carbide abrasive papers at a sliding velocity of 3,5cm/sec under a low constant load and noted that the rate of wear increases very rapidly with decreasing grit size until a critical grit diameter is reached after which wear rate levels out. The value of this diameter falls between 40 - 80μm. Larsen-Badse et al (18) undertook further studies of copper, aluminium and iron and found similar results; however no levelling out of the material removal rate for aluminium was observed. Misra et al (19) also recognised this size effect and have attempted to explain this phenomenon in terms of clogging of the fine abrasive papers, grit damage, elastic contact, adhesive wear and ploughing effects.

2.2.3 Abrasive shape

Single point tools resembling a wide representation of abrasive grit geometries were traversed across the surface of M6 tool steel by Dean et al (20) in order to determine the effect of grit morphology in fine abrasion. It was concluded that metal removal is strongly affected by the shape of the tool in contact with the workpiece. For example; a smooth tool of negative rake 68^{o} removed material by ploughing while the same tool with a negative rake angle approaching 90^{o} removed no material but instead displaced material laterally by plastic deformation. Moore (21) postulated that if surface hardness of the wearing material and load on the

particle during abrasion are constant then the projected area will remain constant; however during abrasion the cross-sectional area of the groove formed will depend on the particular particle shape and therefore so will the volume of wear. Nevertheless the characterisation and quantification of abrasive particle shape in practice is difficult; both because of the range found in any particular environment and because only 10 - 30 percent of the total surface area of the abrasive particle contact is involved (13).

2.3 Effect of variables other than the abrasive

2.3.1 Load

Clearly as the applied load increases so too will the depth of indentation of the abrading particles. Investigations by Archard and Hirst (7) of a ferritic stainless steel undertaken on the pin and ring machine revealed a relatively sharp transition from *mild* to *severe* wear at a critical load of 3,5kg. This transition was also recognised by Moore (12) who found volumetric wear to be proportional to the applied load up to a critical load. This critical load is determined by the onset of gross deformation of the specimen or by instability of the abrasive surface. Richardson (22) found that for Armco iron, wear per unit load decreases by about 8 percent as the load is increased over the range 200 - 500g on 180 grit paper. However Khruschov (23) states that under an established

wear regime, linear wear is proportional to the normal stress. A similar relationship was documented by Noël (24) who revealed a direct proportionality between volumetric loss and normal load up to 10kg on the pin and disc apparatus for mild steel.

2.3.2 Sliding velocity

Larsen-Badse (18) found that for low loads and velocities the material removal rate of aluminium at a sliding speed of 0,5mm/sec is 20 - 50 percent greater than at 82mm/sec. Contrarily it has been established (12) that volumetric wear increases slightly as sliding speed increases in the range 0 - 2,5 m/sec. This is in agreement with Allen et al (14), Fogel (25) and Noël (24) who all found that the effect of increasing the speed of abrasion, on the pin and disc wear rig, from 20mm/sec to 450mm/sec results in an increased material loss or a decrease in abrasion resistance of selected grades of stainless steels. Mild steel however shows low sensitivity to the belt velocity in this range.

2.3.3 Abrasive path length

After an initial running in period of abrasion, during which time the wear rate fluctuates due to changes in the condition and structure of the material surface layers (7), volumetric wear becomes constant and proportional to the abrasion path length (4, 12, 24, 25) under conditions of constant load, sliding velocity and grit size.

2.3.4 Attack angle of abrasive particle

After studying various coarse, bonded silicon carbide abrasive papers Mulhearns and Samuels (26) utilized a single point tool of known geometry to similate the point of contact of idealised abrasive particles. By changing the attack angle α (Fig. 2.1) on plain carbon steel, the *critical attack angle* was established to be 90°; above which a microchip was cut and below which ploughing occurs (Fig. 2.2).

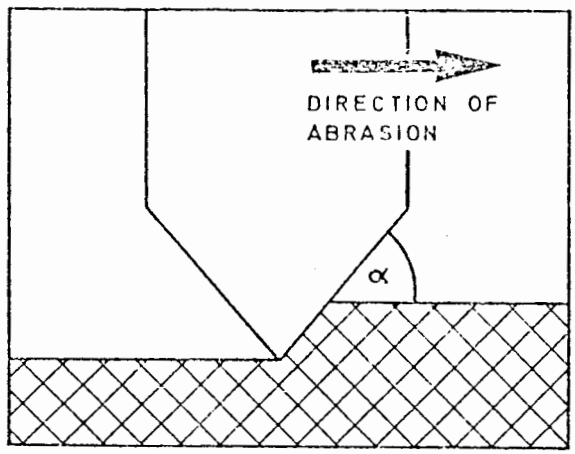

Fig. 2.1 Schematic diagram demonstrating the attack angle (α) of a single point tool or of an abrading particle.

Murray et al (8) conducted identicle single point scratch experiments, however no distinct α critical was observed but the major change from ploughing to machining for copper appeared to take place between 30° and 60° and for 1040 and

1082 steels between 20^{o} and 30^{o} respectively.

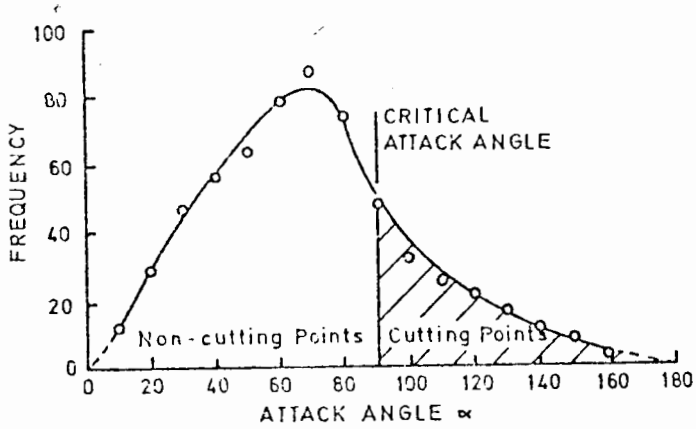

Fig. 2.2 Frequency distribution of contacting abrasive particles in unused 220-grade silicon carbide abrasive paper.

Similar work was conducted by Graham et al (27) whose findings are principally in agreement with the aforementioned workers, i.e. a transition from ploughing to microchip formation occurs when a critical attack angle, the angle between the abrasive particle and the undergrooved surface, is exceeded.

2.4 MECHANISMS OF DEFORMATION

2.4.1 Models of abrasive wear

Various theoretical mathematical relationships (8, 13, 26, 28, 29, 30, 31, 32) have been developed to model and to explain abrasive wear processes in order to quantify the volumetric removal of material in practice when a contacting abrasive particle forms a groove by plastic deformation.

Parameters used to gauge abrasive wear included: abrasive particle shape (attack angle); cross-sectional area of the groove; the proportion of groove volume that forms wear debris as opposed to that which is deformed to the sides of the groove; the probability that material is actually removed; load on the abrasive particle; depth of indentation; hardness of the surface; number of contacting particles per unit area; mean particle diameter; the coefficient of friction and the contribution due to ploughing.

The outcome of one such model is that proposed by Moore (13) who postulated that the volumetric wear per unit area, V, is equal to $K_1.K_2.K_3 \frac{\sigma}{H}$, where K_1 is the summed probability of wear debris formation, K_2 is the wear proportion of groove volume formed, K_3 is a constant which depends on the shape of the abrasive particles, σ is the applied load per unit area and H, is the surface hardness.

Clearly no single parameter can be used to gauge abrasive wear which is a complex function incorporating many variables and the particular experimental or service conditions.

2.4.2 Plastic deformation processes

The abrasive action of rigidly supported hard particles on softer ductile materials causes surface degradation by plastic deformation mechanisms.

These processes may or may not lead to material removal of metal. Two extreme causes of groove formation have been identified (8). Fig. 2.3 as ploughing (microploughing) and as cutting or machining (microcutting or micromachining).

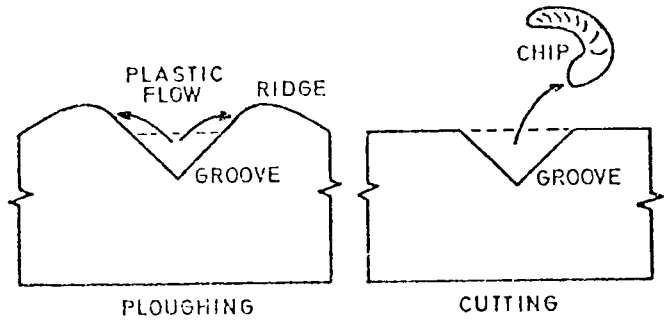

Fig. 2.3 Schematic diagram showing two mechanisms of groove formation in metals.

Ploughing or plastic grooving occurs when a prow is formed ahead of the abrading particle, continually displacing material laterally to form ridges adjacent o the developing groove. Ideally no detachment of metal from the surface occurs and hence there is no overall volume loss. The second mode of groove formation, i.e. cutting occurs via the separation of metal particles from the surface in the form of primary microchips by a process of micromachining. Ideally groove volume equals the volume of the detached metal chips. The generation of secondary microchips via material deformation to the sides of the grooves is possible for both cases of material

removal. Torrance (32) recognised this as *side wall stripping* where ridges are detached to form semicontinuous chips. It must be noted that although material removal is controlled by fracture, the rate controlling process will be determined by how much plastic strain the wearing material can sustain before fracture occurs.

The *delamination theory* was proposed by Suh (30, 33, 34, 35, 36) to explain the formation of platelike debris observed in sliding wear situations via the following sequential events, (a) the accumulation of plastic shear deformation with repeated abrasion, (b) subsurface crack nucleation, (c) crack propagation parallel to the abraded surface and ultimately, (d) the delamination of long, thin wear sheets when these cracks finally shear to the surface.

In conclusion, the work necessary to remove material was measured by Larsen-Badse (17) to be the sum of several contributions. Of these, the work to form ridges and the work against friction in shearing processes contribute over 80 percent, while the work to form actual chips is less than 10 percent of the total.

2.4.3 Flow and fracture properties

During groove formation plastic deformation is not confined to the worn surface but extends to considerable depths due to strain hardening. A hydrostatic stress system is developed ahead of the abrading particle while behind the particle

the stress is likely to be tensile (21). Because this hydrostatic stress opposes or suppresses ductile fracture processes, i.e. void formation and growth, the strains at the worn surface are very high. This pseudo-triaxial state of stress is known to raise the fracture stress by a factor of three or four (37).

It is well known that strain hardening is due to dislocation interaction and multiplication. Zum-Gahr (38) differentiated between *cellular* and *planar* dislocation structures. Brass (low stacking fault energy) favours planar arrays while copper (high stacking fault energy) favours cellular dislocation structures. Cells form more abundantly in high stacking fault materials since the tangled cell walls form more readily if dislocation climb and cross-slip are easier (39).

Moore et al (37) who correlated the flow stresses of worn and annealed (unstrained) surfaces, observed that pure metals have the highest degree of strengthening and that work hardening is a direct function of dislocation density. However for martensitic materials, with inherently high dislocation densities, strengthening at high strains is reduced because excessive work hardening is not possible. Clearly the ability to absorb strain prior to fracture is an important criterion for a wear resistant microstructure.

Larsen-Badse (40) used the familiar power law to describe the stress-strain relationship of pure metals, i.e. $\sigma = A\varepsilon^n$, where σ is the true flow stress, ε the true strain, n the strain hardening

exponent and A a constant. Therefore abrasion resistance plotted against hardness should give a straight line through the origin with some scatter due to the spread in the strain hardening exponent. Clearly this scatter would be reduced if surface hardness as opposed to bulk hardness was plotted against wear resistance.

2.5 Mechanical properties and abrasion resistance

Since hardness controls the depth of indentation of abrading particles, it is clearly an inherently important property when determining wear resistance.

It is well documented (8, 22, 23, 41) that a direct relationship between bulk hardness and wear resistance exists for pure annealed metals (Figs. 2.4 and 2.5), however for heat treated steels this relationship is not so simple.

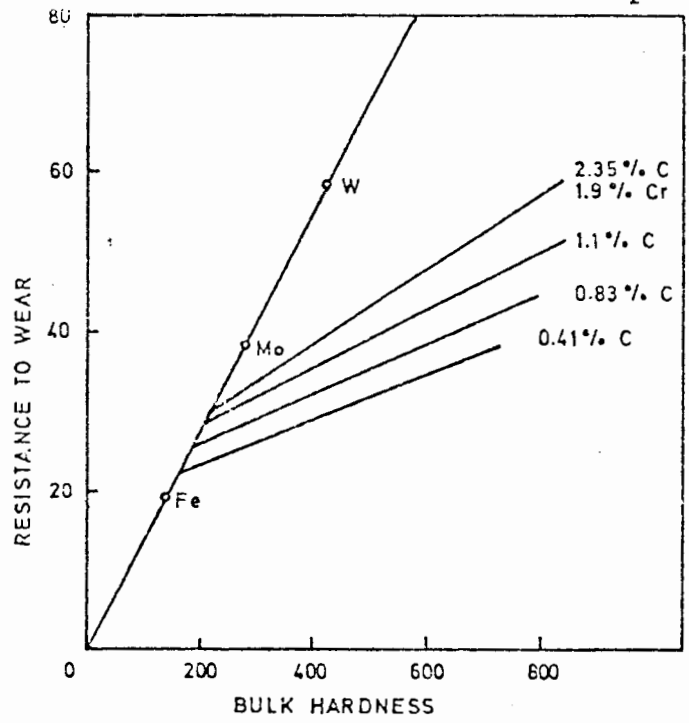

Fig. 2.4 Wear resistance as a function of bulk hardness for pure metals and heat treated steels as plotted by Khruschov (41).

Khruschov (41) found a linear relationship between wear resistance and bulk hardness for particular grades of steel. Notably with increasing carbon content the lines for each grade of steel lie higher on the graph and the slope becomes steeper (Fig. 2.4). Murray et al (8), on the other hand, found that data for steels form on a series of sigmoidal curves which are displaced to higher wear resistance as the carbon content is increased.

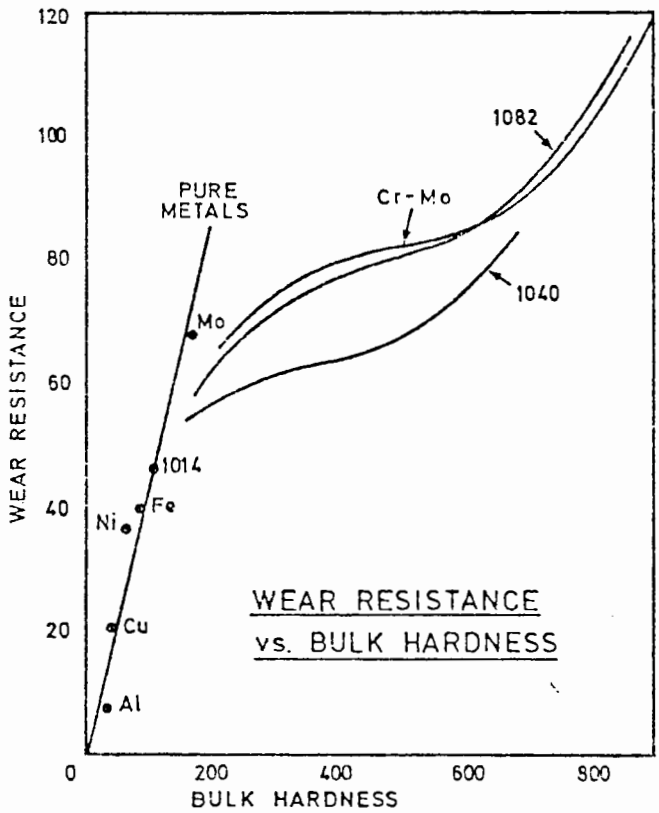

Fig. 2.5 Wear resistance as a function of bulk hardness for pure metals and heat treated steels (after Murray et al (8)).

Murray et al (8) attempted to explain the transition wear behaviour i.e. a change in mechanism of material removal from predominantly ploughing to predominantly cutting, of steels in terms of increasing hardness values (Fig. 2.6).

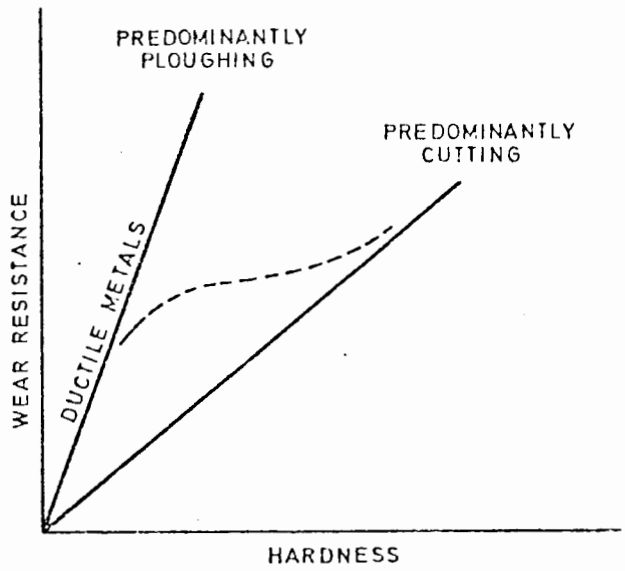

Fig. 2.6 Two possible relationships between metal hardness and wear resistance predicted by considerations of ploughing and cutting mechanisms of groove formation. The dotted curve shows the transitional behaviour found in steels (after Murray et al (8)).

The steel curve is shown to be asumptotic to the two linear extreme limits of ploughing and cutting, and the transitional behaviour is due to an increase in the number of contacting points able to remove metal as the hardness of the steel increases.

Borik et al (42) found little correlation between gouging wear resistance and bulk hardness for a wide variety of steels; however good correlation between

wear resistance and the hardness of the worn, work hardened surface was noted (Fig. 2.7).

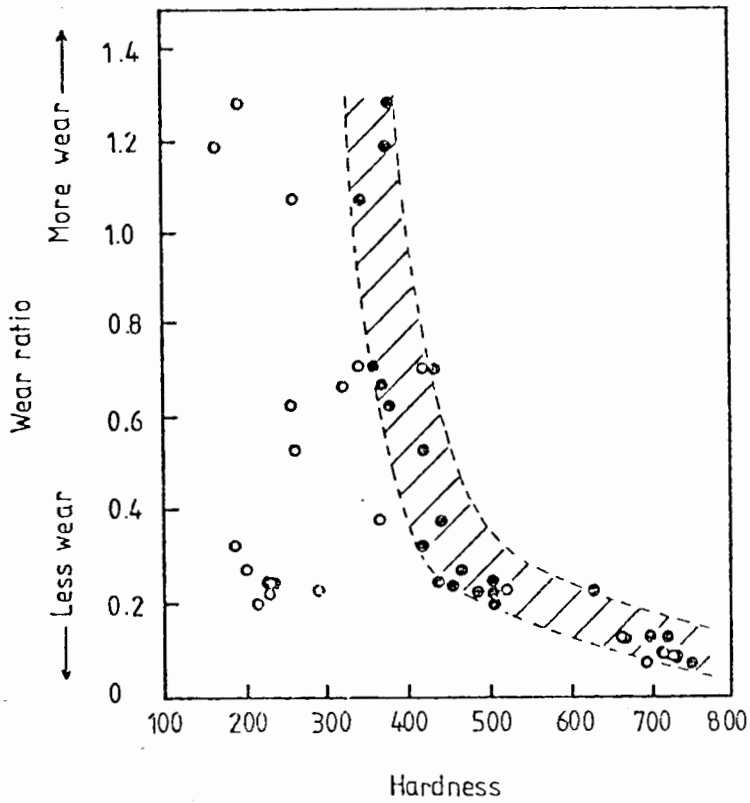

Fig. 2.7 Wear ratio versus non-work hardened hardness (open points) and work hardened hardness (solid points) for a wide variety of steels (after Borik et al (42)).

Hence higher work hardened hardness values favour increased wear resistance. This phenomenon principally supports the theory proposed by Khruschov (41) in that the rate of abrasive wear is a function of the hardness of the strain hardened surface.

Nevertheless Silence (43) states that for alloys with similar composition and microstructure, bulk hardness can be a useful indication of wear resistance. This statement is exemplified by Moore (44) who found a

linear relationship between relative wear resistance and bulk hardness and the square root of the carbon content for martensitic steels.

Increasing the bulk hardness of a material by work hardening prior to abrasion has been found to have a detrimental effect on wear resistance (4, 23), since the surface of a material during wear becomes heavily cold worked and the hardness may reach a limiting value. Richardson (45) measured the maximum hardness of a range of materials by measuring the microhardness of surfaces strained by shot peening, wear in a stony soil and by working with a blunted tool. The highest and most uniform results were obtained by trepanning and these were taken as the maximum hardness. When the maximum hardness values of the worn surfaces were correlated with wear resistance, an approximately proportional relationship was observed (46).

Clearly the bulk hardness or unworked hardness alone is insufficient to predict abrasive wear resistance in practice, since high plastic deformation in the surface of materials leads to strain hardening and in some alloys to microstructural transformations.

2.6 Microstructural properties

The wear resistance of white cast irons was studied by Zum-Gahr (16). It was noted that wear resistance increased with increasing carbide volume in both austenitic and martensitic materials, however a limit is reached when the presence of hard undissolved carbides becomes detrimental to both hardness and toughness. Consequently a trade off between hardness (which increases with

carbide volume fraction), toughness and wear resistance is necessary (47, 48).

Suh (36) states that raising the hardness reduces subsurface deformation and hence crack nucleation rate while raising the toughness decreases the crack growth rates. Bauschke et al (46) and Filippov et al (49) ascribed the outstanding performance of austenitic steels in abrasive wear environments to an ability to facilitate extensive plastic deformation by dislocation interactions, twin and stacking fault formations and the transformations of austenite to hexagonal martensite and/or to body centred cubic martensite.

Prasad et al (20), showed that the wear resistance of pearlitic and spheroidised microstructures in plain carbon steels are similar. The wear resistance of spheroidised materials generally increases with inter-carbide spacing. Moore (44), on the other hand, found that the wear resistance of pearlitic steels increases linearly with volume fraction of pearlite. Pearlite confines the ferrite grains and constrains any plastic deformation within the grains. Since material removal involves plastic deformation any constraint on plastic deformation will increase wear resistance.

Steels with unstable microstructures of martensite and retained austenite exhibit high resistance to wear (51). It has been shown that retained austenite increases fracture toughness (52) and hence increases wear resistance by decreasing subsurface crack growth rates. Salesky (53) found that the superior wear resistance

behaviour of iron/4% chromium/0,3% carbon/2% manganese steels is due to the presence of dislocated lath martensitic structures in association with continuous layers of retained austenite. This was confirmed by Fogel (25) and Bhat et al (47) who showed that the optimum microstructure for resistance to pure sliding wear in high carbon steels to consist of a combination of martensite, retained austenite and bainite.

2.7 Abrasive-corrosive wear

It is known that the high rates of metal removal in corrosive environments e.g. subterranean minewaters, are due to the combined action of abrasion and corrosion.

Previously because abrasion had only been perceived in isolation, harder metals were substituted for mild steel in an attempt to solve wear-related problems. However it is now recognised that corrosion and not hardness is the dominant factor in *low stress* wet-abrasive wear (54). In environments where very aggressive acidic minewaters with low pH and high chloride and sulphate contents are abundant, this is especially true. Abrasive particles affect corrosion rates by repeatedly removing protective films and exposing fresh metal to the environment (55) while plastic deformation generates high internal energy.

Corrosion can be defined as the deterioration of solids (e.g. metals) by liquid electrolytes (e.g. aqueous solutions). Since these reactions involve electron transfer, corrosion is an electrochemical process involving an electrochemical cell consisting of the anode (which corrodes and is supplying electrons to the external

circuit) and the cathode (which is receiving electrons from the external circuit). Thus the anode is undergoing an oxidation reaction because the valence state is being increased (56).

The type of galvanic cell relevant to the investigation is the *stress cell*. Distorted high energy zones are created adjacent to the abrasive wear grooves and it is here that corrosion products e.g. rust, are nucleated. Multiple high and low energy zones due to the inhomogeneous deformation of the abrasion surface are the cause of many localized anodes and cathods resulting in accelerated corrosion of the abraded surface. Noël (24) investigated the problem of abrasive-corrosive wear in the gold mining industry and from simulated laboratory experiments the following observations were concluded:

(a) about $^{2}/3$ of the volume loss of mild steel on shaker conveyors is due to corrosion, while the remainder is due to abrasive wear,

(b) reduced wear resistance is caused by the synergistic action of abrasion and corrosion,

(c) increasing load has only an incremental affect in volume loss due to corrosion and

(d) the frequency of abrasion and corrosion is important.

From (c) and (d) it was concluded that for a set duration of corrosion, increasing the load decreases the proportion

of the corrosion effect; and that in an abrasive-corrosive environment under conditions of continual abrasion under high loads, the proportional effect of corrosion can become negligible.

3.0 EXPERIMENTAL PROCEDURES

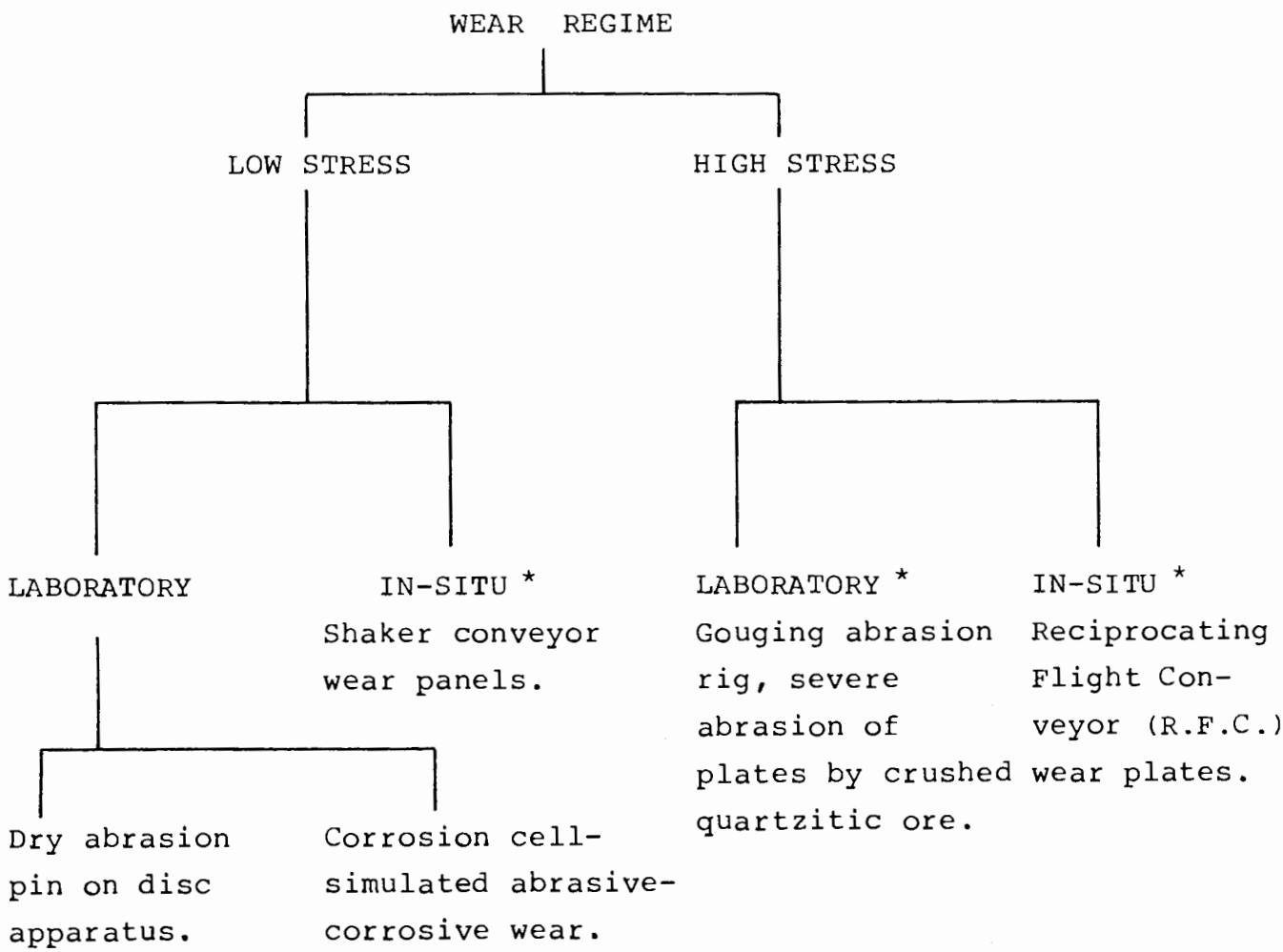

Fig. 3.1 Different wear environments.

* supervised by Chamber of Mines

The low stress abrasion rig was used to test and to evaluate the dry abrasion resistance of materials in the laboratory while the abraded surfaces of materials worn in all four environments were studied to compare the mechanisms and effects of abrasive wear.

3.1 Materials and heat treatments

3.1.1 Materials

The choice of materials and their heat treatments was largely determined by the Chamber of Mines for underground and laboratory wear testing and evaluation. (Chemical analysis of materials, Fig. 3.2.) Materials studied can be sub-divided as follows:

Standard reference material: mild steel

Proprietary abrasion resistant materials: Quatough, A-R-Col 360, Roqlast AH400, Roqlast AH360, Benox, RB390 and Wearalloy.

Quatough and A-R-Col 360 were selected for dry abrasion evaluation because of their toughness to-strength ratio and dual phase microstructure.

A Hadfield manganese steel (BW10) was studied because of its well known extraordinary work hardening ability, while the effect of spheroidisation on dry abrasion resistance of En9 and En31 and the effects of prior cold work on mild steel were also examined. Various stainless steels

were also studied because of their good abrasion-corrosion resistance.

3.1.2 Heat treatments

The heat treatment of Quatough was based on similar work undertaken by Salesky (53) to produce a microstructure of martensite and retained austenite, while the choice of heat treatment for A- R-Col 360 was such to produce a micro-structure that gave optimum wear resistance for this particular alloy system.

(a) Quatough (Iron/ 0,3% carbon / 2,0% manganese / 4,0% chromium)

i) Single heat treatment (S.H.T.)
Heat to 1100°C for 30 minutes (austenitize), oil quench, heat to 200°C for 30 minutes (temper), water quench.

ii) Double heat treatment (D.H.T.)
Heat to 1100°C for 30 minutes (austenitize), oil quench, heat to 200°C for 30 minutes (inter-temper), water quench, heat to 870°C for 30 minutes (re-austenitize), oil quench, heat to 200°C for 30 minutes (temper), water quench.

(b) A-R-Col 360 (Iron / 0,2% carbon / 1,2% manganese / 0,1% silicon / 0,8% chromium / 0,4% molybdenum)

i) Heat to 850°C for 30 minutes (austenitize), water quench.

ii) Heat to 950°C for 30 minutes, water quench.

iii) Heat to 1050°C for 30 minutes, water quench.

Tests were undertaken in both the as-received (hot rolled) and heat treated conditions. Heat treatments at high temperatures necessitated that the specimens be embedded in a fine grained sand pot to prevent scaling and oxidation at the surface.

(c) Spheroidisation heat treatment of En 9 (Iron / 0,3% carbon / 0,7% manganese / 0,1% silicon) and En 31 (Iron / 1,2% carbon / 0,4% manganese / 0,2% silicon / 0,5% chromium / 1,8% nickel)

All specimens were austenitized for 45 minutes at 800°C and then air cooled. Specimens were then spheroidised at 700°C for various durations (ranging from 1 - 30 hours) and then cooled in air.

(d) Effect of prior cold work on the abrasion resistance of mild steel. Mild steel (En3B) plate was received in the cold-drawn condition. A sample was cold rolled in the laboratory to an 11 percent reduction in thickness. Abrasion specimens were then machined and tested on the pin and disc rig. The identicle specimens were normalised at 880°C for a duration of 30 minutes and then tested in the wear rig under standard conditions.

FIG. 3.2 CHEMICAL ANALYSIS OF MATERIALS

MATERIAL	%C	%Mn	%Si	%S	%P	%Cr	%Ni	%Mo	%B	%Nb	%Zr	%V	%Ti	%Cu	%Bo	%Al	Bal. Fe
A-R-Col 360	0,17	1,23	0,14	0,017	0,013	0,75	0,023	0,40	0,0001	0,0001	0,0001						
Quatough	0,294	1,00	0,04	0,003	0,012	3,95	0,03										
3CR12	0,030	0,81	0,36			10,70	0,53	0,07				0,08	0,3				
431	0,16	0,86	0,49	0,017	0,022	16,14	1,98							0,39			
44OB	0,88	0,48	0,30	0,012	0,024	17,45	0,28	1,11						0,06			
En9	0,32	0,70	0,09	0,016	0,005												
En31	1,24	0,36	0,16	0,021	0,016	0,48	1,75										
304L	0,035	1,38	0,42			18,80	8,4	0,11				0,09	0,02				
Mild Steel	0,15	0,44	0,08			0,02	0,03	0,01				0,01			0,001		
316L	0,035	1,32	0,55			16,60	10,4	2,2				0,08	0,02				
Hadfield BW10	0,81	14,46	0,79			0,14	0,08										
Abrasalloy	0,39	0,85	0,17	0,018	0,012	0,43	0,60	0,16						0,05		0,04	
Roqlast AH400	0,35	0,59	o,26			0,89	0,02	0,19				<0,01	<0,0001		<0,0001		
Wearalloy 400	0,21	0,97	0,24			0,02	0,03	<0,01				<0,01	0,03		0,001		
Benox	0,48	0,86	0,14			0,01	<0,01	<0,01					<0,01				
Roqlast AH360	0,21	0,56	0,29			0,05	0,13	0,61				<0,01	0,02		0,004		
RB390	0,24	0,53	0,29			1,54	1,3	0,56				0,09	0,03		0,002		
430	0,060	0,65	0,37			17,4	0,27	0,05				0,09	0,02				

3.2 Dry laboratory abrasion testing (low stress wear)

3.2.1 Description of pin and disc apparatus

All abrasion testing was carried out on a pin and disc-type abrasion test rig devised by Allen (4). This apparatus has been constructed from a Rockwell proprietary disc/belt sander which has been extensively redesigned and re-modified to function as a semi-automatic abrasion test rig. In operation a dead loaded cylindrical specimen (8,9mm diameter) is abraded against a bonded abrasive belt. The belt was horizontally at a constant velocity while the specimen runs traversely across the belt at a constant velocity; thus the specimen at all times abrades against unworn particles.

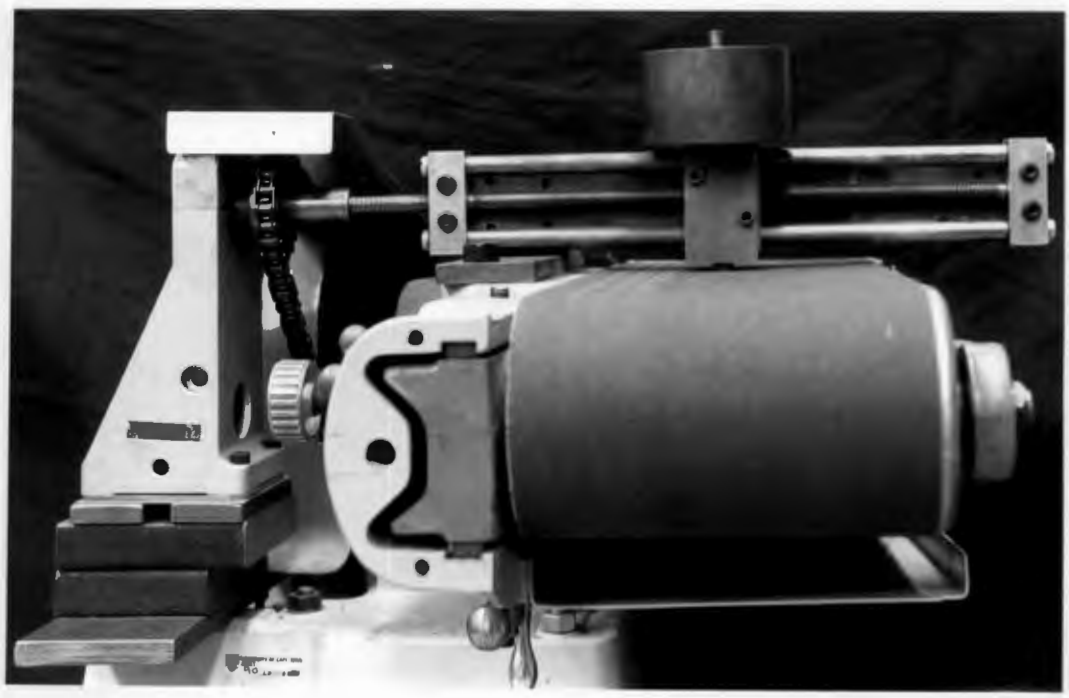

Fig. 3.3 Pin on disc apparatus.

The accelerated laboratory abrasion test rig was chosen since it is simple, well known and a reproducible wear test. Reproducibility of the test was previously gauged and found to be within $\pm$4% (25). Since this work is part of an ongoing project it was necessary to adhere to predetermined experimental constants which were set by previous workers (4, 24, 25) when testing to evaluate material ranking performance.

3.2.2 Standard experimental conditions

Parameter	Standard Condition	Motivation for use
Type of abrasive cloth	Al_2O_3	Readily available, hardness closely approximates hardness of quartzites.
Abrasive particle size	80 grit (300µm)	Wear profile approximates profile of worn in-situ shaker conveyor pan.
Load	2kg (19,6N)	Load approximates to forces exerted during low stress in-situ sliding wear.
Path length	4 x 1m	Length sufficient to overcome non-linear wear during stop/start procedures.
Velocity	260mm/sec	Velocity of the same order of magnitude as the sliding speed of quartzitic ores on shaker conveyor pan.

3.2.3 Method of testing

Machined specimens are pre-abraded for a minimum distance of 1m, washed in alcohol, dried and then weighed on a Mettler analytical balance to a precision of 0,1mg. Specimens were then abraded according to standard conditions for 1m, washed, dried and re-weighed. The average of four such tests was taken as the mass loss. The measured volume loss of a specimen was then calculated and used to compute relative abrasion resistance (R.A.R.) as shown below.

$$\text{RAR} = \frac{\text{volume loss of mild steel per metre of abrasion path length}}{\text{volume loss of specimen x per metre of abrasion path length}}$$

Additional loads of 2N and 68,6N, as well as an increased abrasion path length of 4,88m were utilized to facilitate studies of abrasive wear mechanisms.

3.3 Abrasion-Corrosion Testing

A technique of laboratory testing was devised by Noël (24). This involves timed corrosion followed by abrasion. The specimens were mounted in such a way that only the abraded surface was exposed to the corrosive environment, the other surfaces being protected by a coating called Micromask. This eliminates corrosion on the side of the specimen where it is in contact with the holder. Samples were abraded, weighed and placed in the corrosion rig for 46 hours after which time they were removed,

abraded for 25cm under a load of 2kg and re-weighed. The volume loss was then recorded. A corrosion solution similar in composition to underground mine-water (24) was used. The corrosion solution was made up as follows: 12ℓ of distilled water, 28,8g $Na_2SO_4.10H_2O$ and 7,7g $CaCl_2.2H_2O$. The solution was maintained at a constant temperature of 30^{o}C by a thermoregulator.

Laboratory Relative Wear Resistance (R.W.R.) of the test specimens was then calculated to a reproducibility of within 8%.

$$\text{Lab.R.W.R.} = \frac{\text{volume loss of mild steel}}{\text{volume loss of specimen x}}$$

(After a series of 46 hours corrosion and 250mm abrasion under a load of 2kg.)

3.4 Mechanical properties

The following methods were used to determine the mechanical properties of various materials.

3.4.1 Tensile testing

Tensile tests were undertaken on an Instron Tensometer at a strain rate of 0,1 min^{-1}. Load elongation curves were obtained from which yield stress, fracture stress and percentage elongation to fracture were determined for specimens of gauge length 12,6mm and cross-sectional area of 10 square mm.

3.4.2 Impact fracture testing

The Izod energy of impact fracture of materials was determined at room temperature.

3.4.3 Hardness testing

The bulk and surface hardness of materials that had undergone wear was determined on a Vickers Hardness testing machine.

3.5 To permit studies of wear mechanisms, experimental procedures can be subdivided into the following sections:

3.5.1 Mechanisms of material removal

3.5.2 Depth of deformation

3.5.3 Microstructure

3.5.1 Mechanisms of material removal

(a) Scanning electron microscopy

The scanning electron microscopy (S.E.M.) was used to study the surface topography of materials that had undergone wear in the laboratory and underground. Prior to examination specimens were immersed in an ultrasonic acetone bath and finally cleaned by mechanical stripping of cellulose acetate. This procedure ensured a relatively uncontaminated surface. A gold-palladium coating was applied to specimens which were then observed

in the S.E.M. at an accelerating voltage of 20kV. Stereopairs at tilt angles of 8^{o} were taken at low and medium magnification while separate micrographs were made at higher magnifications when a particular feature was to be studied.

(b) Low magnification optical photomicrography

The surface profiles of selected materials from low and high stress wear environments were investigated. All specimens were sectioned perpendicular to the direction of wear and coated with a protective layer of electroless nickel to facilitate edge retention during mounting and polishing procedures. Low magnification micrographs were recorded, from which surface profiles were subsequently traced.

(c) Profilometric studies

Talysurf profilometric studies were conducted in order that the profiles of abraded materials could be measured. Specimens were immersed in an ultrasonic acetone bath and finally cleaned by mechanical stripping of cellulose acetate sheet to ensure uncontaminated working surfaces. Surface profile measurements were carried out perpendicular to the direction of abrasion. A method of establishing a datum from which numerical values of surface texture may be specified is the Centre Line Average System (57). Centre Line Average (C.L.A.) which is measured in microns, is the average value of the departure of a profile both above and below its centre line over a

prescribed sampling length. Experiments were carried out using a constant traversing length of 1,9mm which, when increased, resulted in greater C.L.A. values incorporating the combined effects of both surface roughness and waviness.

3.5.2 Depth of deformation

(a) Microhardness traverses

Tapered surfaces of wear specimens at 2 and/or 5 degrees for microhardness evaluation were obtained by mechanically polishing specimens (8,9mm diameter) retained in holders at premachined angles. The polishing procedure commenced with initial grinding with 800 silicon carbide grit followed by 3 micron and subsequently 2,5 micron diamond paste. The C.E.J. Mikrokator Microhardness tester was used to conduct microhardness traverses on tapered surfaces (Fig. 3.4) commencing between the abraded grooves and progressively traversing at increments of 0,1mm along the taper. A numerical measurement of microhardness, the Diamond Pyramid Hardness (D.P.H.) was obtained from the following equation:

$$D.P.H. = \frac{1854 \times P}{D^2}$$

where P is the load in grams (either 50g or 100g) and D is the diagonal of impression in microns.

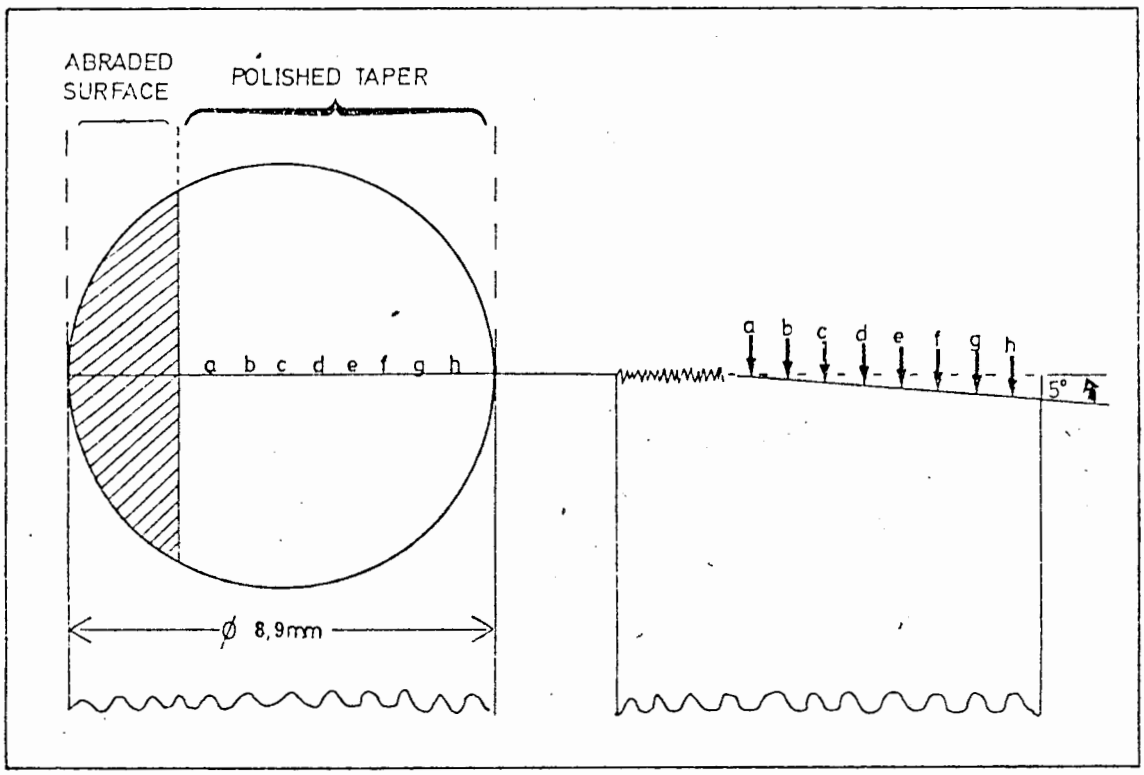

Fig. 3.4 Microhardness traverse of taper section.

Using simple geometry the traverse length (ℓ) along the taper can be converted to depth (d) below the abraded surface, i.e. $d = \ell \sin \theta$, where θ is the taper angle in degrees.

(b) Optical metallography

The depth of deformation due to abrasion was measured from optical micrographs of polished and etched sections.

(c) Technique of split specimens

Cylindrical specimens of selected materials were sectioned longitudinally using a low speed diamond saw on the MR microslice, mounted and polished to 0,25 microns. The sections were protected, rejoined and the re-assembled pin abraded under a load of 7kg for 4,88m. Micrographs of the polished surface were recorded and the depth of deformation, if any, was measured.

3.5.3 Microstructure

(a) Transmission electron microscopy

T.E.M. studies were undertaken on selected materials. Foils were prepared as follows:

(i) slices 0,2 - 0,6mm were cut parallel to the worn surface at low cutting speeds on a MR microslice.

(ii) standard 3,05mm diameter discs were punched from these slices and polished to the appropriate thickness for thinning.

(iii) foils were prepared in a Bainridge Unithin (80V, 103mA) using a solution composed of 7% $HClO_4$ in absolute ethanol.

Care was exercised to ensure minimal mechanical deformation of the foils during the preparatory procedures.

(b) X-Ray Diffraction to determine the volume fraction of retained austenite in a martensitic matrix.

Quantitative XRD analysis (24, 25) for the determination of relative amounts of two phases in a mixture requires comparison of two suitable reflections of both phases. For the retained austenite-martensite mixture, the diffraction lines best meeting these requirements are the (200) reflection of the martensite and the (220) reflection of the austenite. For a molybdenum x-ray tube these peaks are found at a Bragg angle of 28,6° and 32,5° respectively.(Fig. 3.5). Integrated intensities are used to compare the two pea peaks. P, the integrated intensity ratio

$$= \frac{\text{(220) austenite total counts - background counts}}{\text{(200) martensite total counts - background counts}}$$

$$= \frac{\text{austenite peak counts}}{\text{martensite peak counts}}$$

$$\text{Volume fraction of retained austenite} = \frac{P}{P + 1{,}31}$$

EXAMPLE

Background1	Martensite	Background2	Austenite	Background3
26,85-27,65	28,10-29,70	30,20-31,00	31,00-32,6	32,6-33,40
= 0,8°	= 1,6°	= 0,8°	= 1,6°	= 0,8°
21380	69852	16899	35672	16488

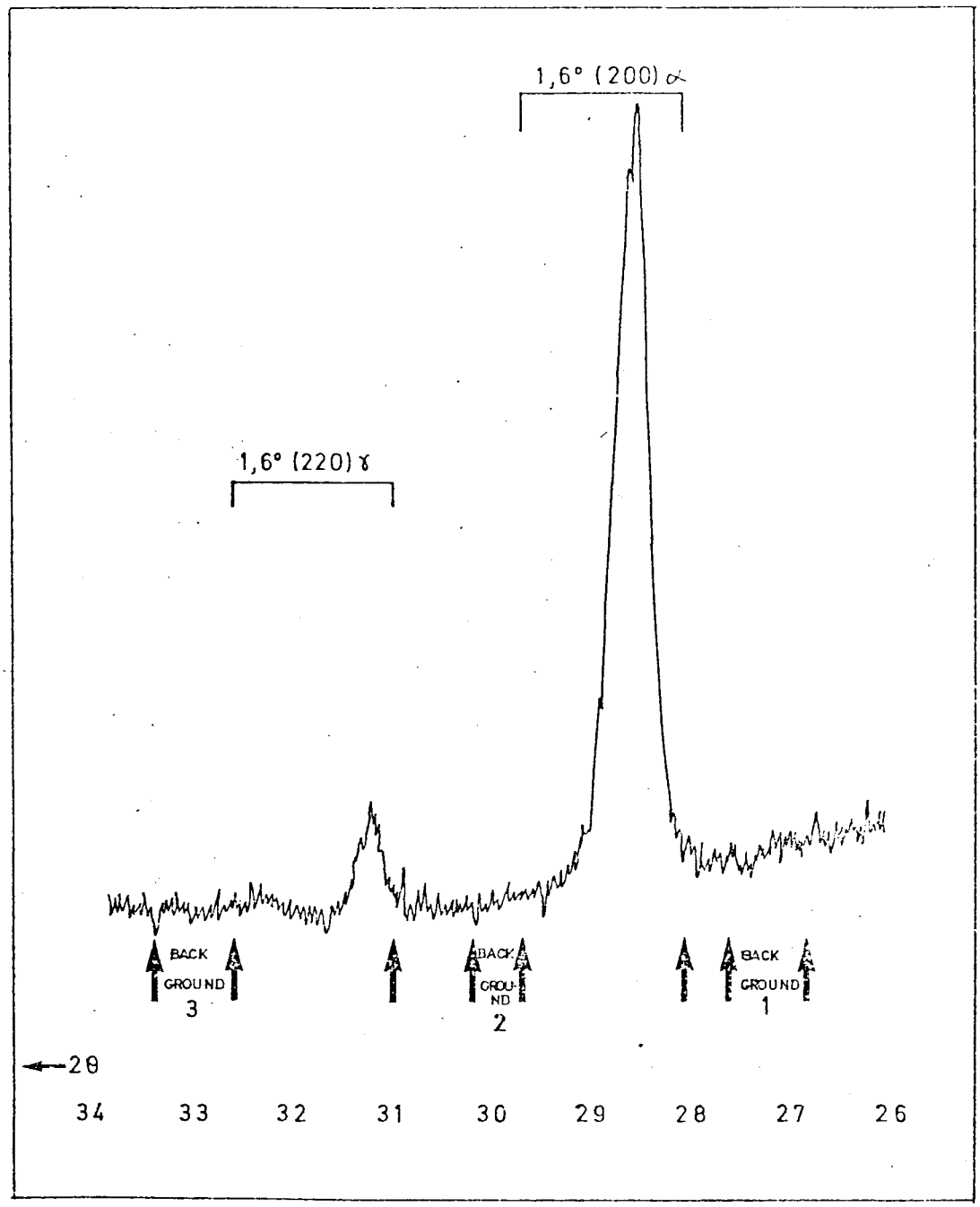

Fig. 3.5 XRD trace of retained austenite in a martensitic matrix.

Austenite peak = 35672 - (16899 + 16488)
= 2285

Martensite peak = 69852 - (21380 + 16899)
= 31573

$P = {}^{2285}/_{31573}$

= 0,0724 and V, ret. aust = 5,24%.

4.0 RESULTS

4.1 The effect of heat treatment of Quatough and A-R-Col 360 can be examined under the following sections;

(a) dry abrasion performance
(b) abrasion-corrosion resistance
(c) mechanical properties
(d) microstructural properties

4.1.1 Dry abrasion performance

From Figs. 4.1 and 4.2 it is observed that both proprietary wear resistant materials, at constant load, exhibit a linear relationship between abrasion path length and volume loss. Quatough in the as-received condition performed marginally better than the S.H.T. condition which in turn fared better than the D.H.T. condition. Optimum A-R-Col 360 resistance to dry abrasion was revealed by the WQ 950°C condition (WQ = water quench); however this performance was only marginally superior to the as-received condition. The poor performance of the WQ 1050°C condition of A-R-Col 360 corresponds to the low hardness of the alloy in this condition. It can further be noted that both the as-received and heat treated conditions of Quatough and A-R-Col 360 perform considerably better than mild steel. From Figs. 4.3 it can be noted that Quatough exhibits a linear relationship between volume loss per metre of dry abrasion and normal load.

4.1.2 Abrasion-corrosion resistance

Fig. 4.4 shows a linear variation between cumulative volume loss and abrasion path length for both materials. Quatough (S.H.T.) exhibited the best laboratory R.W.R. whereas A-R-Col 360 (WQ 850°C) was found to be superior to the as-received condition of A-R-Col 360. The corrosion contribution was calculated to account for 65% and 61% of the total volume loss of Quatough and A-R-Col 360 respectively. Noël(24) found corrosion to contribute about 66% of the total volume loss of mild steel.

4.1.3 Mechanical properties

From Fig. 4.5 it can clearly be observed that abrasive wear (under standard conditions) results in a nett hardness increase i.e. hardness at the worn surface is greater than the hardness of the bulk material. From the same table it can be noted that heat treatment of Quatough results in a considerable decrease in bulk hardness (approximately 100 VPN units) since the as-received condition had not undergone any tempering treatment. A-R-Col 360 (WQ 850°C) exhibits a greater hardness compared to the as-received condition which in turn is not as hard as Quatough in the same condition. The WQ 1050°C condition of A-R-Col 360 exhibits a hardness which is considerably less than the as-received condition. This low hardness value is verified by the low tensile strength recorded for this material, (Figs. 4.6 and 4.7).

A-R-Col 360 in the as-received, WQ 850°C and WQ 950°C heat treated conditions all exhibited similar tensile properties. Quatough in the as-received and S.H.T. condition exhibit similar mechanical properties i.e. tensile strength and impact fracture energy, while the D.H.T. condition of Quatough demonstrates a greater elongation to fracture but half the notch-toughness. Relative to mild steel (21J), the as-received and heat treated conditions of A-R-Col 360 all show better resistance to failure by impact fracture.

4.1.4 Microstructural properties

The major difference in microstructure (Fig. 4.8) between the as-received and S.H.T. condition of Quatough is that there appears to be some sort of overall grain refining action (Fig. 4.8(b)) of the finely divided acicular martensite. The martensite laths of the D.H.T. condition are broader and fatter than those of the as-received and S.H.T. conditions due to the extra re-austenitize sequence. The fine pronounced needles of Quatough (S.H.T.) produce superior wear resistance compared to the softer D.H.T. condition. A-R-Col 360 in the as-received condition as well as in the heat treated conditions exhibit microstructures of fine needle-like martensite (Fig. 4.9) which become more pronounced as the steel is quenched from higher temperatures and subsequently yield less resistance to abrasive wear. Fig. 4.10 demonstrates evidence of

interlath films of retained austenite while a trend of increasing volume fraction of retained austenite with improved wear resistance for Quatough was found to exist; this relationship however is not as well defined for A-R-Col 360. Ductile fracture can be observed on the impact fracture surface of Quatough (Fig. 4.11) and on the tensile fracture surface of A-R-Col 360 (Fig. 4.12) which demonstrates macroscopically a cup-cone type mode and microscopically many dimples as shown in Fig. 4.12. These dimples are formed as a result of the coalescence of microvoids after plastic tensile overloading. The abraded surfaces of Quatough (Fig. 4.11) and A-R-Col 360 (Fig. 4.12) show evidence of predominant ductile plastic grooving, micro-machining and, where excessive deformation occurs, microfracture.

EFFECT OF VARYING DRY ABRASION PATH LENGTH
ON THE ABRASIVE WEAR OF QUATOUGH

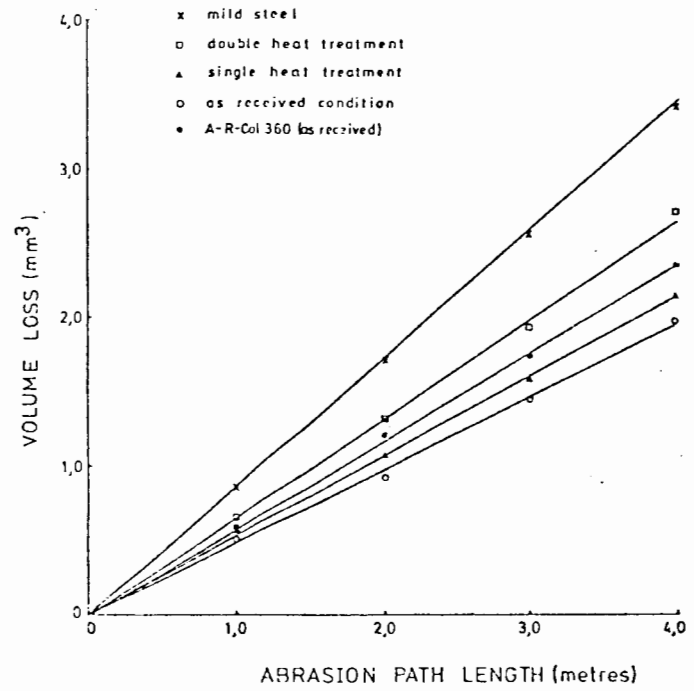

Fig. 4.1

EFFECT OF VARYING DRY ABRASION PATH LENGTH
ON THE ABRASIVE WEAR OF A-R-Col 360 (for a 2Kg load)

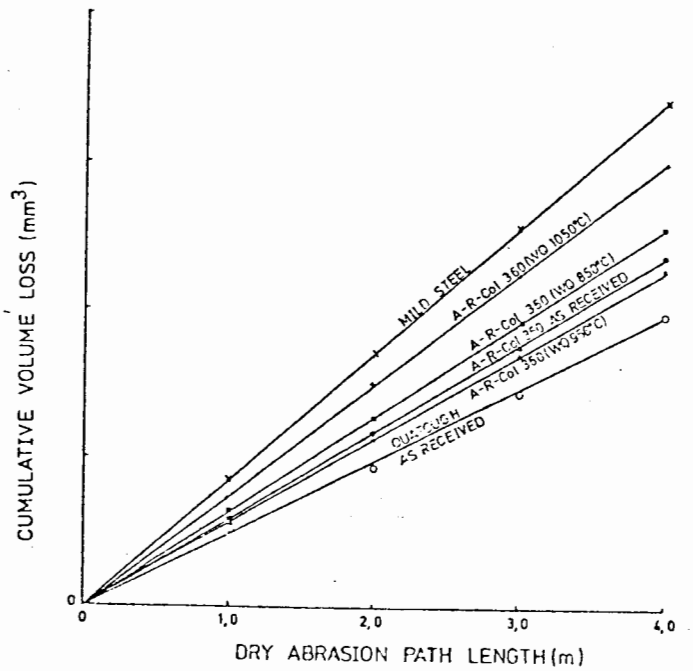

Fig. 4.2

EFFECT OF VARYING LOAD
ON THE ABRASIVE WEAR OF QUATOUGH

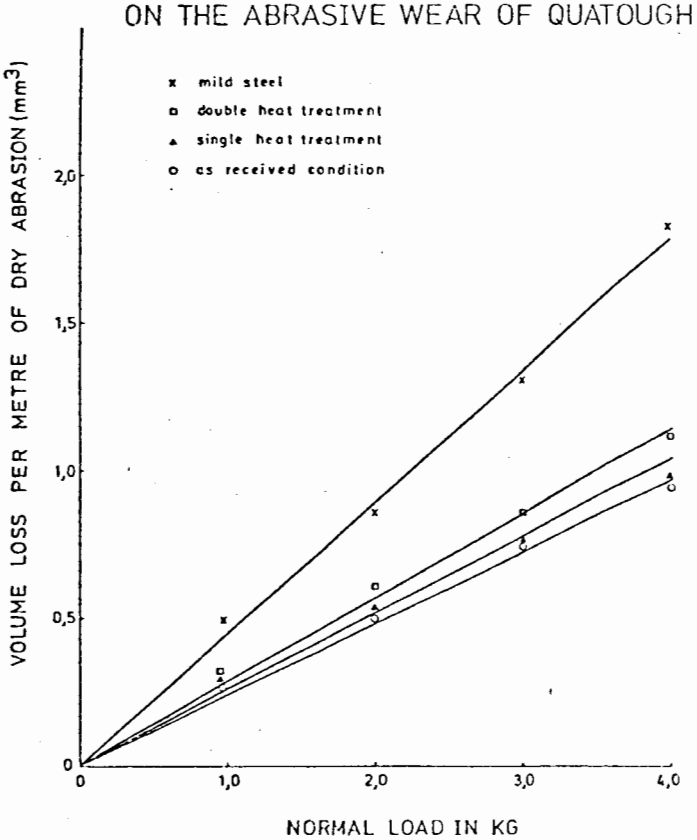

Fig. 4.3

WEAR OF QUATOUGH AND A-R-Col 360 (FOR 1METRE
ABRASION (2KG LOAD) AND 184 HOURS CORROSION)

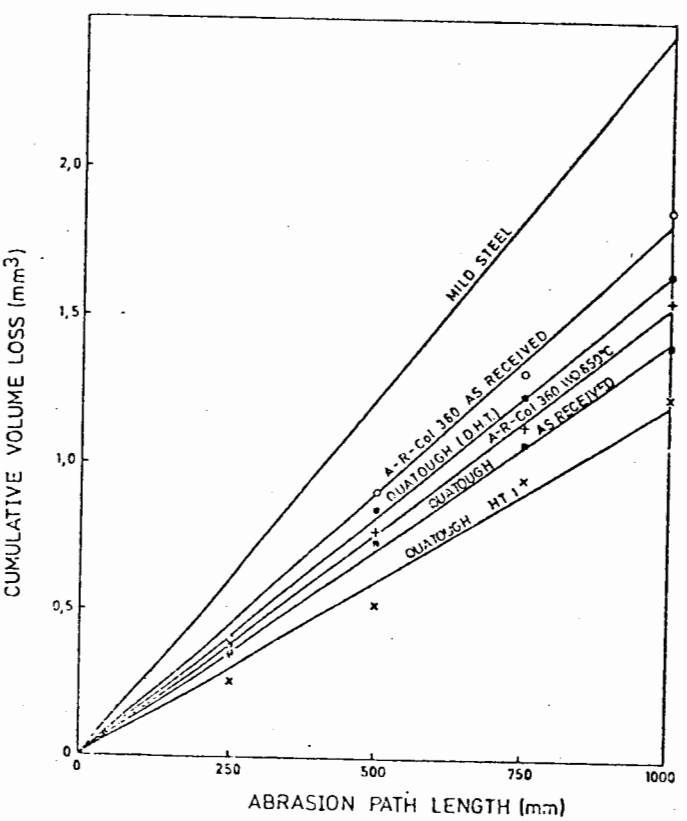

Fig. 4.4

MATERIAL	HEAT TREATMENT	BULK HARDNESS (H_V 50)	SURFACE HARDNESS AFTER ABRASION (H_V50)	LOW STRESS R.A.R.	LAB.R.W.R.
Quatough	As received	509	533	1,70	1,73
Quatough	S.H.T.	407	489	1,59	2,05
A-R-Col 360	WQ 950°C	438	465	1,49	-
A-R-Col 360	As received	399	399	1,44	1,33
A-R-Col 360	WQ 850°C	430	434	1,33	1,59
Quatough	D.H.T.	398	445	1,32	1,50
A-R-Col 360	WQ 1050°C	347	390	1,12	-
Mild Steel	As received	126	170	1,00	1,00

Fig. 4.5 Low stress dry abrasion performance of Quatough and A-R-Col 360.

MATERIAL	HEAT TREATMENT	(i) σy (MPa)	(ii) σu (MPa)	(iii) σf (MPa)	(iv) $\%\varepsilon_f$	IZOD IMPACT ENERGY (J)	% RETAINED AUSTENITE
A-R-Col 360	As received	934	1219	912	19	31	5,65
A-R-Col 360	WQ 850°C	1001	1246	918	18	45	4,92
A-R-Col 360	WQ 950°C	868	1159	845	18	41	3,98
A-R-Col 360	WQ 1050°C	712	901	601	20	31	5,42
Quatough	As received	1335	1642	1290	20	27	5,35
Quatough	S.H.T.	1335	1660	1120	21	28	5,04
Quatough	D.H.T.	659	958	706	24	14	4,41

(i) σy = yield stress

(ii) σu = ultimate tensile strength

(iii) σ_f = fracture stress

(iv) ε_f = strain to fracture

Fig. 4.6 Mechanical properties of A-R-Col 360 and Quatough.

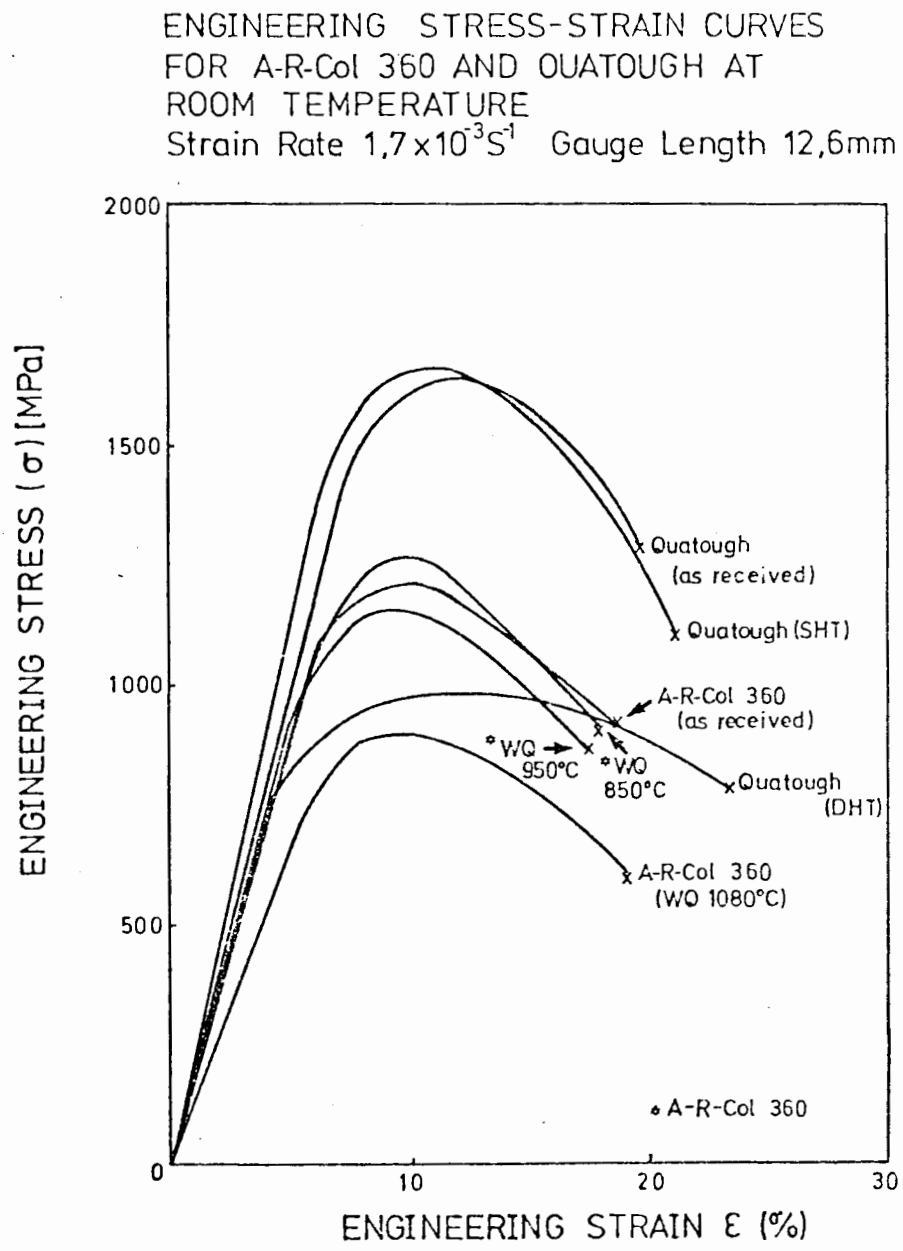

Fig. 4.7 Stress-strain diagrams of A-R-Col 360 and Quatough

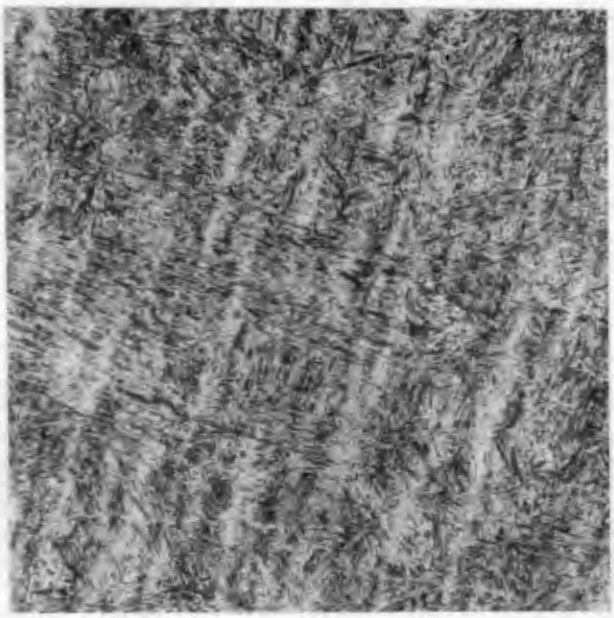

(a) As-received condition (400x)
R.A.R. 1,70 Hardness 50VPN 509

(b) Single heat treated condition (400x) R.A.R. 1,59 Hardness 50VPN 407

(c) Double heat treated condition (400x) R.A.R. 1,32 Hardness 50VPN 398

Fig. 4.8 Optical micrographs of Quatough
(Etched in 2,5% Nital for 90 seconds.)

(a) As-received condition
R.A.R. 1,44 Hardness 50VPN 399

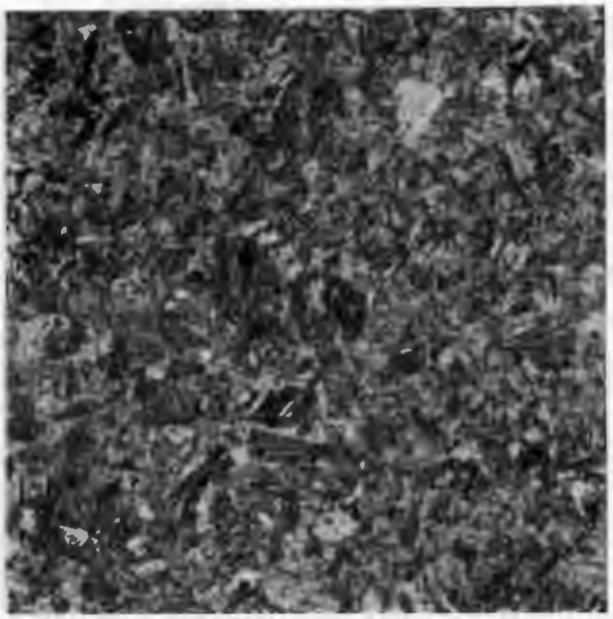

(b) WQ 850°C (750x) R.A.R. 1,33
Hardness 50VPN 430

10 µm

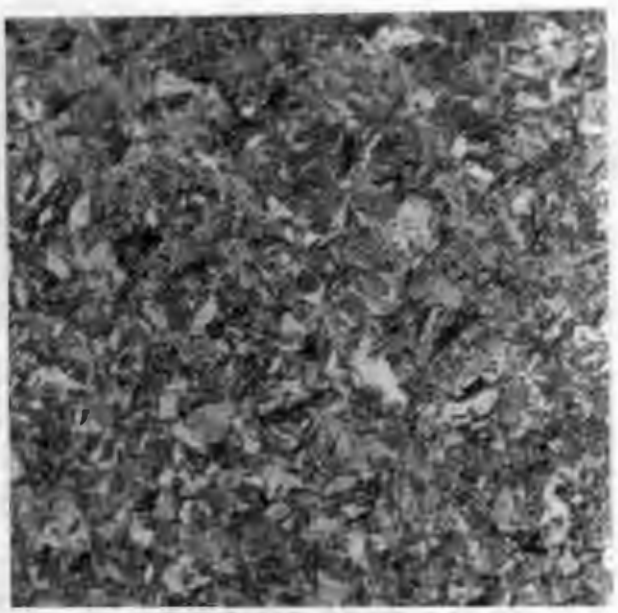

(c) WQ 950°C
R.A.R. 1,49 Hardness 50VPN 438

(d) WQ 1050°C
R.A.R. 1,12 Hardness 50VPN 347

Fig. 4.9 Optical micrographs of A-R-Col 360
(Etched in 5% Nital for 30 seconds.)

(a) Bright field
(41000x)

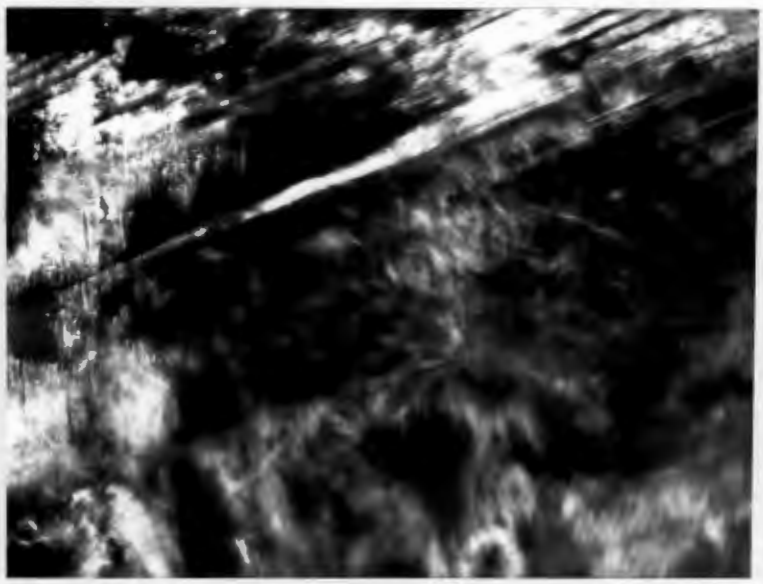

(b) Dark field
(41000x)

Fig. 4.10 Bright field-dark field pair of Quatough. The white streaks observed in the dark field micrograph delineate possible evidence of retained austenite.

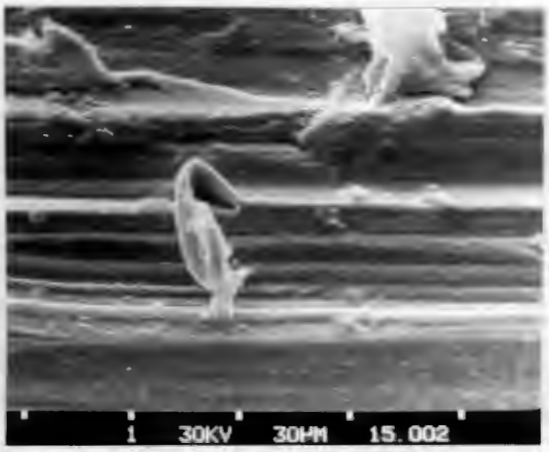

(a) Undetached chip on abraded surface which appears plastically deformed (ductile).

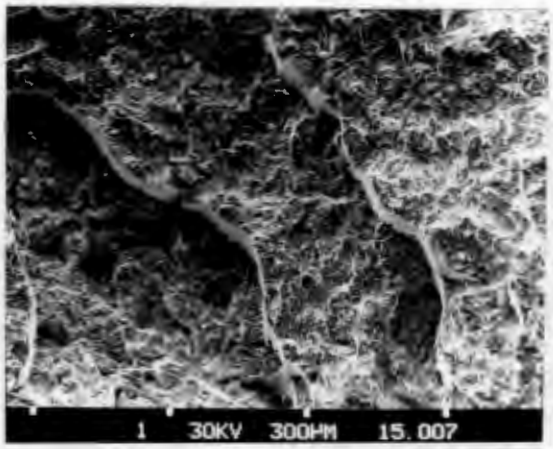

(b) Tiered impact fracture surface.

Fig. 4.11 S.E.M. micrographs of Quatough.

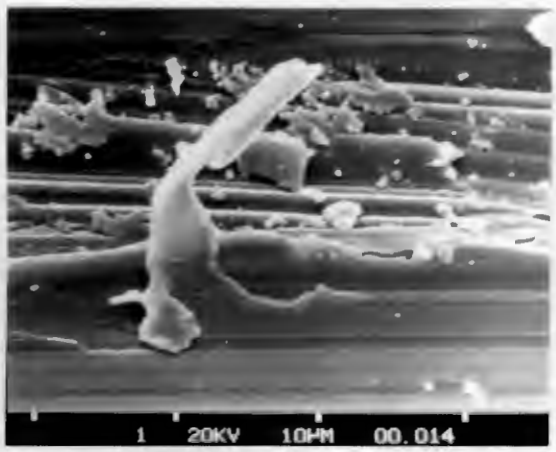

(a) As-received condition; attached wear chip (300x).

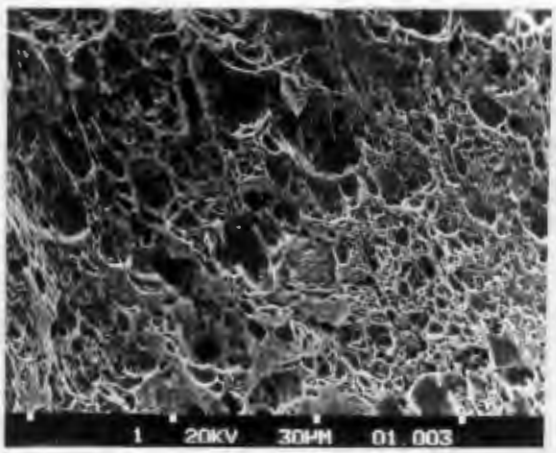

(b) Ductile tensile fracture. (1000x)

Fig. 4.12 S.E.M. micrographs of A-R-Col 360.

4.2 Spheroidisation heat treatment of En9 and En31

(a) The effect of spheroidising anneal time on the abrasion resistance of En9.

From Fig. 4.13 it can be noted that there is a trend of decreasing abrasion resistance with spheroidising time up to about 7 hours after which R.A.R. improves. The trend of decreasing R.A.R. corresponds to a systematic reduction in hardness which is associated with the spheroidisation of coarse laminated cementite which balls up into rounded masses. Abrasion resistance is known to be a function of both hardness and toughness. It can be noted that with extended spheroidising times (i.e. greater than about 7 hours) the ferrite matrix becomes depleted in carbon and hence tougher, while the carbides become increasingly coarse. Although the hardness continues to decrease, the increased toughness of the ferrite would explain the improved R.A.R. at extended spheroidising times.

(b) The effect of spheroidising anneal time on the abrasion resistance of En31.

Fig. 4.13 demonstrates a maximum value of abrasion resistance for En31 This maxima corresponds to a spheroidisation time of about 12 hours. For shorter heat treating durations a trend of increasing abrasion resistance with reduction in hardness can be observed; however for longer durations a trend of decreasing R.A.R. with a reduction in hardness is apparent.

From Fig. 4.16 it can be observed that material removal during the abrasive wear of Silver Steel (En31) occurs via two processes i.e.

(i) the preferential removal of the harder spheroidal cementite fraction from the softer ferrite matrix leaving behind voids or cavities (a) within the worn surface, and

(ii) the grooving (b) of the ductile ferrite matrix by brittle cementite spheroids which become trapped within the abrading medium and which subsequently act themselves as abrading particles.

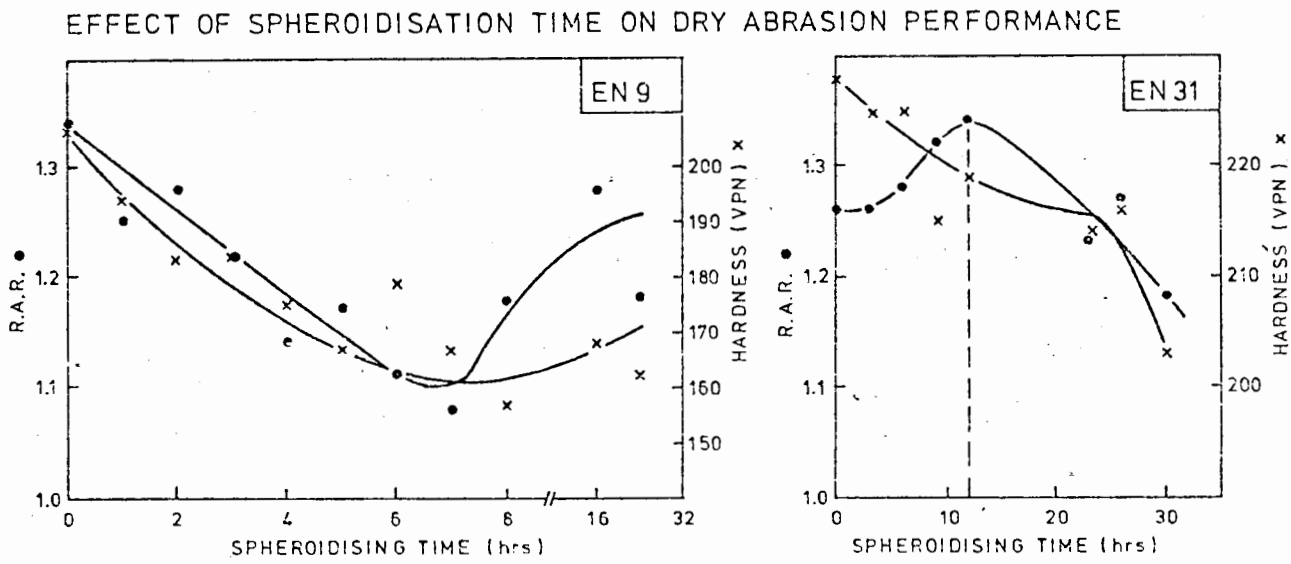

Fig. 4.13 The effect of spheroidisation time on dry abrasion performance.

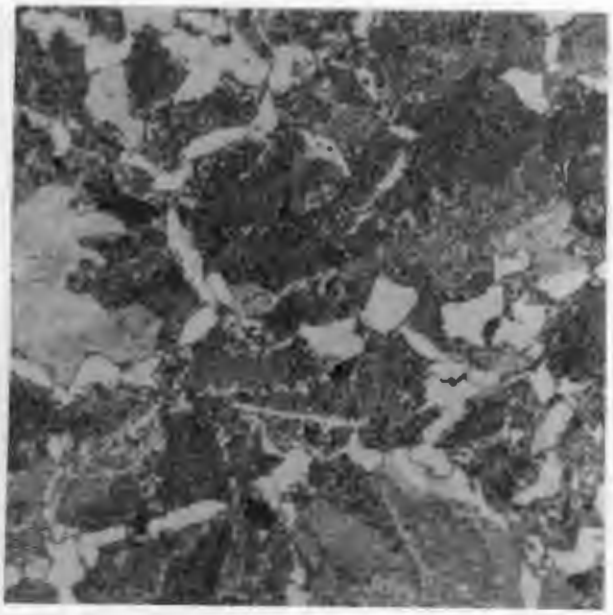

(a) 3 hours.

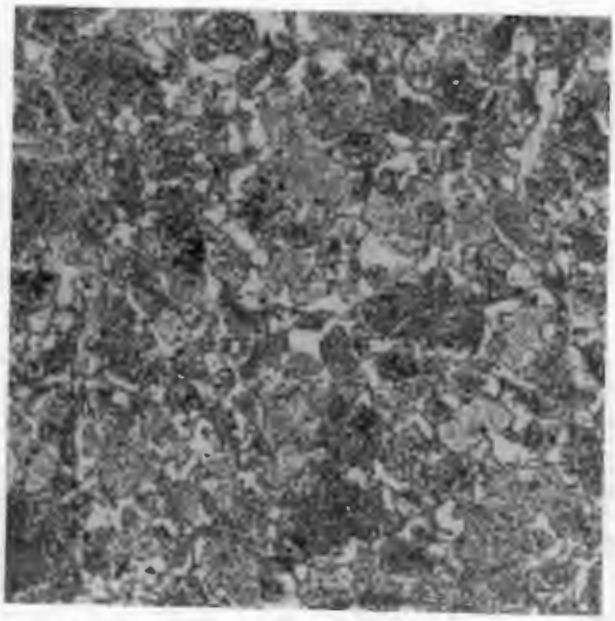

(b) 7 hours.

40μm

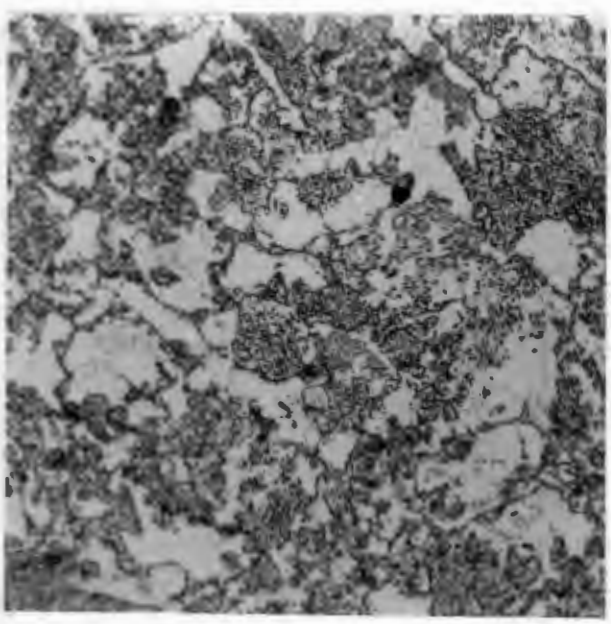

(c) 20 hours.

Fig. 4.14 Microstructures of En9 after various annealing times at 700°C.

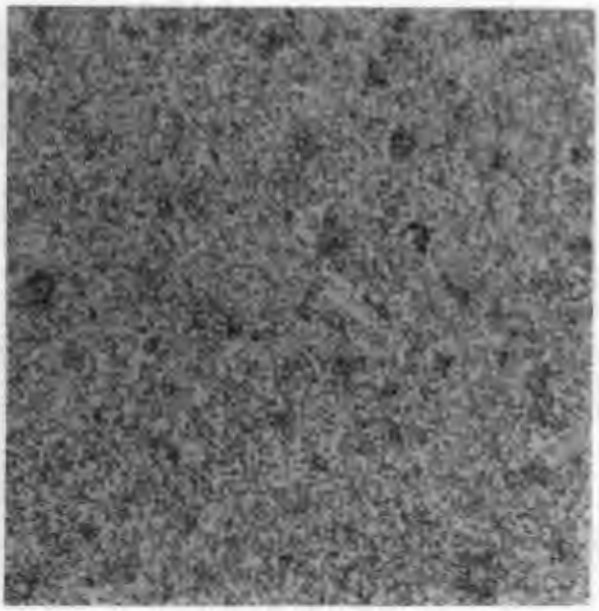

(a) 0 hours.

(b) 12 hours.

40μm

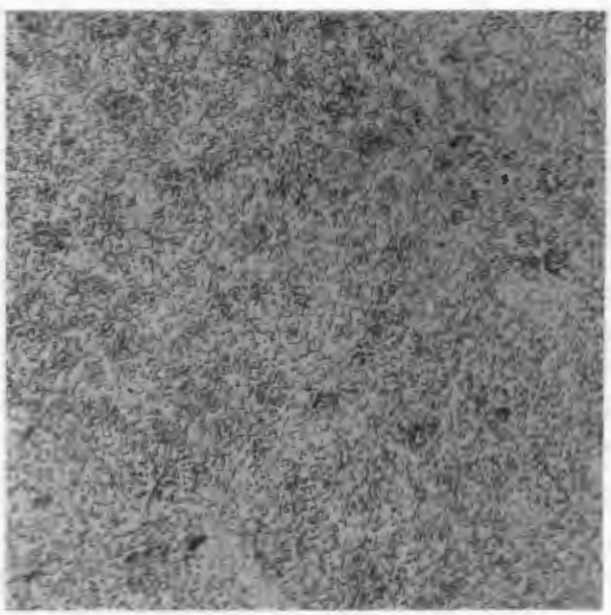

(c) 26 hours.

Fig. 4.15 Spheroidised microstructures of En31 as a function of annealing time at 700°C.

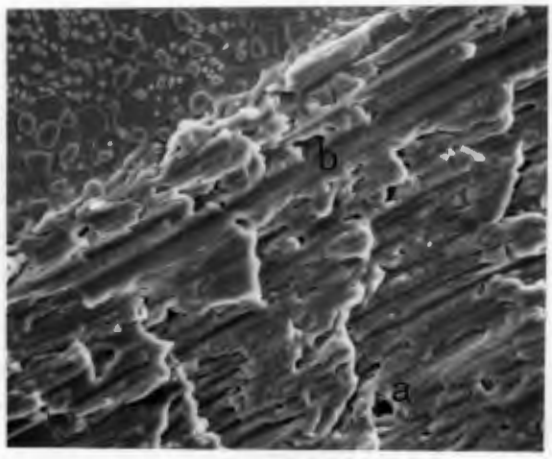

Fig. 4.16 S.E.M. micrograph of the abraded surface of spheroidised silver steel showing:
(a) cavity
and (b) groove formation
(3000x).

4.3 The effect of prior cold work on the abrasion resistance of mild steel

From Fig. 4.17 it can be observed that mild steel in a normalised condition has superior abrasion resistance to mild steel which has been cold worked. Factors associated with improved wear resistance due to the normalization heat treatment are:

(a) reduction in hardness (Fig. 4.17)
(b) refinement of ferrite/pearlite microstructure (Fig. 4.18).

It is clear that prior cold deformation does not improve the dry abrasion resistance of mild steel.

Material	Condition	R.A.R.	Hardness Hv30
Mild steel	11% cold work	0,94	213
Mild steel	Normalised	1,05	164

Fig. 4.17 Effect of prior cold-work on abrasion resistance of mild steel.

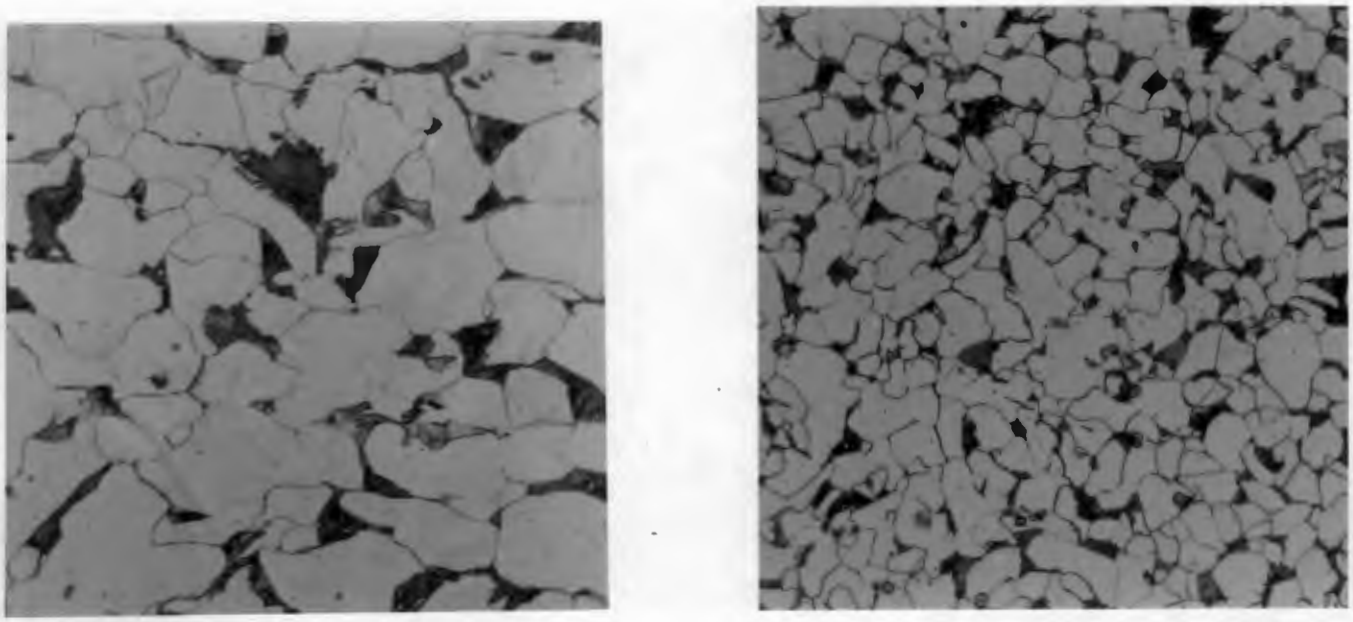

(a) cold worked (b) normalised

Fig. 4.18 Optical micrographs of mild steel showing the effect of cold work and heat treatment on microstructure.

4.4 To facilitate an understanding of the mechanisms responsible for material removal and to measure the depth of deformation incurred during wear, the following work was carried out. This investigation can be divided into the following sections:

4.4.1 Surface studies

4.4.2 Depth of deformation

4.4.3 Structural changes

4.4.1 Surface studies

Topographical studies undertaken to examine surface damage caused by abrasive wear can be sub-divided as follows:

(a) profilometric studies
(b) photomicrography of surface profiles
(c) S.E.M. studies
(d) effect of wear on surface hardness

(a) Profilometric studies.

The profiles generated during *low stress* wear on the worn surfaces of materials tested *underground* (Fig. 4.19) are less exaggerated than those generated by pure dry abrasive wear in the *laboratory* (Fig. 4.20). This phenomenon applies for the stainless steels as well as for the proprietary wear resistant materials

and is probably due to combined effects of differing modes of material removal e.g. cross-flow, in-situ corrosion and contamination. From Fig. 4.21 for *low stress* abrasion of Quatough in the *laboratory*, surface roughness (or C.L.A.) increases with normal applied load. In other words, the more severe the load, the more exaggerated the surface relief due to a deeper indentation of abrading particles. Fig. 4.22 demonstrates this effect for Abrasalloy. The surface profiles generated during *high stress* wear of low bulk hardness materials e.g. mild steel and 304L stainless steel tested underground (Fig. 4.23) are less exaggerated than those generated by pure *dry abrasion* (Fig. 4.24). However a reverse effect is apparent for materials with higher bulk hardness values and it can be observed that the surface profiles generated by severe *high stress* wear underground are greater than those measured for *laboratory* abraded materials.

IN-SITU - LOW STRESS

MATERIAL	NO. OF TRAVERSES	TRAVERSE LENGTH (mm)	AVERAGE C.L.A. (μm)
Abrasalloy	11	1,9	5,39
AISI 431	9	1,9	4,24
3CR12	15	1,9	3,46
Mild Steel	7	1,9	4,06
AISI 304	10	1,9	4,05
A-R-Col 360	5	1,9	2,60
Wearalloy 500	5	1,9	3,44
Wearalloy	5	1,9	3,84
Roqlast C400	5	1,9	2,48

Fig. 4.19 Surface profile measurements.

LABORATORY - LOW STRESS

MATERIAL	LOAD (N)	NO. OF TRAVERSES	TRAVERSE LENGTH (mm)	AVERAGE C.L.A. (μm)
Quatough	2,0	3	1,9	3,67
	19,6	3	1,9	5,90
	68,6	3	1,9	7,77
Abrasalloy	2,0	3	1,9	5,43
	19,6	3	1,9	7,37
	68,6	3	1,9	8,27
AISI 431	2,0	3	1,9	5,17
	19,6	3	1,9	7,00
	68,6	3	1,9	8,07
3CR12	2,0	3	1,9	8,13
	19,6	3	1,9	8,37
	68,6	3	1,9	>10
Mild Steel	2,0	3	1,9	6,53
	19,6	3	1,9	9,53
	68,6	3	1,9	7,80
AISI 304L	2,0	3	1,9	5,57
	19,6	3	1,9	7,97
	68,6	3	1,9	8,97

Fig. 4.20 Surface profile measurements.

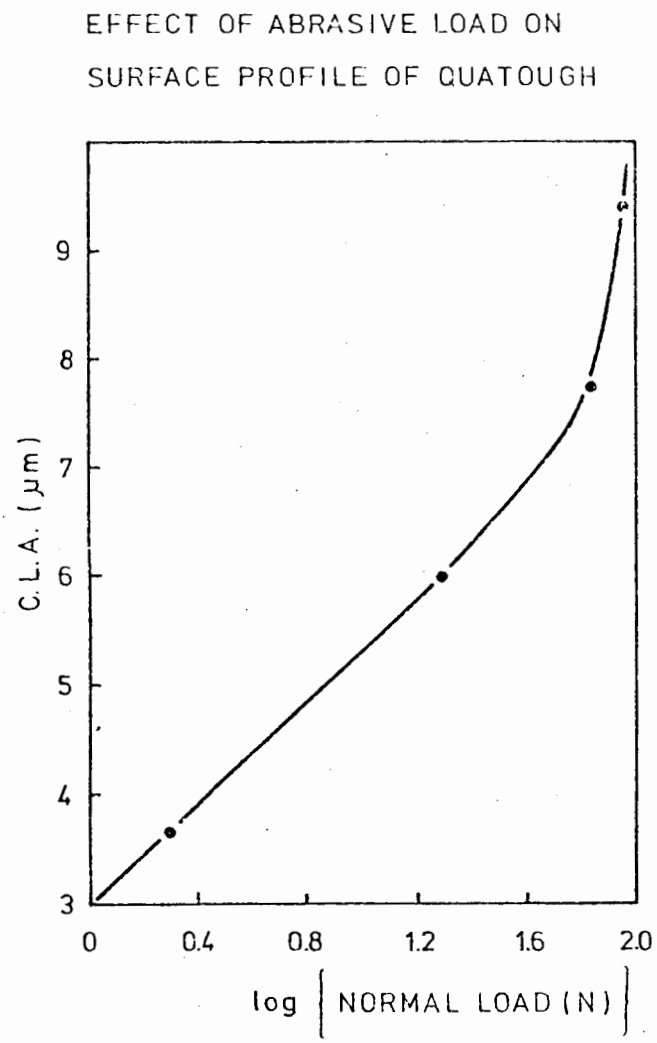

Fig. 4.21 Low stress laboratory abrasion of Quatough.

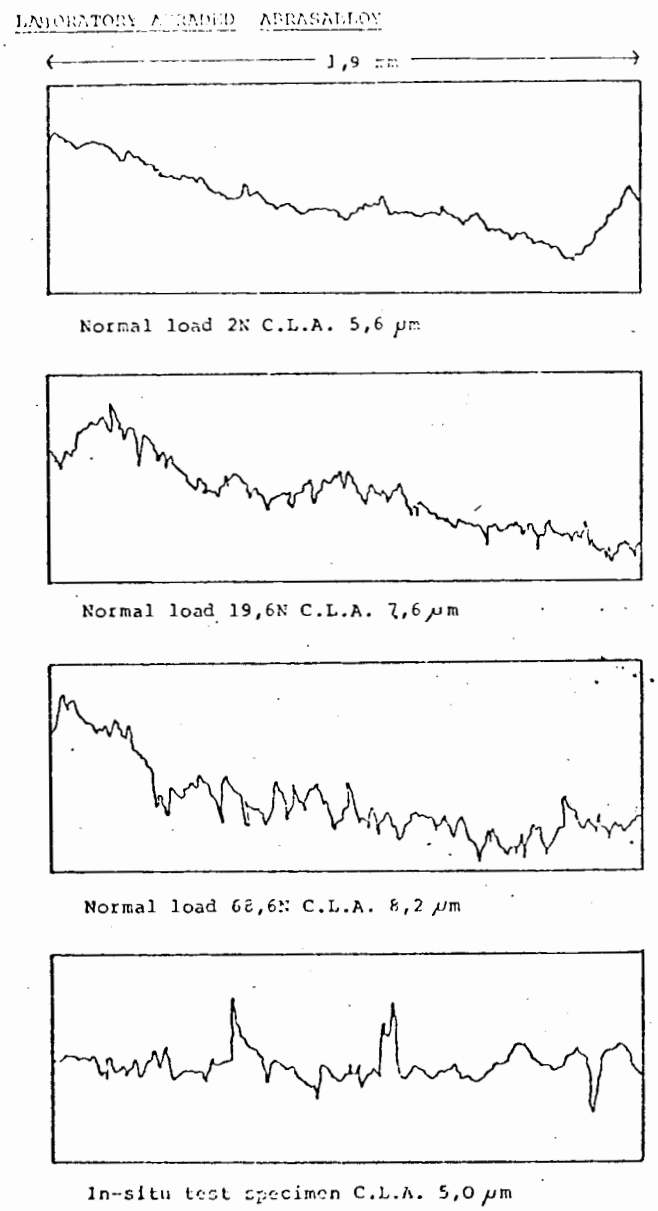

Fig. 4.22 Talysurf traces of Abrasalloy that has undergone low stress wear in the laboratory and underground.

IN-SITU - HIGH STRESS

MATERIAL	TRAVERSE LENGTH (mm)	NO. OF TRAV-ERSES	AVERAGE C.L.A. (μm)	TRAVERSE LENGTH	NO. OF TRAV-ERSES	AVERAGE C.L.A. (μm)
Roqlast AH360	1,9	5	5,24	3,8	5	>10
Mild Steel	1,9	5	4,84	3,8	5	8,32
Wearalloy	1,9	5	6,06	3,8	5	>10
Wearalloy 500	1,9	5	6,25	3,8	5	>10
304L	1,9	5	3,52	3,8	5	6,58
Hadfields BW10	1,9	5	7,40	3,8	5	>10
Abrasalloy	1,9	5	4,98	3,8	5	7,14
Benox	1,9	5	7,72	3,8	5	>10
3CR12	1,9	5	3,78	3,8	5	7,54
316L	1,9	5	3,00	3,8	5	7,24
3CR12 Ni 800°C	1,9	5	6,14	3,8	5	>10
3CR12 Ni 700°C	1,9	5	6,06	3,8	5	>10

Fig. 4.23 Surface profile measurements.

Benox	1,9	5	4,24	3,8	5	>10
Vidalloy	1,9	5	0,32	3,8	5	1,18
316L	1,9	5	3,38	3,8	5	5,48
Wearalloy 400	1,9	5	4,92	3,8	5	8,62
Kyle Dua Plate	1,9	5	4,76	3,8	5	>10
Mild Steel	1,9	5	5,62	3,8	5	>10
AL 745 7F	1,9	5	4,92	3,8	5	7,60
Quatough	1,9	5	2,02	3,8	5	2,52
304L	1,9	5	4,48	3,8	5	7,78
Abrasalloy	1,9	5	3,76	3,8	5	4,92
BS 4360 43A	1,9	5	5,64	3,8	5	8,12
3CR12 Ni	1,9	5	4,12	3,8	5	7,96
Wearalloy 500	1,9	5	2,96	3,8	5	7,40
Roqlast AH400	1,9	5	2,42	3,8	5	4,66

Fig. 4.24 Surface profile measurements.

(b) Photomicrography of surface profiles.

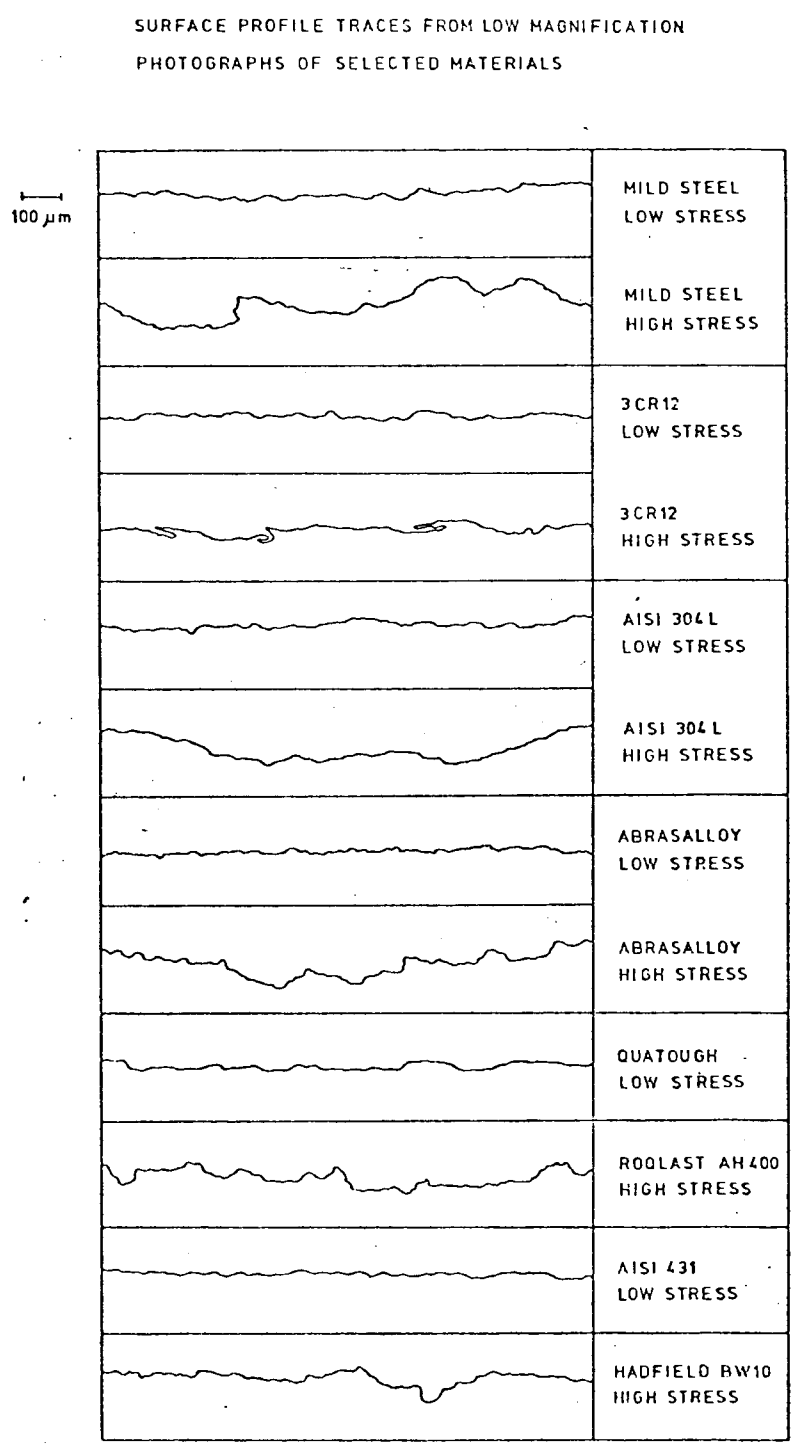

Fig. 4.25 Surface profiles demonstrating the effects of *low* and *high stress* wear on various materials abraded in the laboratory and in-situ respectively.

Fig. 4.25 demonstrates the difference between the surface topography of materials which have undergone *low stress* wear (68,6N load) in the laboratory and *high stress* wear underground.

LOW AND HIGH STRESS OPTICAL MICROGRAPHS OF MILD STEEL

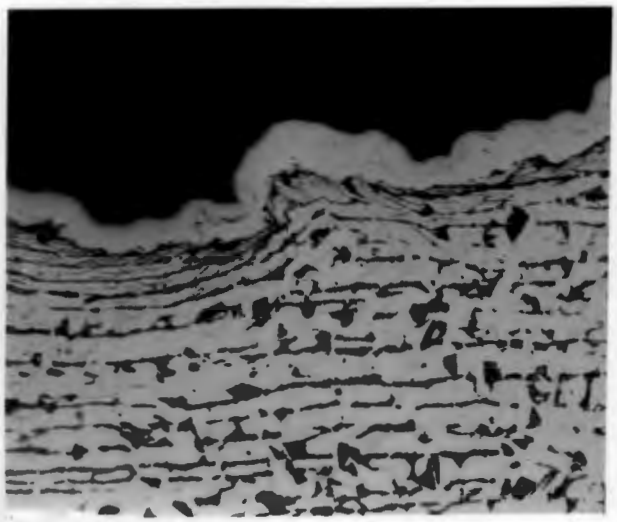

100µm

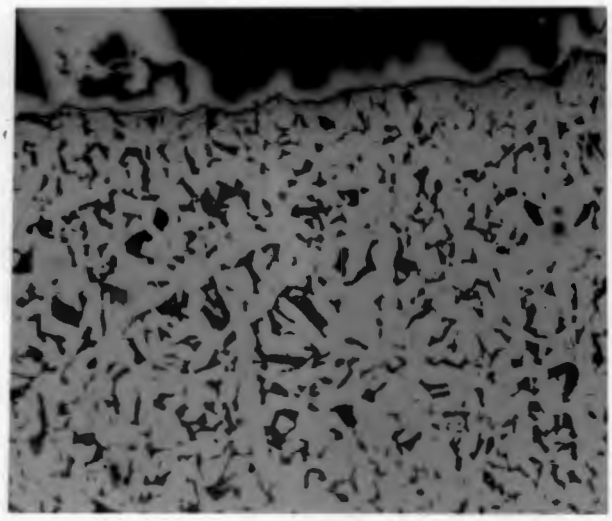

100µm

Fig. 4.26 (i) (ii)

Note extent of microstructural damage induced by high stress wear (i) compared to low stress wear (ii). Mag. 150x.

In conjunction with Fig. 4.26 it can be observed that as the severity of stress of the wear environment increases so too does the topography become enhanced in the following fashion:

(i) by an increase in amplitude or the groove peak-to-valley height,

(ii) by an increase in wavelength or the peak-to-peak distance for consecutive grooves and

(iii) by an increase in depth of deformation or distortion of microstructure.

(c) S.E.M. studies.

The worn surfaces of materials from the following environments were examined.

(i) Laboratory *low stress* wear.

All materials were abraded according to standard conditions at a load of 19,6N. In order to determine the effect of abrasive load on the mechanism(s) of material removal, 3CR12 was abraded on the pin and disc rig at low medium and high loads i.e. at 2N, 19,6N and at 68,6N loads respectively. The direction of abrasion is from left to right.

(ii) In-situ *low stress* wear.

The surfaces of worn shaker conveyor wear panels were examined. Because of excessive corrosion and contamination underground only the corrosion resisting or stainless steels were included in this examination.

(iii) Laboratory *high stress* wear.

Single scratch tests were carried out on a number of materials. Rough experiments were conducted by manually abrading the surfaces of materials with fragments of quartzitic ore.

(iv) In-situ *high stress* wear.

The surfaces of worn reciprocating flight conveyor wear plates were examined.

S.E.M. micrographs of the abraded surfaces of various materials and identification of various major characteristic features are presented.

(i) LABORATORY LOW STRESS DRY ABRASION - WORN SURFACE TOPOGRAPHY

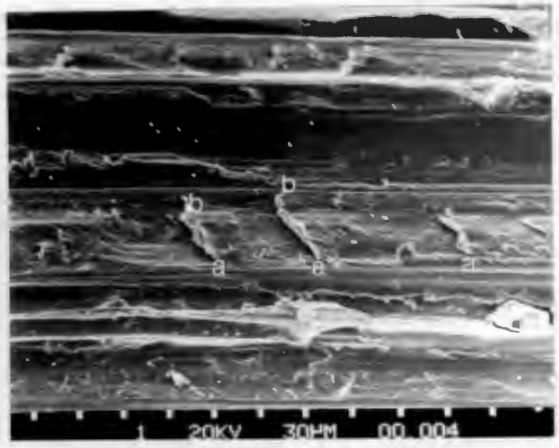

Fig. 4.27 Mild Steel (340x)
Sub-surface shearing (a) and periodic spalling (b).

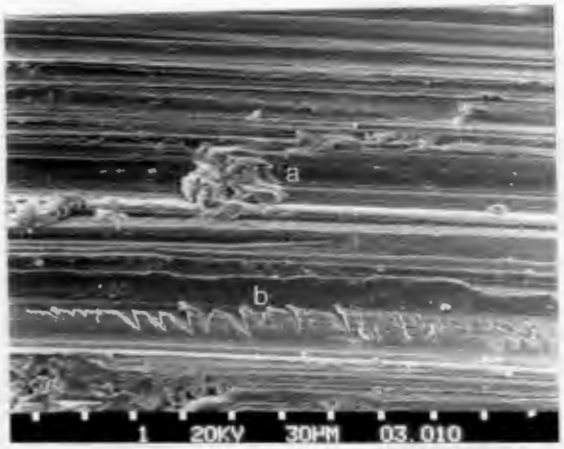

Fig. 4.28 Abrasalloy (310x)
Large wear debris cluster (a) and extensive shear lip microcracking (b)

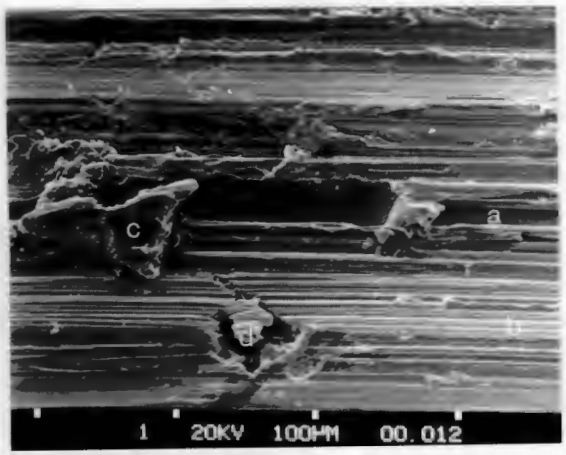

Fig. 4.29 304L Stainless Steel
Unidirectional macrogrooving (a) and microgrooving (b). Wear debris (c) and wear spall (d).

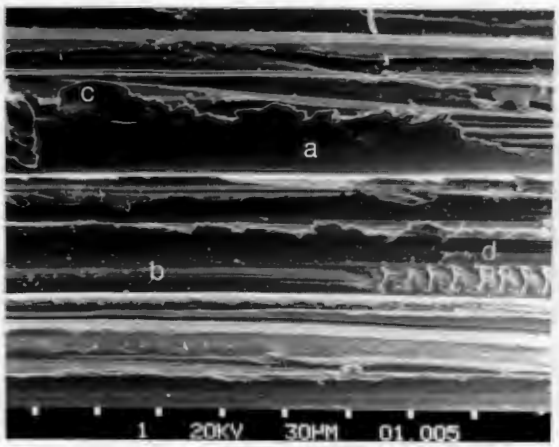

Fig. 4.30 Quatough (390x)
Clear distinction between macrogrooving (a) and microgrooving (b). Semi-detached laterally extruded ridge (c). Repeated spalling at base of groove (d).

(ii) IN-SITU LOW STRESS - WORN SURFACE TOPOGRAPHY

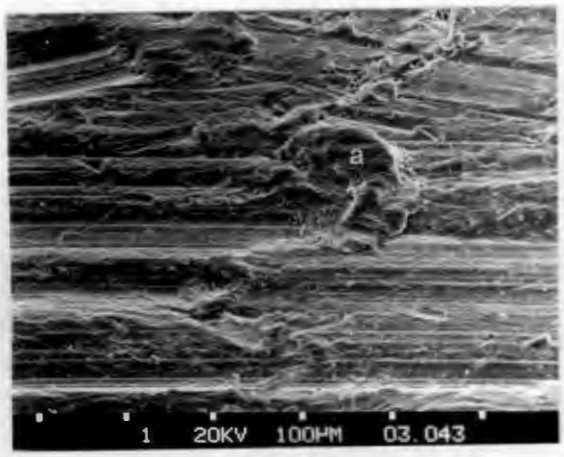

Fig. 4.31 431 Stainless Steel (192x) "Bulldozing effect" (a). Material displaced laterally and forward by abrading particle

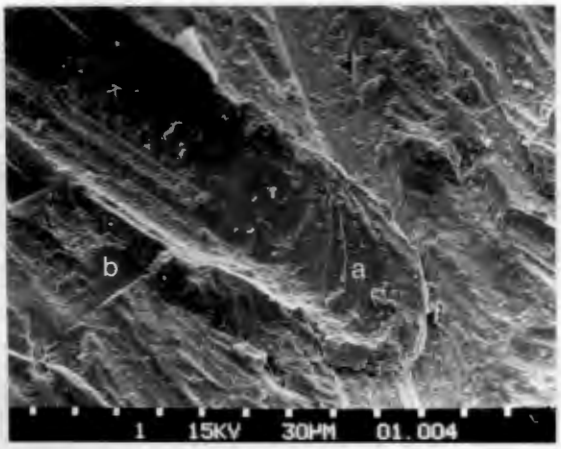

Fig. 4.32 3CR12 (300x) Stacked prow formation (a) - result of bulldozing. Wedge indentation (b) - evidence of impact wear.

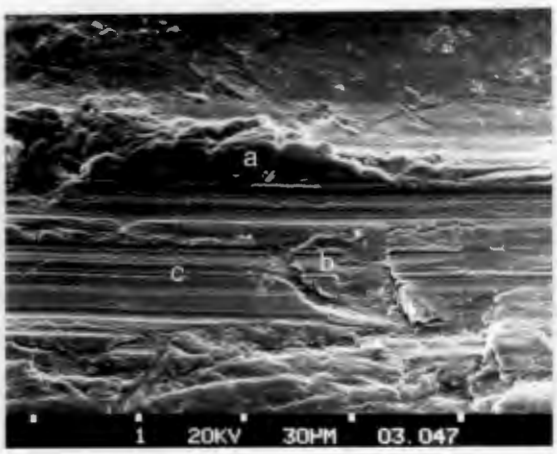

Fig. 4.33 304 Stainless Steel Sideways displacement of material to form an extruded ridge (a). Repeated spalling (b within wear groove (c).

(iii) LABORATORY HIGH STRESS - WORN SURFACE TOPOGRAPHY

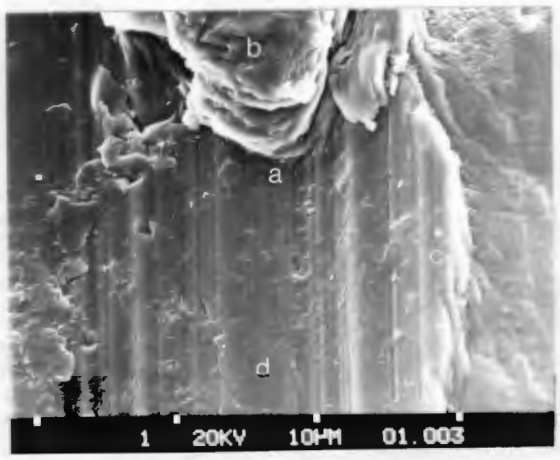

Fig. 4.34 Mild Steel (950x): Material build-up ahead of developing groove (a) contains a stack of thin sheets (b) - remnants of prior delaminated wear. Extensive lateral displacement of material to form ridges (c) adjacent to developing groove (d).

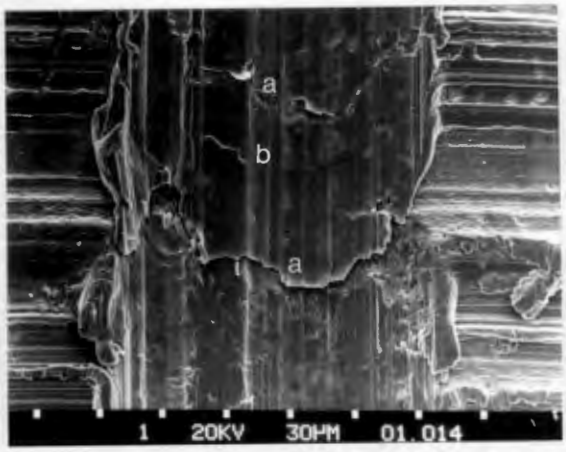

Fig. 4.35 Abrasalloy (400x): Series of concentric cracks (a) nucleating below the surface. Centre crack (b) has yet to propagate fully to the surface while others have already done so and exhibit repeated spalling or delaminated-type wear.

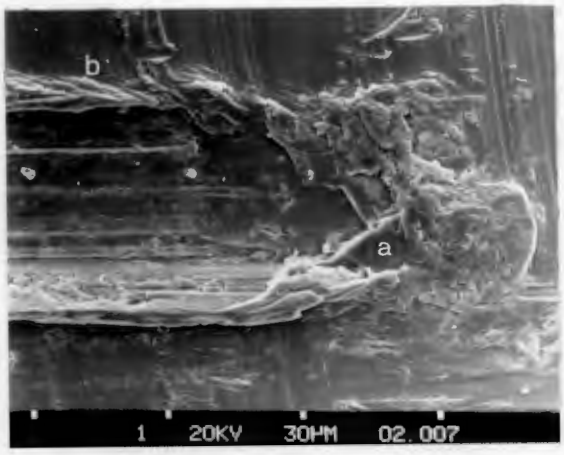

Fig. 4.36 Wearalloy (830x): Bulldozing effect - forward (a) and lateral (b) displacement of material ahead of abrading particle.

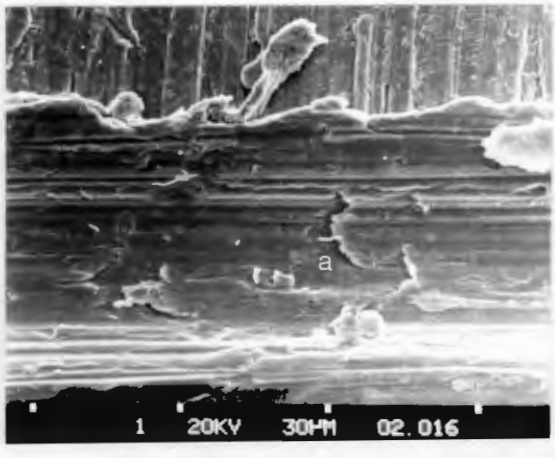

Fig. 4.37 316L Stainless Steel (800x): Delaminated wear i.e. plastic deformation of the surface layer, sub-surface crack nucleation and propagation resulting in delamination of thin sheets (a) of material - subsequently removed.

(iv) IN-SITU HIGH STRESS - WORN SURFACE TOPOGRAPHY

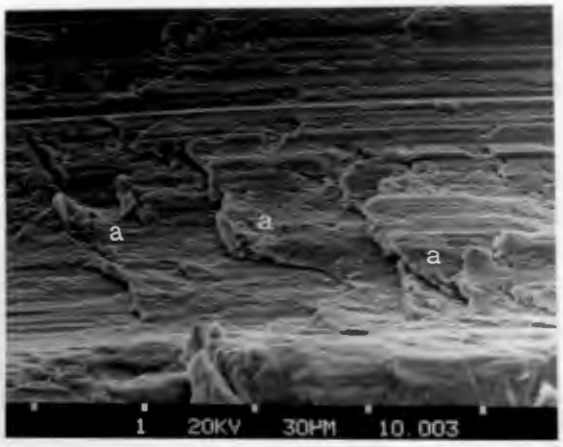

Fig. 4.38 3CR12 (690x) Repeated delamination of worn surface (a).

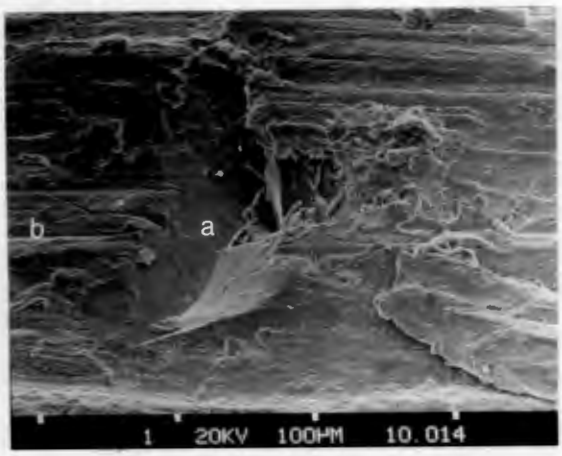

Fig. 4.39 304L Stainless Steel (1000x): Impact crater (a) on severely deformed wear track (b)

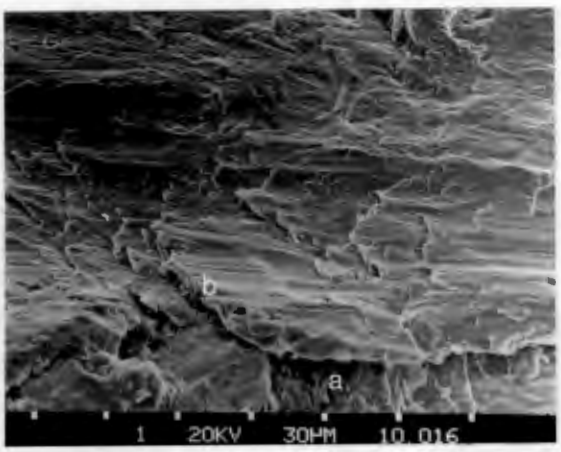

Fig. 4.40 304L Stainless Steel (450x): Severe delamination i.e. sub-surface degradation (a) and fracture (b).

(v) THE EFFECT OF LOAD ON MECHANISM(S) OF MATERIAL REMOVAL OF 3CR12

Direction of abrasion ⟶

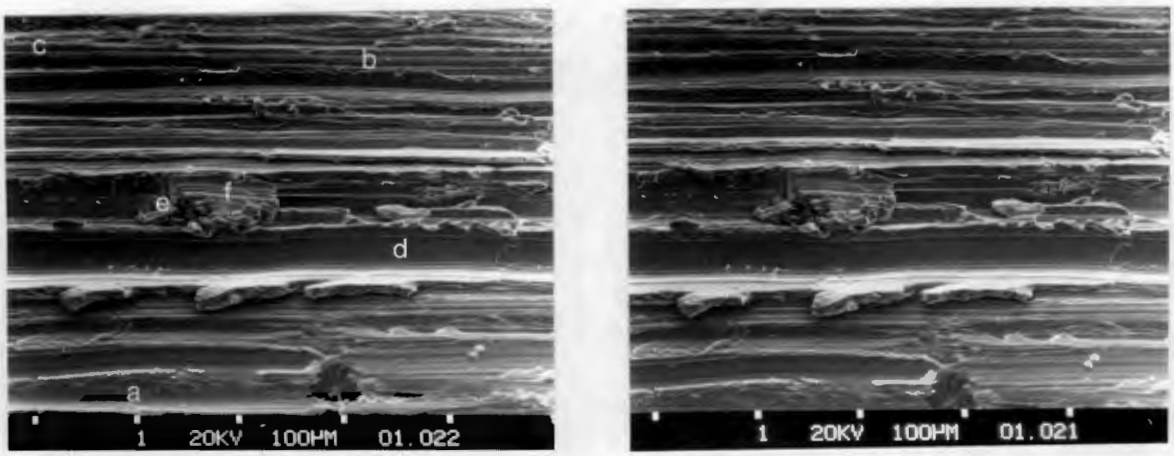

Fig. 4.41 3CR12 Medium load (Stereopair 8° tilt, 225x)

The abraded surface as seen in Fig. 4.41 consists of a series of coarse textured unidirectional macro-grooves (a) parallel to the direction of motion of the abrading particles. Interspaced within these grooves are ridges, some are sharp edged (b) - a result of microcutting or micromachining, while others are rounded (c), these being formed by the ploughing action of abrading particles. Within each coarse groove a series of microgrooves (d) can be seen. Clusters of wear-debris pile up (e), reside on alternating ridges and grooves. Microgrooves (f) are clearly visible on the upper surface of wear plates.

During severe plastic deformation ductile ridges are laterally extruded to form undetached wear chips (g). Remnants of these severely deformed or sheared ridges (g) actually "arrow" the direction of abrasion.

Direction of abrasion 

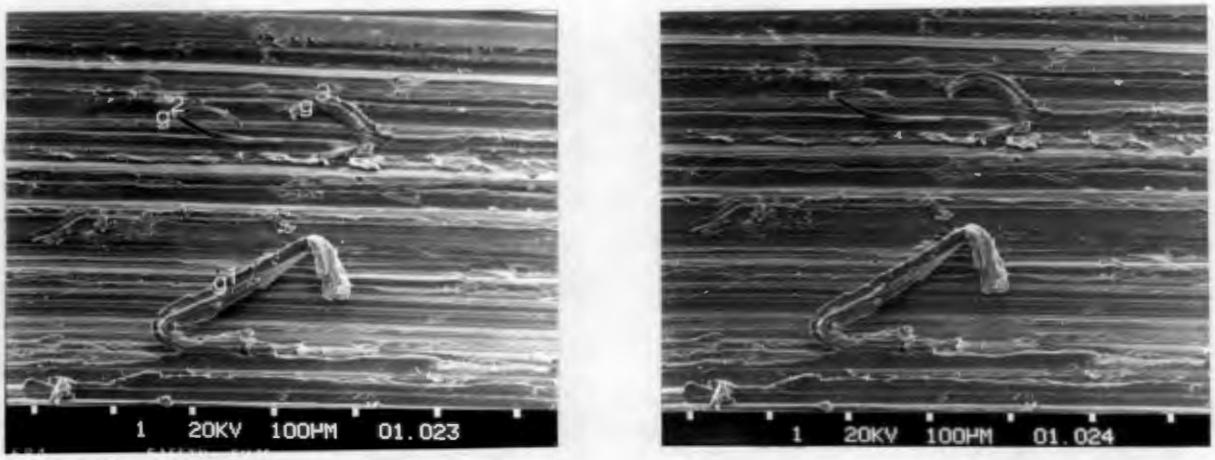

Fig. 4.42 3CR12 High Load (Stereopair 8° tilt, 175x)

Many of the characteristic features described for 3CR12 when abraded under a medium load can be observed in Fig. 4.42. These features are inter alia, a,b,c,d,e and g. The most distinctive feature is the extent of the semi-detached wear ridge (g). A ridge greater than 200µm in length appears to have been laterally extruded under high compressive stresses applied normal to the direction of abrasion causing shearing to occur. Further abrasion has deformed and twisted this ridge. Two

similar but smaller features appear near the top of this micrograph. One of these chips (g^2) appears to have been lifted vertically from the surface while the other appears to have been deformed laterally (g^3).

Direction of abrasion 

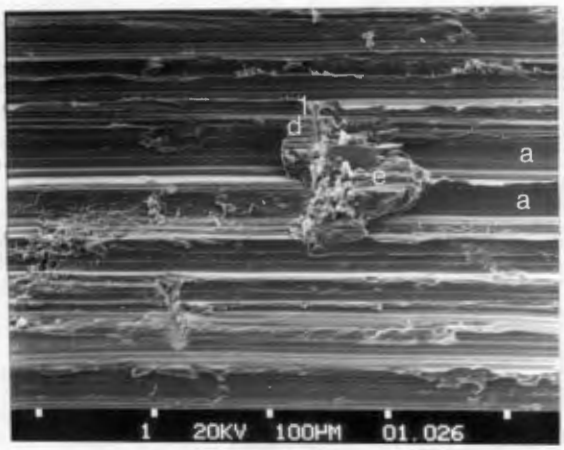

Fig. 4.43 3CR12 High Load (253x)

Fig. 4.43 is a close-up of a wear debris cluster (e). Wear debris formation, constitution and orientation can assist one in the elucidation and characterisation of the various mechanisms by which abrasion can occur. A delaminated sheet (d^1), as well as other debris (e.g. abrasive grit in various stages of disintegration due to crushing and grinding) constitute the debris cluster. The striations described (d^1) remain aligned parallel to the direction of motion of wear while the bulk of the debris cluster resides on two adjacent (a) grooves.

Direction of abrasion ⟶

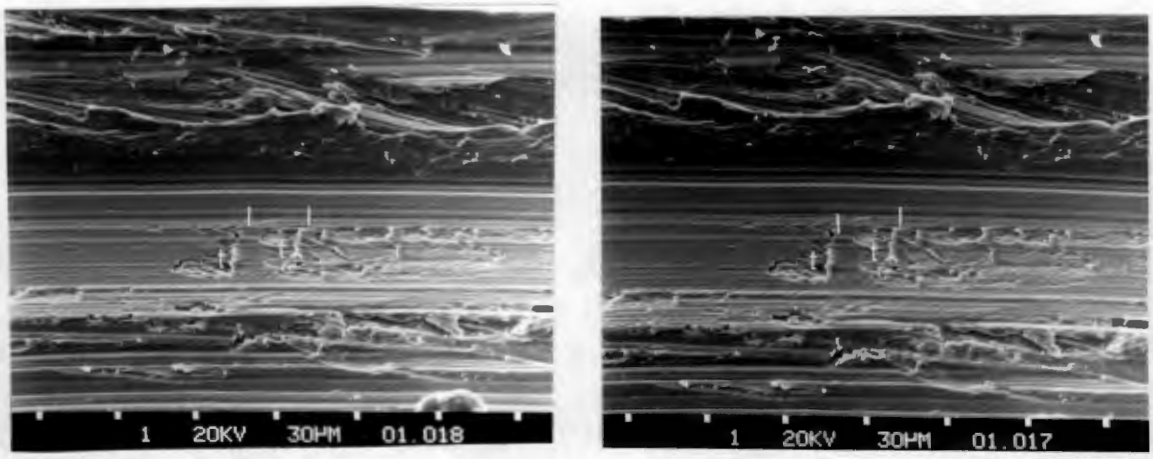

Fig. 4.44 3CR12 Low Load (Stereopair 8^{o} tilt, 580x)

The following features apparent in Fig. 4.44 are, inter alia, a,b,c,d and g. A repeated spalling mechanism appears to account for the intra-groove surface damage and subsequent material removal.

(d) The effect of wear on surface hardness.

From Fig. 4.45 and Fig. 4.46 it can be observed that the hardness of the worn surface when compared to the unworn or bulk hardness of a material which has undergone wear either remains constant, increases (i.e. work hardening occurs), or decreases (i.e. work softening, recovery or recrystallization takes place). Fig. 4.45 can be summarised in terms of bulk microstructure as follows:

(i) for ferritic (b.c.c.) materials, $4 \geqslant \Delta Hv(\%) \geqslant -3$.
(ii) for austenitic (f.c.c.) materials, $14 \geqslant \Delta Hv(\%) \geqslant -6$.
(iii) for martensitic (b.c.c. tetragonal) materials, $17 \geqslant \Delta Hv(\%) \geqslant -7$.

Fig. 4.46 can be summarised as follows:

(i) for ferritic materials, $89 \geqslant \Delta Hv(\%) \geqslant 36$.
(ii) for austenitic materials, $162 \geqslant \Delta Hv(\%) \geqslant 64$.
(iii) for martensitic materials, $12 \geqslant \Delta Hv(\%) \geqslant -28$.

It can be observed that the severe abrasion of reciprocating flight conveyor wear plates causes greater surface hardening to occur, for all materials, compared to wear on the shaker conveyor wear panels with the exception of Wearalloy 400.

The austenitic materials which have undergone both *high* and *low stress* wear all exhibit extensive surface hardening.

Fig. 4.45 Hardness values of low stress in-situ (shaker conveyor) wear panels.

	MATERIAL	BULK MICROSTRUCTURE	* NO. OF SAMPLES	HARDNESS H_V 30 UNWORN SURFACE	HARDNESS H_V 30 WORN SURFACE	** ΔH_V %
x	A-R-Col360	Martensite	2	334	342	+ 2
x	Abrasalloy	"	4	354	364	+ 3
x	Roqlast AH400	"	3	477	448	- 6
x	RB390	"	2	442	449	+ 2
x	Wearalloy 400	"	3	395	368	- 7
x	Wearalloy 500	"	1	446	424	- 5
x	Benox	Ferrite/pearlite	2	187	194	+ 4
■	Mild Steel	Ferrite/pearlite	18	134	131	- 3
o	304L	Austenite	2	159	181	+14
o	316L	"	3	179	198	+10
o	304L (15% cold work)	"	1	309	353	+14
o	304L (27% cold work)	"	2	303	321	+ 6
o	430	Ferrite/pearlite	3	166	177	+ 7
o	440B (T200°C)	Martensite	1	500	485	- 3
o	440B (T400°C)	Tempered martensite	1	470	485	+ 3
o	440B (T600°C)	" "	1	393	458	+17
o	431 (T200°C)	Martensite	1	373	393	+ 5
o	431 (T400°C)	Tempered martensite	1	343	343	0
o	431 (T600°C)	" "	1	334	334	0
●	3CR12	Martensite/ferrite	2	149	161	+ 8
●	3CR12 OQ 700°C	Ferrite	1	153	184	+20
●	3CR12 OQ 800°C	Martensite/ferrite	1	155	172	+11
●	3CR12 OQ 900°C	Martensite	1	228	246	+ 8

Key: x proprietary wear resistant material

■ standard reference material

o stainless steel

● corrosion resisting steel

* three hardness tests undertaken on each sample

** percentage change in hardness of worn surface composed compared with unworn surface

MATERIAL	BULK MICROSTRUCTURE	NO. OF* SAMPLES	HARDNESS H_V 30		** ΔH_V %
			UNWORN SURFACE	WORN SURFACE	
x Abrasalloy	Martensite	1	433	485	+12
x Roqlast AH400	"	1	415	419	+ 1
x Roqlast AH360	"	1	432	443	+ 3
x Wearalloy 400	"	1	461	330	-28
x Benox	Ferrite/pearlite	1	203	277	+36
■ Mild Steel	Ferrite/pearlite	1	133	251	+89
o 316L	Austenite	1	170	312	+84
o 304L	"	1	140	230	+64
△ Hadfield BW10	"	1	178	467	+162
● 3CR12	Martensite/ferrite	1	143	187	+31
● 3CR12Ni (800°C)	Martensite/ferrite	1	196	214	+ 9
● 3CR12Ni (700°C)	"	1	229	252	+10

Key:

x proprietary wear resistant material

■ standard reference material

o stainless steel

● corrosion resisting steel

△ cast 14% manganese steel

* three hardness tests undertaken on each sample

** percentage change in hardness of worn surface compared with unworn surface

Fig. 4.46 Hardness values of high stress in-situ (reciprocating flight conveyor) wear plates.

4.4.2 Depth of deformation

It is well known that deformation associated with abrasive wear is not confined to the surface of a worn component. However to what depth below the worn surface does this deformation extend and how can it be identified?

The following techniques were used to identify and to measure the depth to which abrasion induced deformation extends:

(a) microhardness traverses
(b) split-specimen technique
(c) optical metallography

(a) Microhardness traverses

The results of the microhardness traverse data are tabulated in Fig. 4.47.

MATERIAL	ENVIRON	MICROHARDNESS (DPH)			H_M	d_{MAX}
		Bulk	Worn Surface	ΔH_M	$Max\frac{H_M}{H_{BM}}$	(μm)
Mild Steel	Lab-low stress	120	216	98	1,80	78
AISI 304L	"	140	230	89	1,64	60
Abrasalloy	"	297	466	169	1,57	17,5
Quatough	"	307	335	27	1,09	6
3CR12	"	179	227	48	1,27	68
AISI 431	"	292	253	62	1,21	12,5
Mild Steel	In-situ-low stress	165	228	63	1,38	42
AISI 304L	"	143	197	55	1,38	90
Abrasalloy	"	307	384	76	1,25	13
Benox	"	190	211	21	1,11	15
3CR12	"	126	145	19	1,15	15
AISI 431	"	471	537	68	1,14	50,5
Mild Steel	Lab-high stress	181	244	64	1,35	69
AISI 304L	"	250	400	149	1,60	160
Abrasalloy	"	283	518	236	1,83	50
Roqlast AH400	"	349	513	165	1,47	25
Quatough	"	470	653	183	1,39	41,5
Mild Steel	In-situ high stress	183	265	82	1,45	53
AISI 304L	"	244	407	163	1,67	420
Abrasalloy	"	315	347	32	1,10	32
Benox	"	216	279	62	1,29	63
Hadfield BW10	"	443	647	202	1,46	83

d_{MAX} - maximum depth of surface hardening

ΔH_M - maximum - bulk microhardness

$Max\frac{H_M}{H_{BM}}$ - normalised microhardness, i.e. microhardness - bulk microhardness

Fig. 4.47 Tabulation of microhardness traverse data.

To gauge the reproducibility of this technique, microhardness tests were undertaken on tapered surfaces of 304L stainless steel which had been polished to 2^{o} and 5^{o} respectively. The hardness profiles obtained were then plotted (Fig. 4.48) and good correlation was noted.

MATERIAL: AISI 304L
NORMAL LOAD: 68,6 N
TAPER: 2^{o} & 5^{o}
ENVIRON: Laboratory - Low Stress

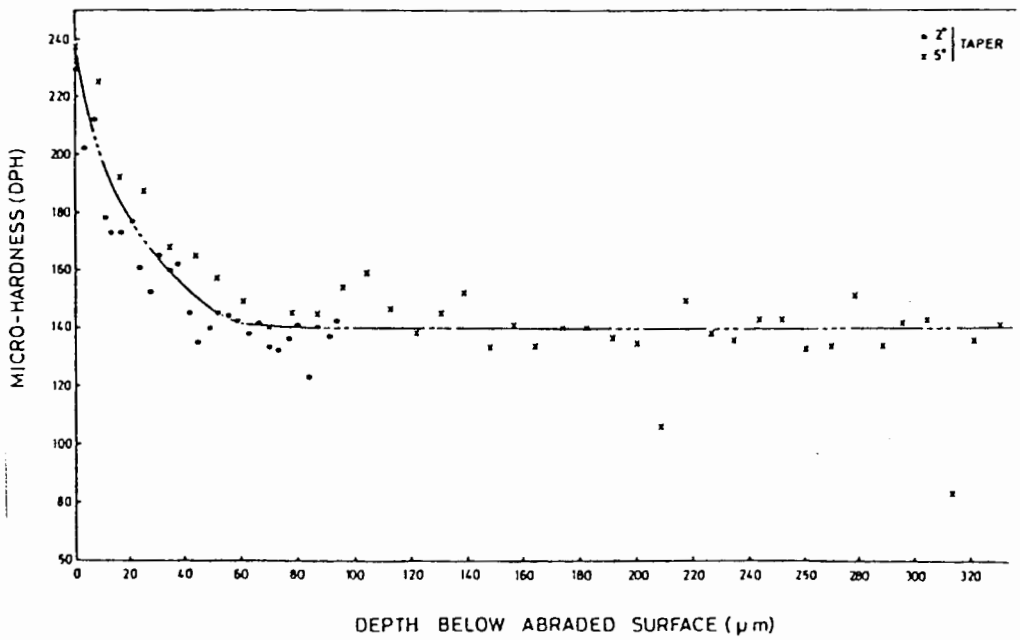

Fig. 4.48 Microhardness profile of 304L stainless steel after abrasion on the pin-and-disc wear rig.

Microhardness traverse profiles of all materials are included in the appendix. From Fig. 4.47 comparisons of surface hardening and depth of deformation phenomena were made. Microhardness tests were undertaken on materials representative of wear occuring in four different environments, i.e.

(i) laboratory, *low stress* (dry abrasion)
(ii) in-situ, *low stress* (abrasion-corrosion)
(iii) laboratory, *high stress* (dry abrasion)
(iv) in-situ, *high stress* (abrasion-corrosion)

Materials exhibiting comparatively low *bulk microhardness* values exhibit correspondingly high *maximum normalised hardness* values. However, the maximum work hardened hardness of these materials is not as high as the maximum hardness of materials having higher bulk hardness values. The maximum hardness values are attained at the critical strain at which fracture or wear occurs.

It is also apparent that *low bulk hardness* materials exhibit extensive depths to which strain induced hardening occurs e.g. 304L stainless steel, while the maximum depth of deformation of martensitic (i.e. high bulk hardness) materials is comparatively shallower. The *change* in *microhardness* (ΔH_M) measured for materials that had undergone *dry abrasion* in both *low* and *high stress* environments is found to be greater than that change in hardness of materials tested *in-situ*.

This is due to the fact that the outer work hardened layer underground is subjected to corrosion and is repeatedly removed during subsequent abrasive wear.

As can be expected the *maximum depth of deformation* induced by *high stress* wear in the *laboratory* was found to be greater than for *low stress* wear (with the exception of mild steel). The same trend was noted for in-situ wear. Some of the anomalies may be explained in terms of corrosive action and softening due to recovery and recrystallization.

(b) Depth of deformation obtained from the split-specimen technique

Fig. 4.49 demonstrates the extent to which deformation occurs below the surface during abrasive wear. The criterion for the maximum depth of deformation was adopted to be that region below the surface where microstructural distortion can no longer be detected and measured e.g. the termination of slip bands in austenitic materials (Fig. 4.50).

Material	Microstructure	Depth of Deformation (μm)
Mild Steel	Ferrite-pearlite	130
Benox	"	90
Abrasalloy	Martensite	Not apparent
3CR12	"	"
AISI 304L	Austenite	160
AISI 316L	"	300
Hadfield	"	330

Fig. 4.49 Measurement of deformation depth induced by abrasive wear.

No noticeable deformation was detected for the martensitic materials, while the ferritic materials demonstrated considerable deformation up to about 100μm. Evidence of the work hardening capacity of the austenitic materials was exhibited by the extensive depth to which deformation can be detected (Fig. 4.50).

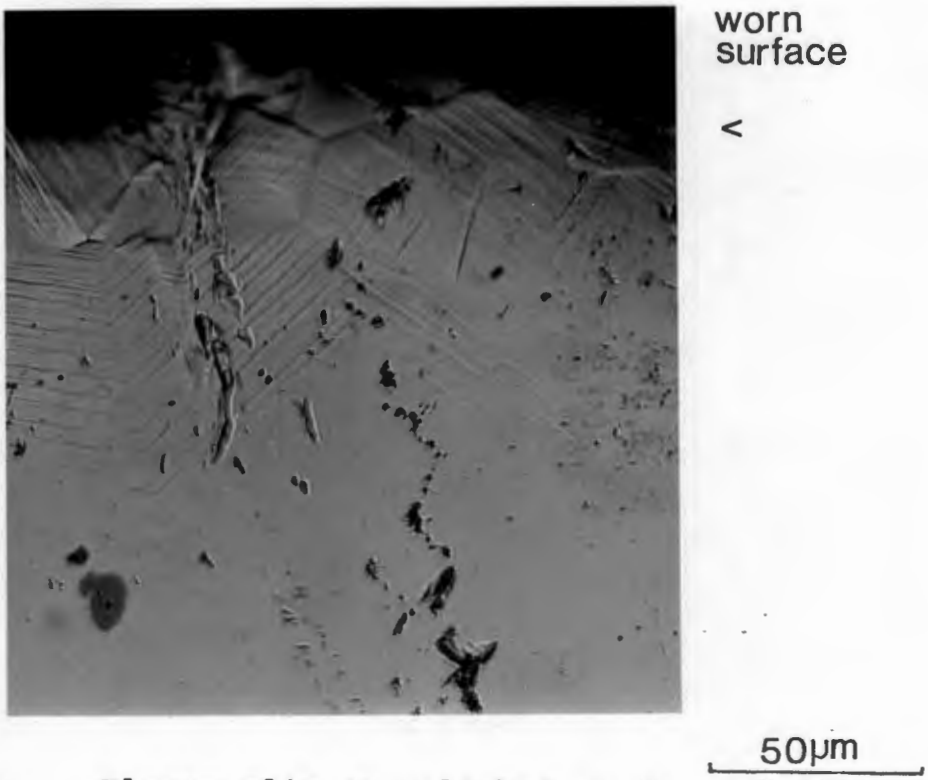

Fig. 4.50 Planar slip on polished surface of 304L after dry abrasion at a load of 7kg.

(c) Depth of deformation as measured by polish-and-etch techniques

The effects of surface deformation due to *high stress* wear can be summarised in Fig. 4.51 below.

MATERIAL	MICROSTRUCTURE	IDENTIFICATION OF DEFORMATION	MEASURED DEPTH OF DEFORMATION
Hadfield BW10	Austenite	Planar slip bands	> 200μm
Quatough	Martensite	Distortion of laths	< 5
316L stainless steel	Austenite	Planar slip bands	> 240
*Mild Steel	Ferrite/ pearlite	Distortion of anisotropic microstructure	> 100
* see Fig. 4.26			

Fig. 4.51 Deformation as measured by optical metallography.

From Fig. 4.51 it is clear that deformation is not confined to the surface but indeed extends to considerable depths below the worn surface and that detection, identification and subsequent measurement of deformation varies as a function of bulk microstructure. It is difficult to pin-point exactly where deformation terminates and where bulk material prevails, for even though slip lines may no longer be discernable, deformation may nevertheless extend further into the bulk material.

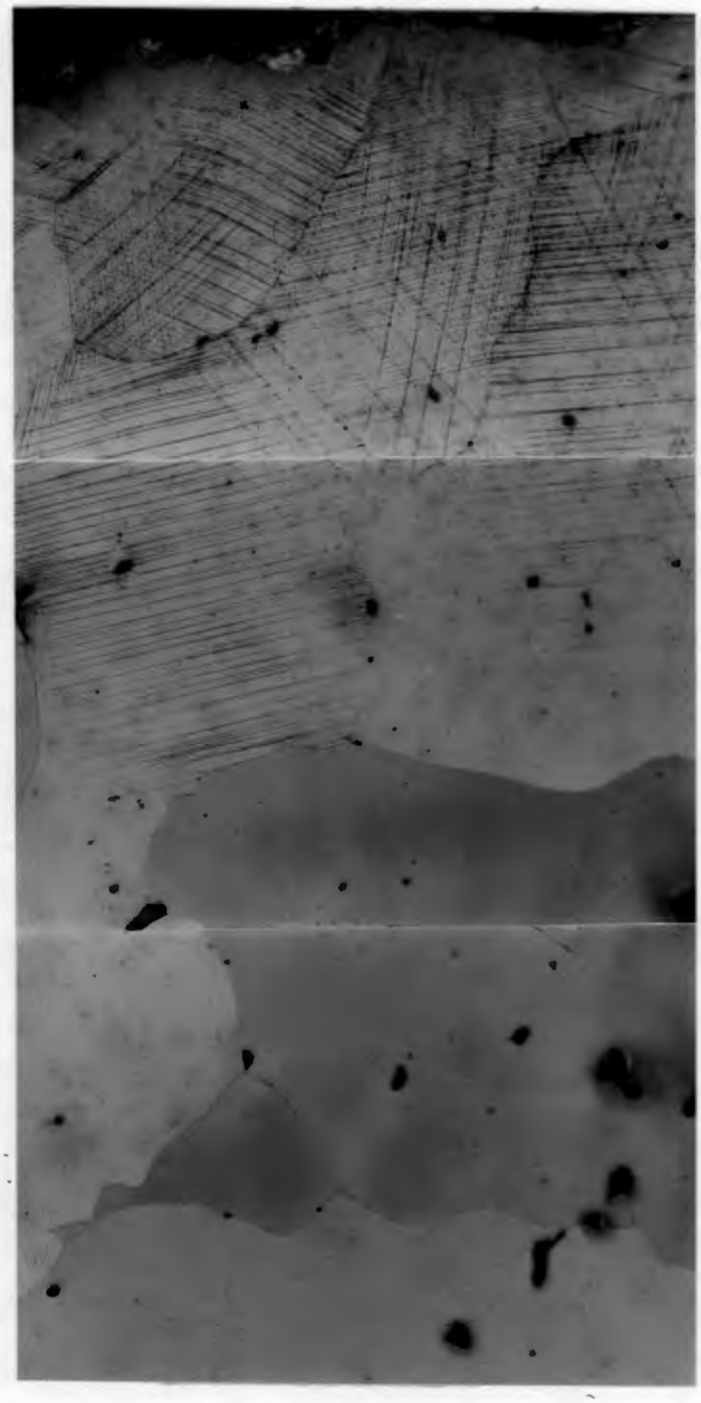

Fig. 4.52 The worn surface of Hadfield BW10 after *high stress* in-situ wear.

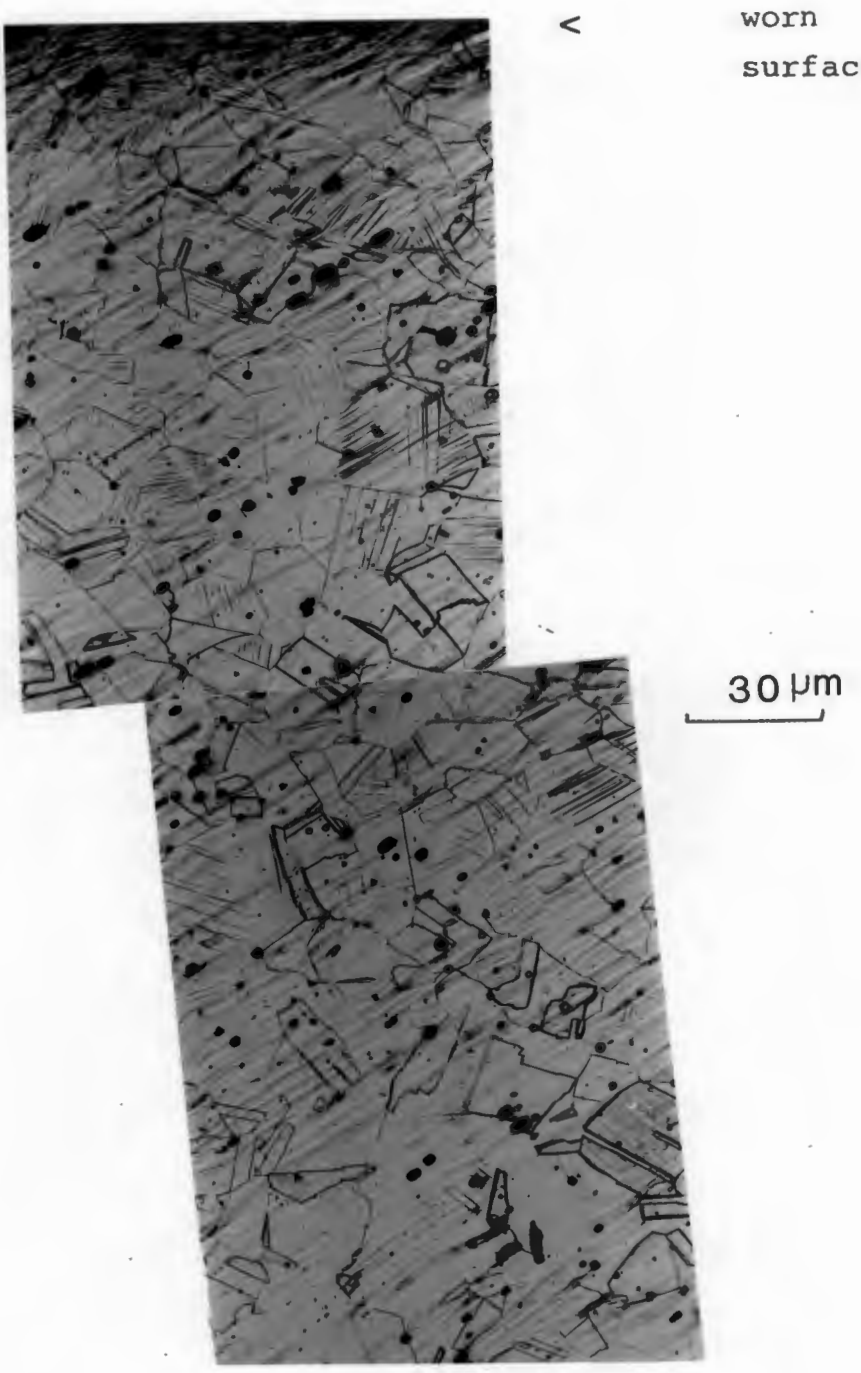

Fig. 4.53 The worn surface of 316L stainless steel after *high stress in-situ* wear.

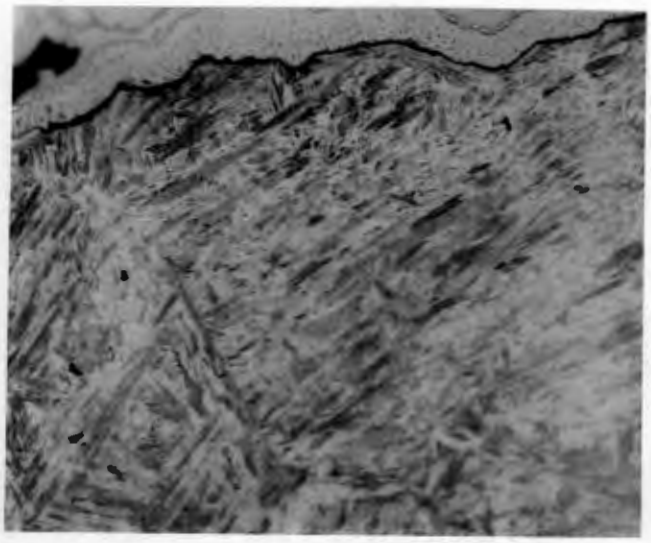

Fig. 4.54 The worn surface of Quatough after *high stress* laboratory wear.

4.4.3 Microstructural changes during abrasive wear

Foils prepared from the worn surface and from the bulk material of the following materials were studied in the transmission electron microscope (T.E.M.) in order to detect any microstructural changes, if any, brought about during the process of abrasive wear.

MATERIAL	BULK MICROSTRUCTURE	WEAR ENVIRONMENT
304L stainless steel	Austenite	Low stress - in-situ, i.e. shaker conveyor
316L stainless steel	Austenite	Low stress - in-situ, i.e. shaker conveyor
Wearalloy	Martensite	" "
Abrasalloy	"	" "
Quatough	"	Low stress - laboratory i.e. (68,6N load)
Hadfield Mn steel	Austenite	High stress - in-situ, i.e. reciprocating flight conveyor

It is apparent that distinction between the worn and unworn microstructures can be made;

(a) the dislocation density of 304L stainless steel and 316L stainless steel is greater on the abraded surface than on the unworn surface. (Fig. 4.55 and Fig. 4.56 respectively.) It is also noted that dislocations tangles are restricted to slip planes of particular orientations, e.g. Fig. 4.56 (a).

(b) stacking fault structures prevail on the abraded surface of 304L (Fig. 4.55 (c)); however their presence is limited to the worn material (Fig. 4.55 (b)). Stacking faults can be observed in both the worn and bulk regions of 316L (Fig. 4.56).

(c) the bulk microstructures of the proprietary wear resistant materials are composed of

dislocated and twinned lath martensite (Fig. 4.57 (b), Fig. 4.58 (b) and Fig. 4.59 (b)). This acicular martensite is still predominant on the worn surfaces of Wearalloy (Fig. 4.58(a)) and of Quatough (Fig. 4.59 (a)); however on the abraded surface of Abrasalloy (Fig. 4.57 (a)) re-organisation of the acicular laths and a decrease in dislocation density demonstrates that recovery and recrystallisation may have possibly occurred.

(d) A phase transformation to martensite of the austenitic Hadfield steel is thought to have occurred and evidence of martensite transformation is presented in Fig. 4.60 (a).

(a) wear surface (27000x)

(b) bulk structure (27000x)

(c) wear surface (41000x)

Fig. 4.55 T.E.M. micrographs of 304L stainless steel showing dislocation tangles and distribution of stacking fault structures - characteristic banded structures between partial dislocations.

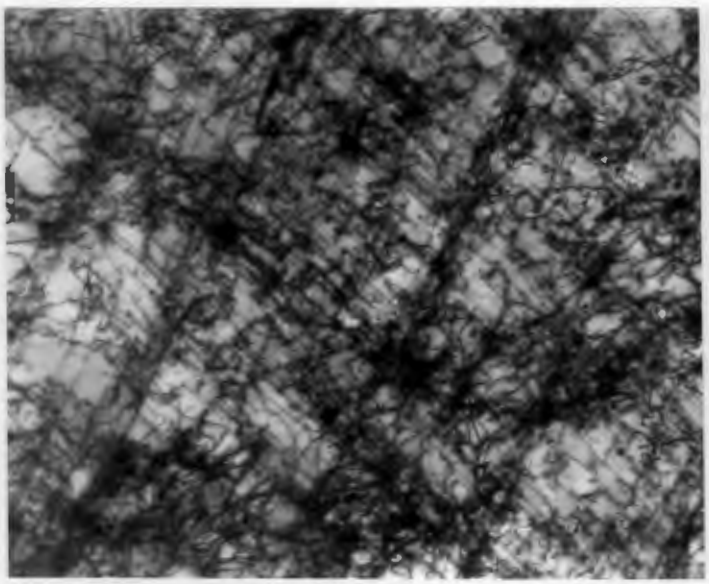

(a) wear surface (27000x)

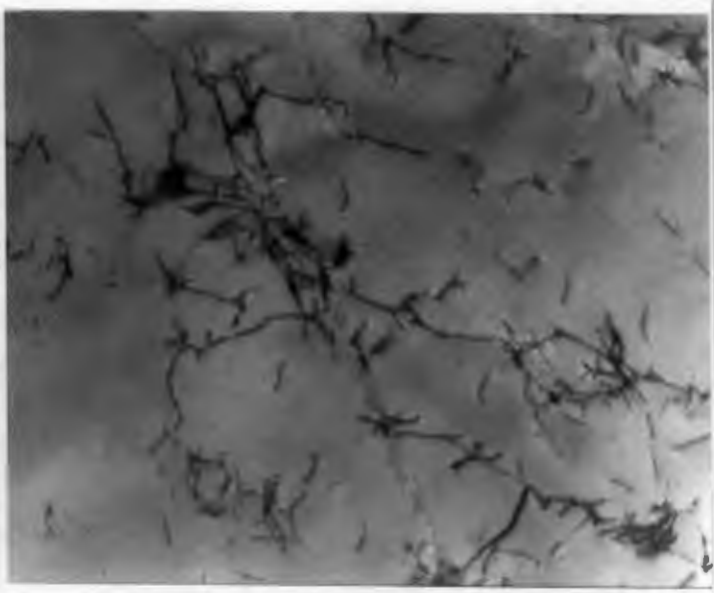

(b) bulk structure (27000x)

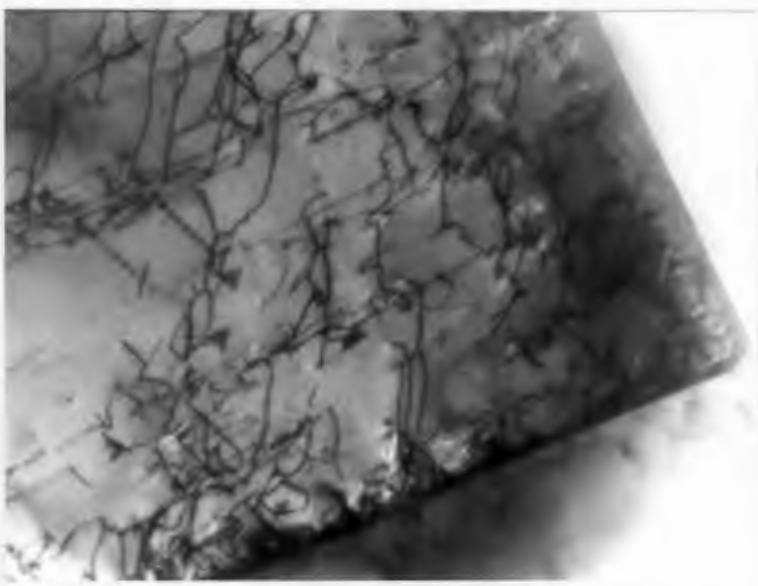

(c) low angle grain boundary - bulk structure (27000x)

Fig. 4.56 T.E.M. micrographs of 316L stainless steel showing dislocation interactions and stacking faults.

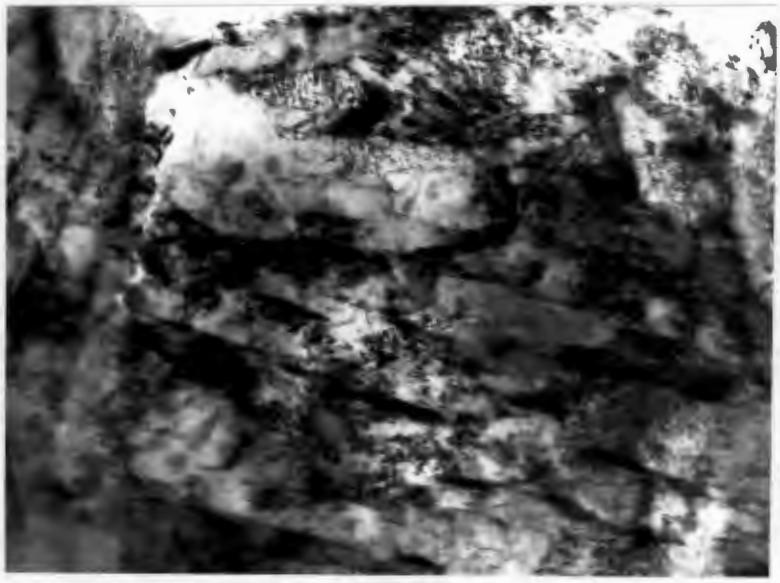

(a) wear surface (41000x)

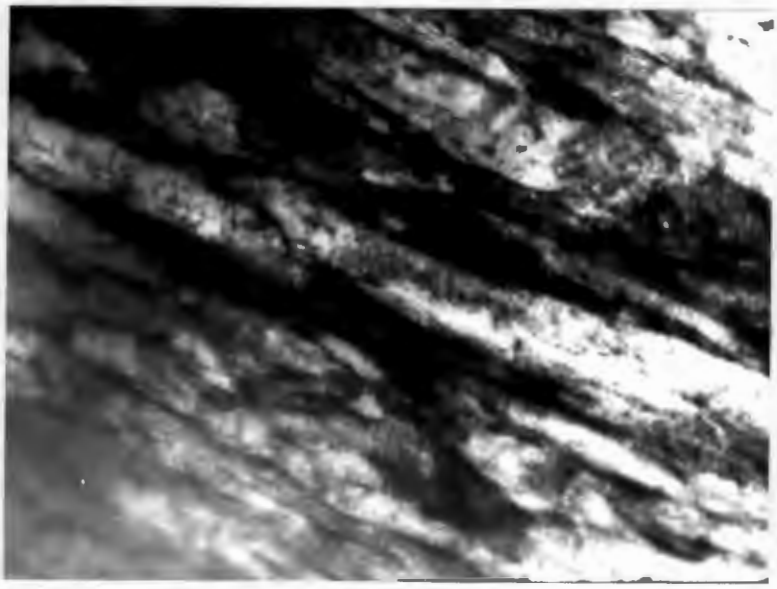

(b) bulk structure (20000x)

Fig. 4.57 T.E.M. micrographs of Abrasalloy - a martensitic proprietary wear resistant material, showing dislocated lath structure of martensite.

(a) wear surface (10000x)

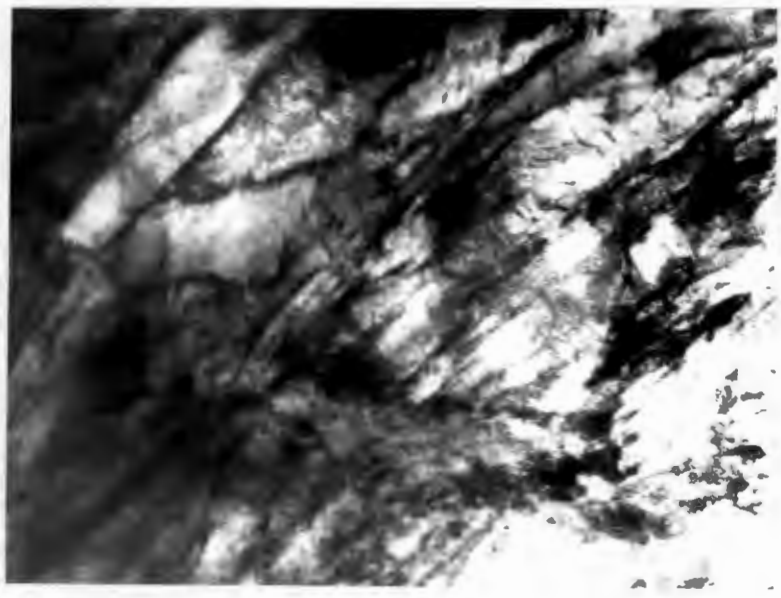

(b) bulk structure (20000x)

Fig. 4.58 T.E.M. micrographs Wearalloy, a martensitic proprietary wear resistant alloy showing internal twinning and dislocated lath martensite.

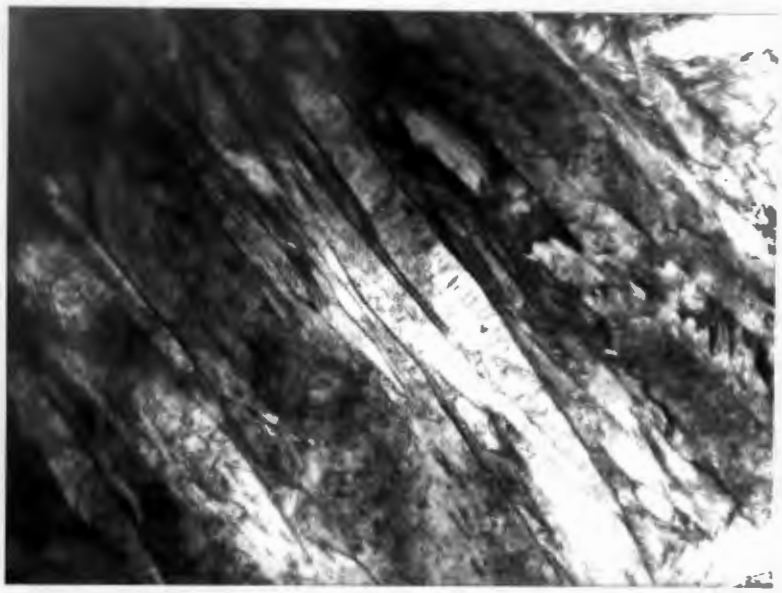

(a) Wear surface (14000x)

(b) Bulk structure (see Fig. 4.10)

Fig. 4.59 T.E.M. micrographs of Quatough. Inter-lath retained austenite is thought to exist within the martensitic microstructure of this proprietary wear resistant material.

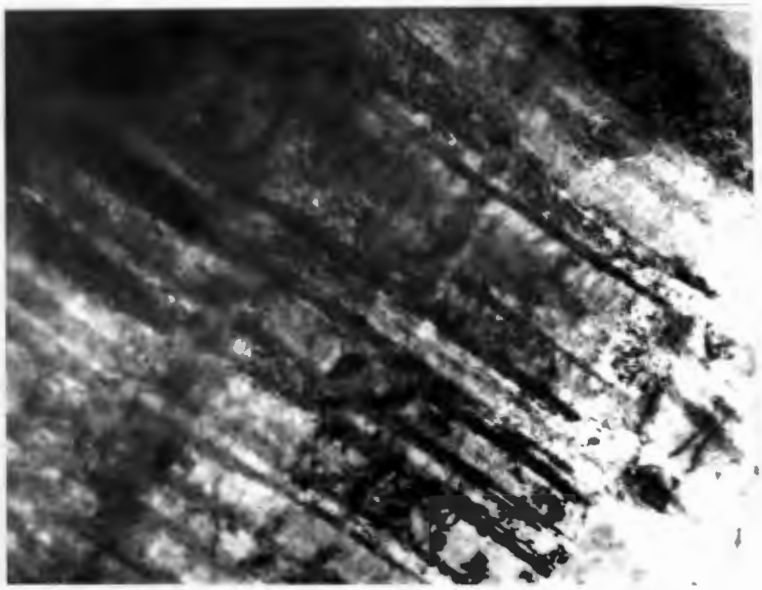

(a) Wear surface (50000x)

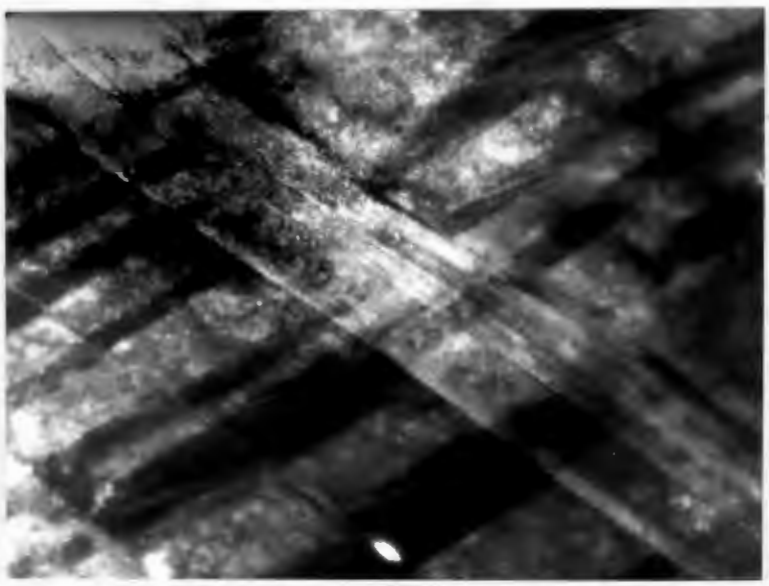

(b) Bulk structure (10000x)

Fig. 4.60 T.E.M. micrographs of austenitic Hadfield steel. Evidence of martensite nucleation and growth can be observed.

5.0 DISCUSSION

5.1 Optimising abrasion resistance via heat treatment.

Khruschov (41) found a linear relationship between wear resistance and bulk hardness for particular grades of steel which had been heat treated to different hardness levels. However, this relationship was not observed for the proprietary wear resistant materials i.e. Quatough and A-R-Col 360 (Fig. 4.5) which is in agreement with the findings of Mutton and Watson (58).

It is clear that wear resistance is not a function of hardness alone, as was previously envisaged (23, 41) but depends on a combination of many parameters including, microstructure (e.g. primary and secondary phases); mechanical properties (e.g. toughness and strength); and deformation characteristics (e.g. flow and fracture properties). Nevertheless, hardness is an important parameter when determining resistance to wear since it controls the depth of penetration of the abrading particles (14).

The superior abrasive and abrasive-corrosive wear resistance of Quatough compared to A-R-Col 360, as gauged by R.A.R. and laboratory R.W.R. values (Fig. 4.5), can be explained in terms of the greater bulk hardness, the greater tensile strength and the partial refinement of the martensitic microstructure of the former. Since hardness controls the depth of indentation of the abrasive and since hardness is a

function of the interstitial carbon which interferes with the passage of dislocations and thus impedes the process of plastic flow, then the superior performance of Quatough can be understood from chemical analyses data (Fig. 3.2) which show Quatough to have a higher carbon content than A-R-Col 360. However, it must again be stated that carbon content alone is not a criterion for abrasion resistance. It can also be argued that the greater notch toughness of A-R-Col 360 accounts for its lower wear resistance as there is little impedence to excessive plastic flow.

Salesky and Thomas (59) ascribe the predominantly superior behaviour of the grain refined and tempered iron- 4%chromium- 0,3%carbon- 2% manganese to be due to the presence of dislocated lath martensite with a fine interlath distribution of Widmanstätten cementite in association with interlath films of retained austenite. T.E.M. micrographs of Quatough (Fig. 4.10) provide evidence of this retained austenite within a martensitic matrix. For the singly heat treated condition of Quatough as opposed to the doubly heat treated condition, a 14 percent increase in retained austenite as measured by X.R.D. technique was correlated with a 20 percent increase in dry abrasion resistance and a 37 percent increase in wet abrasion resistance. Abrasion resistance is enhanced due to the presence of retained austenite which has a dual facility to transform to martensite on deformation while its inherent toughness has the ability to blunt crack propagation during abrasive wear. The excessive increase in abrasion-corrosion resistance is difficult to explain and further work in this direction is recommended. The increase in

retained austenite was found to benefit the V-notch toughness, which doubled, while the tensile strength also increased considerably. Bhat et al (47) found the presence of a higher amount of retained austenite to be beneficial under two body abrasive wear conditions. However for A-R-Col 360 the lowest wear rate did not necessarily correlate with the maximum volume fraction of retained austenite, nor with the maximum V-notch toughness, but with the maximum hardness. It is believed that the high cooling rate of A-R-Col 360, i.e. in the WQ 1050^{o}C condition, affects the microstructure through its influence on the carbon tent of the austenite. With slow cooling rates secondary carbides form and the austenite matrix becomes depleted in carbon. On the other hand, with fast cooling rates there is less time for diffusion which results in a higher dissolved carbon content and more retained austenite is present in the microstructure (15).

From a consideration of the S.E.M. micrographs of the proprietary wear resistant materials (Fig. 4.11 and 4.12) it is apparent that material removal during abrasive wear occurs via both ploughing and cutting mechanisms. It is also apparent that excessive plastic grooving is limited by the tensile strength of the displaced material, as seen in adjacent ridges, which form semi-detached wear chips which ultimately fracture to form wear debris particles (28).

Heat treatment of the initially pearlitic matrices of iron- 0,3%carbon- 0,7%manganese resulted in an increased rate of material removal or a decrease

in abrasion resistance as spheroidisation of the cementite is effected. As was noted by Moore (44), spheroidised annealed steels have lower wear resistances than pearlitic structures of the same composition. This reduction in wear resistance is accompanied with a decrease in hardness. For spheroidised iron- 1,2%carbon- 1,8%nickel the curve of abrasion resistance with tempering time (Fig. 4.13) shows a point of inflection. Wear resistance increases significantly with time then decreases after inflection. Prasad and Kulkarni (50) found this relationship to coincide with a coarsening of the dispersed particles and an increase in inter-carbide spacing up to a maxima while hardness progressively drops off.

On the left hand side of the point of inflection the combination of a fine dispersion of cementite and a partially saturated ferrite matrix give rise to a microstructure which is sufficiently strong to resist indentation by the abrasive and tough enough to resist crack initiation and propagation, while on the right hand side at extended spheroidising times the ferrite matrix becomes progressively softer, the dispersed particles become increasingly coarse and the strengthening effect continually diminishes. As seen in Fig. 4.16 material removal of spheroidised steels during abrasive wear occurs via the dual mechanism of preferential carbide stripping and ductile groove formation. Khruschov (41) and Allen et al (4) found that cold work prior to abrasion fails to increase the wear resistance of plain carbon steels and stainless steels respectively, although hardness increases considerably with the degree of cold deformation. Mild steel which had been

cold worked to yield a 30 percent increase in bulk hardness resulted in a 10 percent decrease in wear resistance relative to a normalised heat treatment of the identical steel. Reduced wear resistance due to prior cold work can be explained by considering the idealized stress-strain curves below (Fig. 5.1).

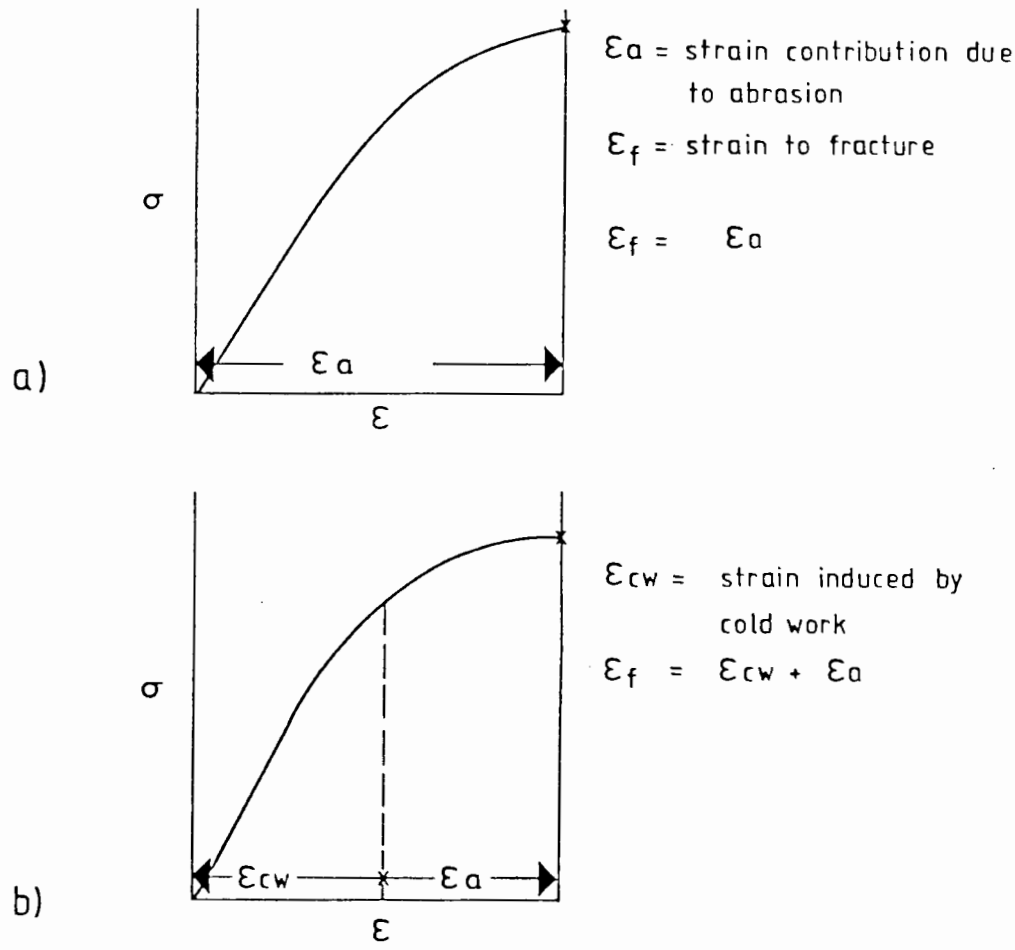

Fig. 5.1 Idealized stress-strain curves for a normalised (a) and cold worked (b) material subjected to abrasive wear.

By comparing the area under the curves the energy expended solely during abrasion of a normalized steel is clearly greater than that of a material which has been cold worked prior to abrasive wear. The strain accomodated during abrasion (ε_a) is reduced to the extent indicated in the diagram (Fig. 5.1 (b)). The effect of increased hardness of the cold worked specimen is offset by its now reduced ductility which explains its reduced wear resistance.

5.2 The effect of wear on surface topography

The accuracy of numerical measurements of surface profiles, when assessing wear of abraded materials, is limited to the extent of horizontal traverse, in this case only 3,8µm, which explains the systematically low C.L.A. values obtained for materials which have undergone *high stress* wear. Fig. 4.25 illustrates a more representative way of gauging the severity of surface deformation brought about by *high stress* wear. Nevertheless it is noticeable that as the severity of abrasive wear increases i.e. as the load on the abrasive particles increases (e.g. Abrasalloy Fig. 4.22), the surface relief or topography is enhanced via the deeper indentation or penetration of the abrading particles to cause extreme surface deformation.

Anomalously low C.L.A. values were measured on the surfaces of materials abraded during *high stress* wear which highlights the shortfalls of this profile measurement technique when trying to categorise the worn surfaces. Besides allowing one to readily

discriminate between the surface deformation profiles associated with *low* and *high* stress wear environments Fig. 4.25 also enables one to study the processes or mechanisms of abrasive wear. In conjunction with S.E.M. micrographs the primary mode of surface deformation can be identified as grooving. Two types of grooving have been outlined by Glaeser (60) i.e. macro-grooving and microgrooving (Fig. 5.2).

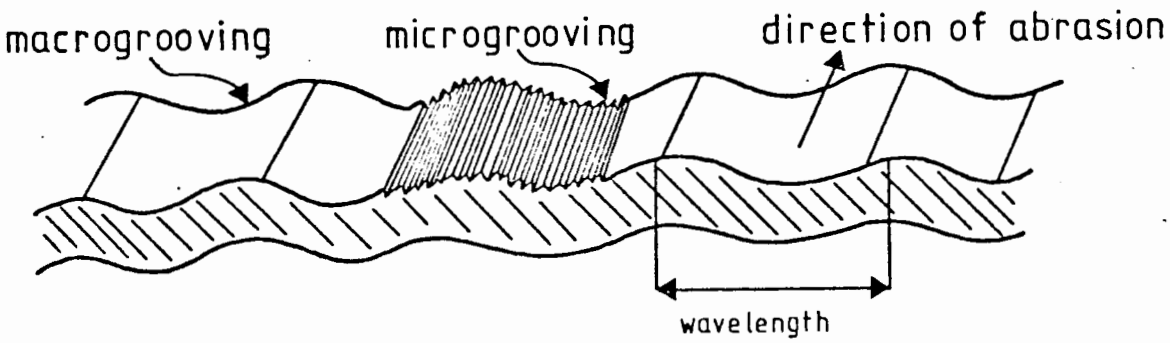

a) Low stress abrasive wear

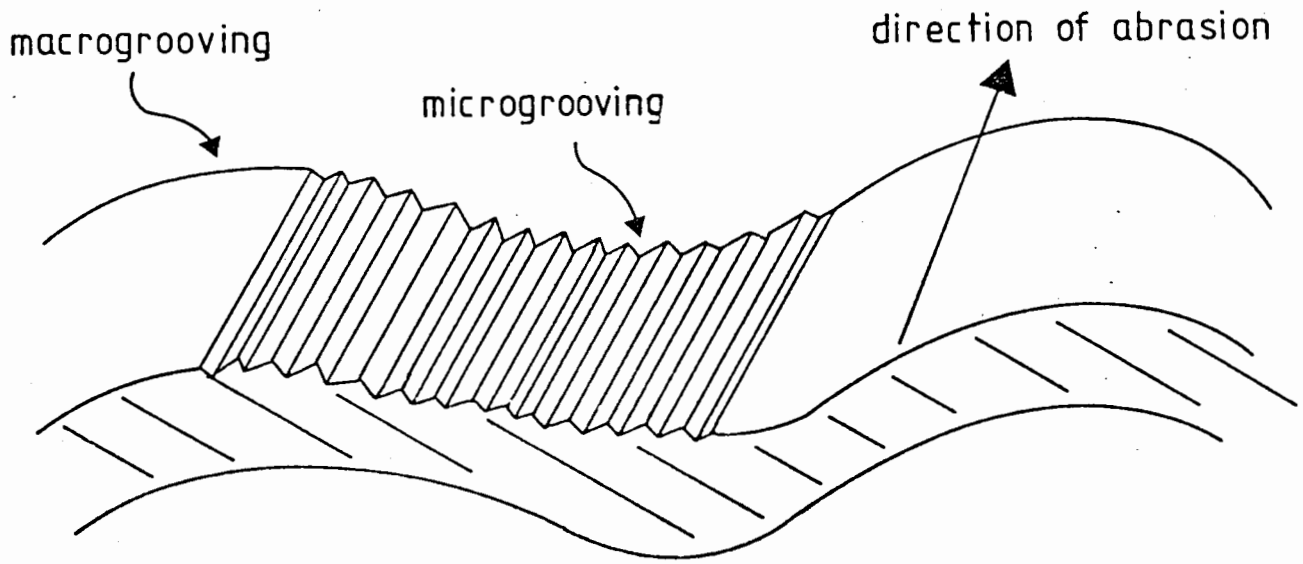

b) High stress abrasive wear

Fig. 5.2 Diagram illustrates modes of idealized groove formation.

The action of rigidly supported hard particles indenting and being forced to move across a softer metal surface results in macrogrooving. It is this type of deformation which causes waviness of the surface profile. Two extreme cases of groove formation have been proposed by Murray et al (8). The first case is ploughing or plastic grooving in which a prow is formed ahead of the abrading particles and material is continually displaced sideways to form ridges adjacent to the developing groove. Ideally no material is detached from the abraded surface. In the second case of macrogroove formation, metal is fully detached from the surface by a mechanism of cutting or micromachining.

Mulhearns and Samuels (26) proposed a model in which either complete ploughing or complete machining occurs depending on the effective rake angle of each individual abrading particle. Clearly a vast variation in rake angle is responsible for material removal in the laboratory and in-situ and hence mixed modes of deformation are responsible for material removal in practice.

The second aspect of groove formation is microgrooving or striation formation. Striations are generated by very small asperity contacts and are superimposed on the larger grooves in the wear surface area. Surface deformation during *low* and *high stress* wear is caused by micro- and macrogrooving parallel to the relative direction of movement of the abrading particles. However the degree of waviness and the profile amplitude of the worn surface is more exaggerated during *high stress* wear due to the

severe action of abrading particles. On successive passes of abrading particles other waves of large amplitude strike the contact area and deform the ridges produced by the initial contacts (60). These repetitive cycles of abrasion cause lateral extrusion of the flattened ridges to produce shear lips (Fig. 5.3) which tear off the side walls of the grooves to form semi-detached chips and wear debris particles.

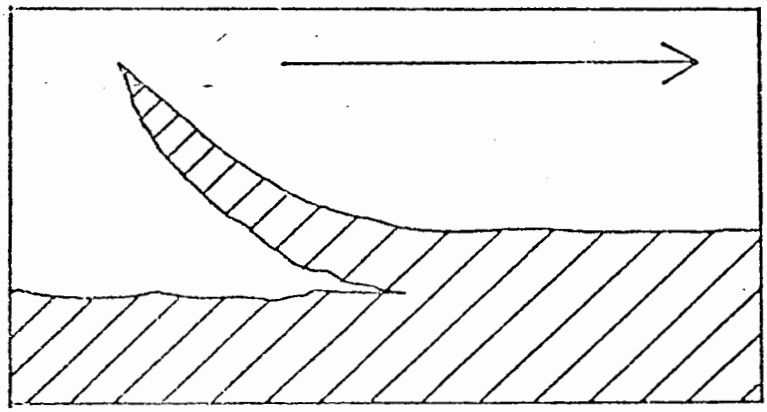

Fig. 5.3 Lateral extrusion of wear ridge. (Arrow indicates direction of abrasion) After Glaeser (60)

Microfracture is initiated due to material mismatch at the interface between the hard work hardened surface and the softer bulk undeformed microstructure.

Periodic spalling is fairly common to *low stress* dry and wet abrasive wear. The nature of these surface tears suggest a repeated spalling process in which prow adhesion stretches the surface until it tears and the prow slips to the next point of adhesion. It appears that a tensile fracture zone (t) at the

rear of each lip (ℓ) is coincident with the border of the next lip (Fig. 5.4).

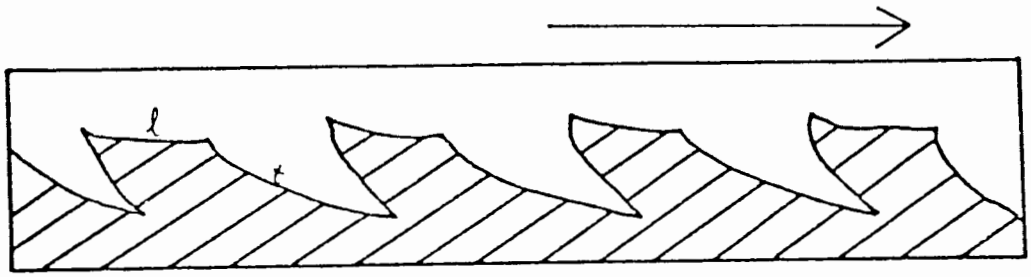

Fig. 5.4 A pictorial representation of surface damage due to abrasion showing transverse lips (ℓ) and tensile fracture zones (t). (Arrow indicates direction of abrasion.) After Glaeser (60)

This suggests a deformation process of tensile tearing and sub-surface shearing. A bulldozing process of abrasive wear appears to be primarily responsible for surface deformation encountered during underground *low stress* wear (Fig. 4.31 and 4.32). Material accumulates ahead of the abrading particle during prow formation and simulates a "bulldozing" action of material removal. Grooves are not parallel, as encountered during dry abrasive wear, but cross-flow delineates a multidirectional abrasive action.

Materials subjected to single scratch *high stress* wear exhibit a delaminated type wear mechanism (Fig. 4.35 and 4.37). Delaminated wear in conjunction with impact wear is also noticeable on the worn surface of materials which have undergone in-situ wear.

It is clear that although no single wear mechanism

is peculiar to a particular wear environment or to a particular material type, characteristic features can be observed. Wear is rarely a result of a single mechanism. There are situations where one type changes to another or where two or more mechanisms operate together (61). Dry laboratory abrasion results in unidirectional groove formation while in-situ wear surfaces exhibit cross-flow and evidence of impact abrasion as well. *Low stress* abrasion is characterized by repeated spalling and bulldozing type wear while *high stress* wear is characterized by severe delaminated type of abrasive wear process. It would be presumptuous to argue that changing the applied load on the abrasive demonstrates effects peculiar to the severity of abrasive wear, during *low stress* dry abrasion, however the experiment did demonstrate differing modes of material removal and further analysis of these results together with information obtained from microhardness, T.E.M. etc. could reveal distinct trends for various conditions of abrasion.

5.3 The limiting hardness of worn materials.

When the change in micro- and macro-indentation hardness results are compared (Fig. 5.5), it is apparent that microhardness data are consistently greater than those values obtained from macrohardness testing.

MATERIAL	MACROHARDNESS (ΔH %)		MICROHARDNESS (ΔH_M %)			
	Low stress In-situ	High stress In-situ	Low stress Laboratory	Low stress In-situ	High stress Laboratory	High stress In-situ
Mild Steel	-3	89	98	63	64	82
304L s/s	8	64	89	55	149	163
3CR12	8	31	48	19	56	38
Abras-alloy	0	12	169	76	236	32
Benox	4	36	24	21	46	62

Fig. 5.5 Percentage change in hardness of worn materials.

Apart from the effects of corrosion of in-situ specimens and experimental errors (e.g. vibration), the major difficulty in measuring low load micro-hardness is the avoidance of superficial strain during specimen preparation.

Fig. 5.6 explains the consistently low *macrohardness* values measured on the surfaces of materials worn during *low stress* wear.

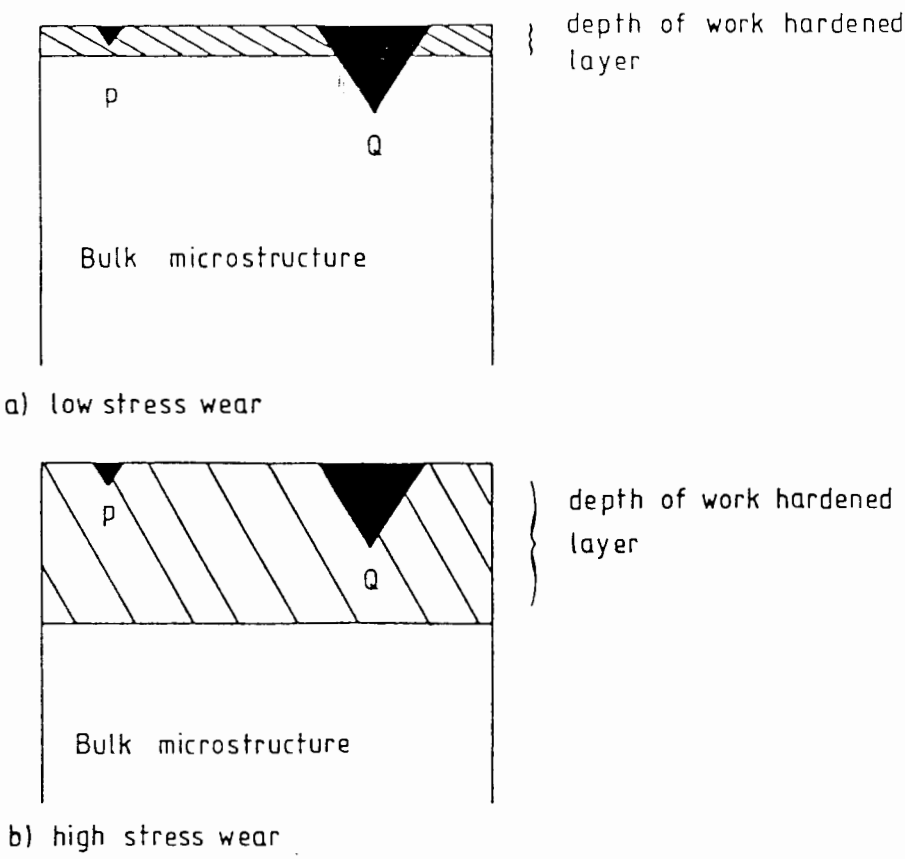

Fig. 5.6 Diagram to illustrate the difference in depth of indentation during micro-hardness (P) and macrohardness testing (Q).

Generally a shallow work hardened layer is generated during *low stress* wear with the result that the depth of indentation during macrohardness testing extends through this layer and penetrates the softer bulk material while microhardness testing is restricted to the hardened surface. On the other hand the depth of indentation during hardness testing, on the surfaces of materials worn during *high stress* abrasion, does not exceed the depth of the work hardened layer and macro- and microhardness results generally agree within experimental error.

Hardness is an important property for describing the contact surface between an abrasive particle and the surface of a material since the static penetration of an abrasive particle into a softer ductile surface is analogous to the process of hardness testing since both are a function of the resistance to local plastic flow (46). Due to the relative movement between the abrasive particles and the metal surface work hardening or strain hardening occurs. This results in an increase in hardness or strength due to excessive plastic deformation (62). Metals clearly are not uniform in their response to plastic deformation. Fig.4.47 shows the various degrees of hardening and also the depth to which hardening occurs.

Richardson (45) measured and plotted the maximum surface hardness, Hu, of a range of materials against relative wear resistance (Fig. 5.7).

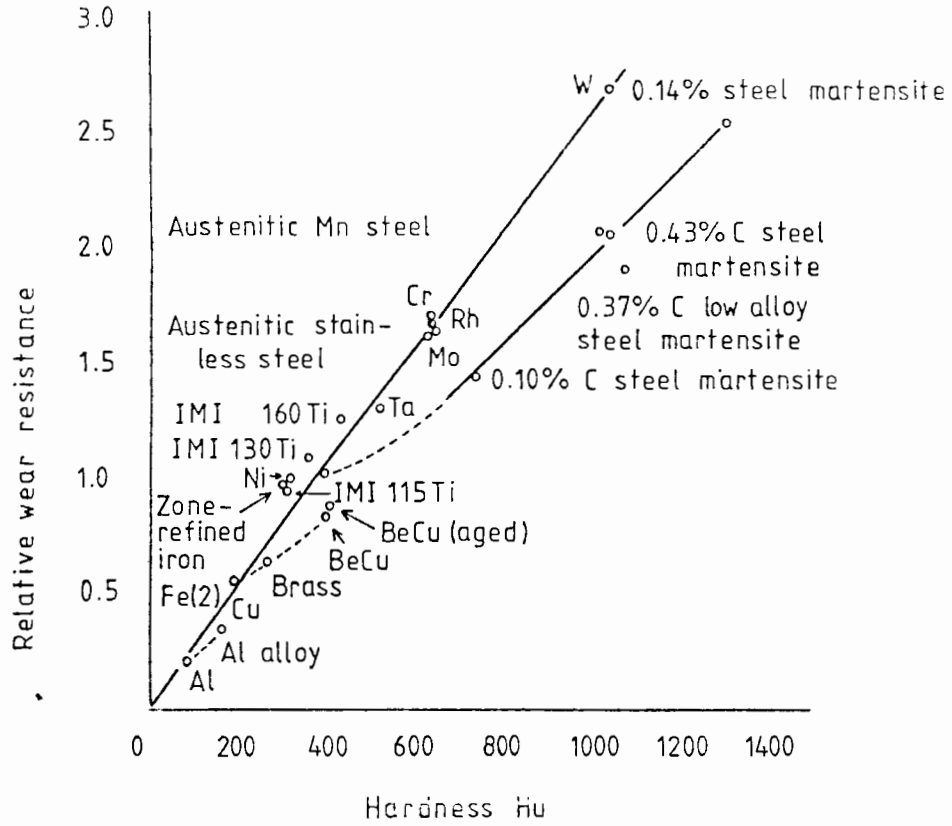

Fig. 5.7 Relative wear resistance on 180 grit corundum cloth as a function of maximum surface hardness (after Richardson (45)).

A proportional relationship between wear resistance and Hu can be observed for some metals, including the austenitic steels. However this trend does not exist for the martensitic materials which plot on the extreme right of the diagram. Richardson (45) postulates that this phenomenon must be due to differences in flow stress as well as to work hardening response. Allen et al (4) theorise that because the magnitude of stress generated in the worn surface regions must always be well in the excess of the yield strength, then the removal of material during wear cannot be combatted by temperate increases in yield strength of ferrous materials but by an improvement in the facility to accommodate the

high shear strains associated with abrasive wear. From S.E.M. micrographs e.g. Fig. 4.42, it is apparent that material is lost by fracture of the extruded shear lips formed adjacent to the wear grooves. The facility of these lips to accommodate high shear strains prior to fracture must be related to the resistance to unstable ductile fracture which is a function of the work hardening characteristics of the metal (4) via the equation $\sigma_t = K\varepsilon_t^n$ (63). Unstable deformation or necking will occur when the true strain (ε_t) equals the strain hardening exponent (n), (where K is the strength coefficient and σ_t is the true stress). McGregor Tegart (63) found n for f.c.c. materials to be greater than that for b.c.c. materials which explains the large degree of work hardening of the austenitic materials (Fig. 5.9).

Moore et al (37) studied the stress-strain system of a copper/silver solder laminate below the worn surface after trepanning wear. Flow stresses were calculated from microhardness data and the uniaxial strain was calculated from the shear angle of the silver solder leaves. Fig. 5.8 depicts this data when plotted against the depth below the worn surface.

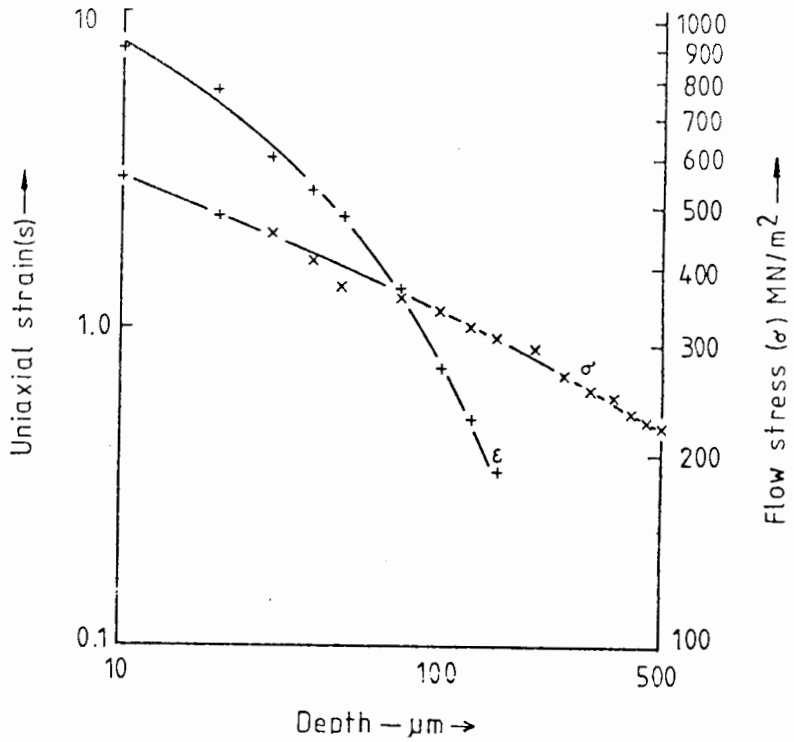

Fig. 5.8 Flow stress and uniaxial strain vs depth below the surface of a trepanned copper/silver solder laminate [after Moore et al (37)].

It can clearly be seen that the strain drops off sharply away from the worn surface and that the strain levels reached at the worn surfaces are extremely high compared to those reached under conventional deformation processes.

Fig. 5.9 shows a comparison of the limiting hardness of the strained surfaces of selected austenitic steels. It can be noted that the work hardened hardness of the strain surfaces of these materials approaches that of the wear resistant martensitic materials (e.g. Abrasalloy Fig. 4.47).

MATERIAL	ENVIRONMENT	MACROHARDNESS UNWORN SURFACE	MACROHARDNESS STRAINED SURFACE	LITERATURE
304 s/s (Iron-18%chromium-8%nickel)	Shaker conveyor	159	181	Author
	R.F.C.	140	230	Author
	Shot peened	158	450	Richardson (45)
	Worn in stony soil		503	
	Trepanned		647	
	Gouging jaw crusher test	165	377	Borik et al (42)
316 s/s (Iron-17%chromium-10%nickel)	Shaker conveyor	179	198	Author
	R.F.C.	170	312	"
	Gouging jaw crusher test	193	381	Borik et al (42)
Hadfield steel (Iron-12% - 14% manganese)	R.F.C.	178	467	Author
	Dry abrasive wear	325	650	Bauschke et al (46)
	Gouging jaw crusher test	199	461	Borik et al (42)

Fig. 5.9 A comparison of the maximum hardness of strained surfaces of 304 and 316 type stainless steels and of Hadfield steel.

What is also noticeable for 304 and 316 type stainless steels in particular, is that as the severity of wear increases so the maximum work hardened hardness increases (64), due to a greater degree of work hardening with associated increased surface deformation.

5.4 Depth of deformation

Depth of deformation studies are summarised in Fig. 5.10 below.

MATERIAL	TECHNIQUE OF DEPTH MEASUREMENT		
	MICROHARDNESS TRAVERSE	SPLIT SPECIMEN	POLISH AND ETCH
Mild Steel	78	130	> 100
Benox	63	90	
Abrasalloy	50	Not apparent	
Quatough	42		< 5
304L s/s	420	160	
316L s/s	-	300	> 240
Hadfield	83	330	> 200

Fig. 5.10 Depth of deformation of selected materials (in μm).

Austenitic materials in general and Hadfields steel in particular demonstrate excessive zones of sub-surface hardening. The depth of the work hardened layer of austenite Hadfield manganese steel as calculated from microhardness data, was found by Bauschke et al (46) and Borik et al (64) to be

approximately 165μm and 1000μm respectively. The depth of the work hardened layer is clearly a function of the severity of the wear medium, e.g. for the latter, extreme deformation was induced by high stress gouging wear in which the compressive strength of the rock was exceeded while the shallower work hardened layer was generated by low stress abrasion under a load of 4,95 MPa.

5.5 Structural alterations induced by abrasive wear

Martensitic transformations of 18% chromium - 8% nickel steels and other materials are well documented. Both hexagonal close packed (ε) and/or body centred cubic (α')martensite are transformed from a face centred cubic (γ) austenitic phase during the process of plastic deformation. It is believed that ε martensite is a transitional phase and constitutes preferred nucleation sites for α' martensite in the $\gamma \longrightarrow M$ transformation. The transformation between γ and ε is coherent since the close packed planes and directions in the two structures are parallel;

$$(111)_\gamma \;||\; (0001)_\varepsilon$$

$$\left[1\bar{1}0\right]_\gamma \;||\; \left[\bar{1}2\bar{1}0\right]_\varepsilon \quad \ldots \text{ after Brooks et al (65)}$$

Lagneborg (66) states that the ε phase is generated by movements of the $\frac{1}{6}\langle 112\rangle$ partials on every slip plane and that new hexagonal layers are added either by loops of partials or by movement of some partial

over several planes by the pole mechanism. Brooks et al (65) however found no evidence for a nucleation process involving a pole mechanism and that ε martensite is formed from randomly spaced overlapping faults in the active slip planes. Orientation relationships between γ austenite and the nucleating α' martensitic phase have been documented according to the Kurdjumov-Sachs relationship;

$$\text{i.e.} \quad (111)_\gamma \;||\; (110)\alpha'$$

$$\left[\bar{1}01\right]_\gamma \;||\; \left[\bar{1}11\right]_{\alpha'}$$

The defects associated with α' martensite nucleations consist of dislocation pile-ups on clearly spaced $(111)_\gamma$ planes.

Stacking fault energy (S.F.E.) influences the nature of dislocation networks in deformed metals. In materials with fairly low S.F.E.'s e.g. 304-type stainless steel (20 ergs cm^{-2} (35)) the dislocation interactions develop nodes in which stacking fault regions are apparent (Fig. 4.55(c)). These arise from the interaction of extended dislocations which, on combination give series of extended and contracted nodes where the dislocations are alternatively dissociated and associated (67). In these low S.F.E. materials e.g. 304L s/s, 316L s/s and Hadfield steel cross-slip is suppressed and planar deformation occurs. (Fig. 4.50; Fig. 4.53 and Fig. 4.52 respectively.) These dislocation interactions promote surface hardening effects (34). Suh et al (35) postulate that S.F.E. may effect wear through its influence on hardness, crack nucleation and crack propagation rates, however

wear resistance is not necessarily a simple function of S.F.E. alone. Substantial evidence, obtained from X.R.D. techniques, for strain induced martensite transformations of austenitic materials has been recorded by Allen et al (4) for various stainless steels, and by Filippov et al (49) and by Zum-Gahr (38) for Hadfield manganese steel respectively. Dislocation multiplication on preferential slip planes (Fig. 4.56 (a)) appear as evidence of martensite nucleation sites in 316L stainless steel. Bauschke et al (46) state that austenitic materials can be divided into two groups:

(a) alloys with M_d < room temperature i.e. austenite is stable under abrasive wear and is not transformed to martensite,

(b) alloys with M_d > room temperature >M_s i.e. austenite transformation is induced during wear; where M_d is defined by Lecroisey and Pineau (68) as the maximum temperature at which the $\gamma \longrightarrow \alpha'$ transformation can be induced during deformation and where M_s is defined as the temperature for spontaneous transformation. 316L s/s has a M_d temperature of $-20^{o}C$ and therefore transformation is somewhat surprising since the austenite of this material is categorically stable.

Various theories as to the mechanism of rapid work hardening of Hadfield manganese steel have been proposed. Work hardening can arise from
a) the strain induced transformation of γ to ε

and/or α' martensite b) fine twinning c) stacking fault - dislocation interactions and d) the interaction of dislocations with carbon atoms.

(a) and (b) can be observed in Fig. 4.60 (a) and Fig. 4.52 respectively. Dastur and Leslie (69) conclude however, that dynamic strain ageing is the principle cause of work hardening in Hadfield manganese steel due to the alignment of otherwise randomly oriented carbon-manganese couples in the strain fields of dislocations during work hardening.

When the bulk microstructure of unworn, unabraded materials is comprised of an inherently high dislocation density and high internal strain (e.g. in martensitic and in cold worked materials) then the facility to work harden and the capacity due absorb plastic strain via dislocation interactions during wear is considerably impaired. Dislocation interactions are affected by slip process so that body centred cubic and hexagonal e.g. ferritic and martensitic materials with limited slip systems would be expected to have lower degrees of strengthening than face centred cubic e.g. austenitic materials.

Moore (13) postulates that the unusual combination of high strain, high strain rate and transient temperature rises can lead to, among other things, strain softening, dynamic recovery and recrystallization. Increasing deformation reduces the temperature at which softening starts. Richardson (45) states that this effect might be exaggerated at

extremes of strain so that recovery and partial recrystallization would occur at room temperature thus set a limit on strength of the metal. Dynamic softening mechanisms may however result in improved wear resistance because the build-up of surface strain and the associated dislocation density may be reversed or retarded and thus provide an extended lifetime for the worn surface layers. The occurrence of such a recovery process will depend on the frictional heating characteristics of the particular material and on the abrasive conditions in relation to the melting point and phase stability. Materials could be selected and tested in order to verify this hypothesis.

5.6 Overview

During abrasive wear material removal from a worn surface occurs when a critical fracture strain criterion is experienced. This critical strain condition may be generated by a single abrasive strike or by a product of successive passes.

During groove formation plastic deformation is not confined to the surface but can extent to considerable depths due to work hardening, phase transformations and other strengthening mechanisms. A hydrostatic stress system is developed ahead of the abrading particle while behind the particle the stress is likely to be tensile. Because this hydrostatic stress opposes or suppresses ductile fracture processes, measured strain at the worn surface is extremely high.

Strain is imparted at an extremely high rate and conditions of pseudotriaxiality exist during abrasion; whilst deformation is dynamic in the sense that as material is lost at the achievement of the critical strain, then material a considerable distance below the worn surface will be at the point of plastically yielding (Fig. 5.11).

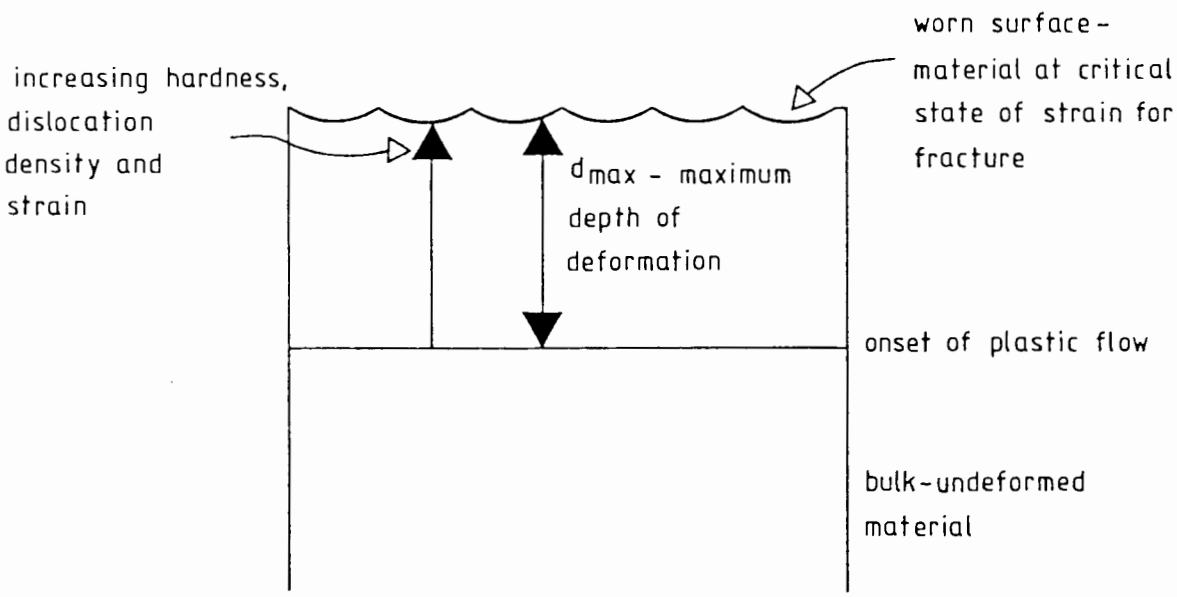

Fig. 5.11 Pictorial representation of a worn surface profile.

Considering a section through an abraded surface, dislocation density and strain, measurable as a function of microhardness, decreases with depth below the worn surface (Fig. 5.12). If one wishes to design an alloy to resist wear then attention must be given to providing a micro-structure which ideally never accumulates the

critical strain under a given abrasive stress.

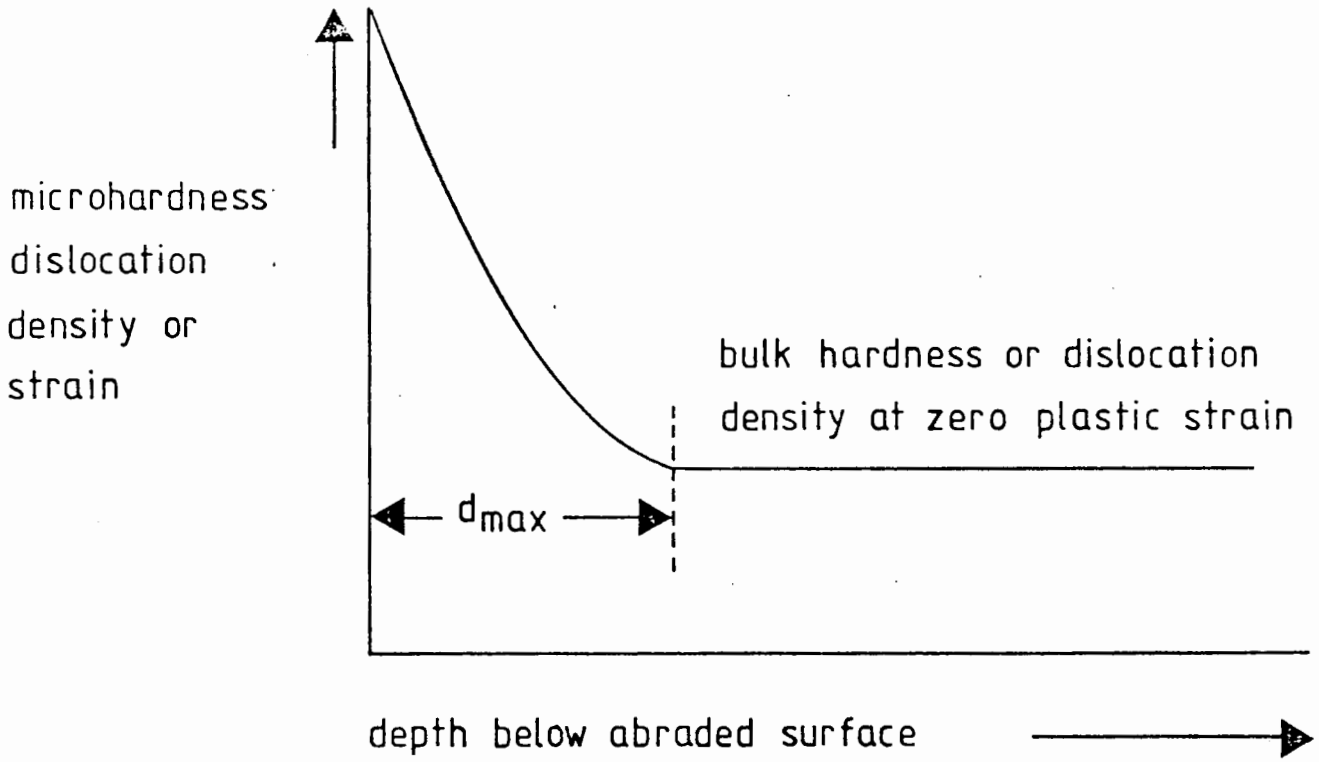

Fig. 5.12 Diagramatic representation of an abraded surface profile as obtained from microhardness traverses.

6.0 CONCLUSIONS

The main objectives of this investigation were;

(i) to continue to test and to evaluate materials presently used in the gold mining industry

(ii) to examine the surfaces of worn materials in order to gain a better understanding of the different wear mechanisms and also

(iii) to examine the extent and depth of deformation induced by abrasive wear.

6.1 *Low stress* dry and wet abrasion testing in the laboratory yielded the following useful results;

(a) the abrasive and abrasive-corrosive properties of the two proprietary wear resistant materials were found to be superior to mild steel.

(b) Quatough performed better than A-R-Col 360 in both the abrasive and abrasive-corrosive environments.

(c) Corrosion is the dominant factor controlling volume loss in the abrasive-corrosive environment. It accounts for about $^{2}/3$ of the total volume loss of ferrous materials while abrasion accounts for the remainder.

(d) Duplex microstructures consisting of dislocated lath martensite surrounded by continuous inter-lath films of retained austenite provide good wear resistance, strength and toughness.

(e) A spheroidising heat treatment can be utilized to optimize the abrasion resistance of 'Silver' Steel. Wear occurs via grooving and the preferential removal of a hard carbide fraction from a softer ductile matrix.

(f) Mild steel in the normalized heat treated condition provides superior abrasion resistance relative to mild steel which has been cold worked prior to abrasion.

6.2 Topographical, mechanical and microstructural studies were undertaken on the worn surfaces of selected materials. It was found that as the severity of wear increased i.e. as the nominal normal load on the abrasive increased, so too did the deformation become more pronounced in the following manner;

(a) exaggeration of topography: This is brought about by an increase in profile or surface roughness or due to a change in the mode of material removal. *Low stress* wear is characterized by repeated spalling and bulldozing wear while *high stress* wear is characterized by severe delaminated wear. Dry abrasion results in unidirectional groove formation while in-situ wear surfaces exhibit evidence of cross-flow and impact wear.

(b) Increase in surface hardness: The extent of surface hardening of austenitic materials

subjected to *low stress* wear is greatly increased when subjected to *high stress* wear. Ferritic and martensitic materials, albeit to a lesser degree, demonstrate the same trend.

(c) Increase in depth of deformation: Work hardening is not confined to the surface but can extend to considerable depths. The maximum depth of deformation induced by *high stress* wear in the laboratory and in-situ was found to be greater compared to low stress wear. Depth of work hardening increases as a function of microstructure from martensitic to ferritic to austenitic materials. Surface hardening is brought about via strain induced phase transformations in conjunction with other deformation mechanisms while recovery and recrystallization account for some surface softening phenomena.

REFERENCES

1. Mokken, A.H., "The viability of the gold mining industry in relation to the rational use of materials of construction and protection", Stainless Steel (Jan/Feb 1978) p. 29.

2. Joughin, N.C., "Potential for the mechanization of stoping in gold mines", Journal of the South African Institute of Mining and Metallurgy (January 1976) p. 285-300.

3. Joughin, N.C., "Progress in the development of mechanized stoping methods", Journal of the S.A. Inst. of Mining and Metallurgy (March 1978) p. 209.

4. Allen, C., Protheroe, B.E. and Ball, A., "The abrasive-corrosive wear of stainless steels", Proc. of Conf. on Wear of Materials, San Francisco (1981) p. 271.

5. Protheroe, B.E., "The causes of metallic wear in hard rock mining conditions with some solutions", Paper presented at Conf. on Fracture, Wits University (1979).

6. "Abrasive Wear 1965", Information Report Handbook Supplement - 1965, Published August 1966 by Society of Automotive Engineers Inc.

7. Archard, J.F. and Hirst, W., "The wear of metals under unlubricated conditions", Proc. Royal Society (London) A238 (1957) p. 401.

8. Murray, M.J., Mutton, P.J. and Watson, J.D., "Abrasive wear mechanisms in steels", Proc. Conf. on wear of Materials, Dearborn, Michigan (April 1979) p. 257-264.

9. Hurricks, P.L., "Some metallurgical factors controlling the adhesive and abrasive wear resistance of steels. A review", Wear, 26 (1973) p. 287.

10. Thomas, C.R., "3CR12 a material for abrasion/ corrosion control", Colloquium on Wear and Abrasion in Industry, Johannesburg (April 1981) p. 2.

11. Avery, H.S., "Fundamentals of abrasion", Materials Selection for the Mining Industry TMS-AIME (March 1977) p. 17-18.

12. Moore, M.A., "A review of two-body abrasive wear", Wear, 27 (1974) p. 78-89.

13. Moore, M.A., "Abrasive wear", American Society of Metals - Materials Science Seminar on Fundamentals of Friction and Wear of Materials (1980) p. 4 - 37.

14. Moore, M.A. and King, F.S., "Abrasive wear of brittle solids", Proc. of Conf. on Wear of Materials, Dearborn, Michigan (April 1979) p. 28.

15. Gundlach, R.B. and Parks, J.L., "Influence of abrasive hardness on the wear resistance of high chromium irons", Wear 46 (1978) p. 104.

16. Zum Gahr, K.-H. and Eldis, G.T., "Abrasive wear of white cast irons", Wear 64 (1980) p. 181.

17. Larsen-Badse, J., "Influence of grit diameter and specimen size on wear during sliding abrasion", Wear, 12 (1968) p. 38-39.

18. Larsen-Badse, J. and Tanouye, P.A., "Strain rate effects in low speed two-body abrasion", Journal of Lubrication Technology, 100 (April 1978) p. 182.

19. Misra, A., and Finnie, I., "On the size effect in abrasive and erosive wear", Wear, 65 p. 361-365.

20. Dean, S.K. and Doyle, E.D., "Significance of grit morphology in fine abrasion", Wear, 35 (1975) p. 128.

21. Moore, M.A., "Abrasive wear", Materials in Engineering Applications, 1 (Dec 1978) p. 97-109.

22. Richardson, R.C.D., "The wear of metals by hard abrasives", Wear, 10 (1967) p. 303.

23. Khruschov, M.M., "Principles of abrasive wear", Wear, 28 (1974) p. 71-87.

24. Noël, R.E.J., "The abrasive-corrosive wear of metals", M.Sc. Thesis 1981, p. 41-128.

25. Fogel, G., "The influence of microstructure on abrasive wear", M.Sc., Thesis 1981, p. 120-122.

26. Mulhearn, T.O. and Samuels, L.E., "The abrasion of metals: A model of the process", Wear, 5 (1962) p. 478-497.

27. Graham, D. and Baul, R.M., "An investigation into the mode of metal removal in the grinding process", Wear, 19 (1972) p. 301-313.

28. Spurr, R.T., "The abrasive wear of metals", Wear, 65 (1981) p. 315-324.

29. Suh, N.P. and Sridharan, P., "Relationship between the coefficient of friction and the wear rate of Metals", Wear, 34 (1975) p. 291-299.

30. Suh, N.P., "The delamination theory of wear", Wear, 25 (1973) p. 111-124.

31. Rigney, D.A. and Hirth, J.P., "Plastic deformation and sliding fraction of metals", Wear, 53 (1979) p. 345-370.

32. Torrance, A.A., "A new approach to the mechanics of abrasive", Wear, 67 (1981) p. 233-257.

33. Suh, N.P., "An overview of the delamination theory of wear", Wear, 44 (1977) p. 1-16.

34. Hirth, J.P. and Rigney, D.A., "Crystal plasticity and the delamination theory of wear", Wear, 39 (1976) p. 133-141.

35. Suh, N.P. and Saka, N., "The stacking fault energy and delamination wear of single phase f.c.c. metals", Wear, 44 (1977) p. 135-143.

36. Suh, N.P., Saka, N. and Jahanmir, S., "Implications of the delamination theory on wear minimization", Wear, 44 (1977) p. 127-134.

37. Moore, M.A., Richardson, R.C.D. and Attwood, D.G., "The limiting strength of worn metal surfaces", Metallurgical Transactions, 3 (1972) p. 2485-2490.

38. Zum Gahr, K.-H., "Formation of wear debris by the abrasion of ductile metals", Wear, 74 (1981-1982) p. 353-373.

39. Rigney, D.A. and Glaeser, W.A., "The significance of near surface microstructure in the wear process", Wear, 46 (1978) p. 246.

40. Larsen-Badse, J., "The abrasion resistance of some hardened and tempered carbon steels", Transaction AIME, 26 (1966) p. 1461 - 1466.

41. Kruschov, M.M., "Resistance of metals to wear by abrasion, as related to hardness", Proc. Conf. on Lubrication and Wear 1957. Institute of Mechanical Engineers London (1957) p. 655 - 659.

42. Borik, F. and Scholz, W.G., "Gouging abrasion test for materials used in ore and rock crushing: Part II - Effect of metallurgical variables on gouging wear", Journal of Materials JMLSA, 6, No. 3 (September 1971) p. 590 - 605.

43. Silence, W.L., "Effect of structure on wear resistance of Co-, Fe-, and Ni - base alloys", Proc. Conf. on Wear of Materials 1977, St. Louis, Missouri (April 1977) p. 77 - 84.

44. Moore, M.A., "The relationship between the abrasive wear resistance, hardness and microstructure of ferritic materials", Wear 28 (1974) p. 59 - 67.

45. Richardson, R.C.D., "The maximum hardness of strained surfaces and the abrasive wear of metals and alloys", Wear 10 (1967) p. 361 - 380.

46. Bauschke, H.-M., Hornogen, E. and Zum Gahr, K.-H., "Abrasive wear of austenitic steels", Z. Metallkde, 72 (1981) p. 1 - 8.

47. Bhat, M.S., Zackay, V.F. and Parker, E.R., "Alloy design for abrasive wear", Proc. Conf. on Wear of Materials 1979, ASME, Dearborn, Michigan (April 1979) p. 286 - 290.

48. Gahr, K.-H., "Relation between abrasive wear rate and the microstructure of metals", Proc. Conf. on Wear of Materials 1979. ASME, Dearborn, Michigan (April 1979) p. 268 - 272.

49. Filippov, M.A., Zil'bershtein, R.A. and Lugovykh,V.E., "Phase transformation and hardening of unstable austenitic steels in plastic deformation and impact action", Met. Sci. Heat Treat. (U.S.S.R.), 23, No. 8-9 (September 1981) p. 640 - 643.

50. Prasad, N. and Kulkarni, S.D., "Relation between microstructure and abrasive wear of plain carbon steels", Wear 63 (1980) p. 329 - 338.

51. Filippov, L.T. and Gol'dshtein, Y.E., "Effect of composition and structure on the wear resistance of steels during abrasive wear", Met. Sci. Heat Treat., 21 no. 1 - 2 (July 1979) p. 90.

52. Zackay, V.F., Parker, E.R. and Wood, W.E., "Influence of some microstructural features on the fracture toughness of high strength steels", Proc. of Third Int. Conf. on the Strength of Metals and Alloys. Vol. 1. Cambridge, England (August 1973) p. 176 - 179.

53. Salesky, W.J., "Sliding wear, toughness and microstructural relationships in high strength Fe/Cr/C experimental steels", M.Sc. Thesis (1980) p. 1 - 25.

54. "New alloy to combat corrosion", Coal, Gold and base minerals of South Africa (January 1981) p. 55 - 61.

55. Steingerwald, R.F., "Corrosion principles for the mining engineer", Climax Moly. Company Materials for the Mining Industry (1974) p. 93 - 101.

56. Van Vlack, L.H., "Materials Science for Engineers", (1970) p. 465.

57. Scarr, A.J.T., "Metrology and Precision Engineering", 1967.

58. Mutton, P.J. and Watson, J.D., "Some effects of microstructure on the abrasion resistance of metals", Wear 48 (1978) p. 385 - 398.

59. Salesky, W.J. and Thomas, G., "Medium carbon steel alloy design for wear applications", Wear 75 (1982) p. 21 - 40.

60. Glaeser, W.A., "Wear experiments in the scanning electron microscope", Wear 73 (1981) p. 371 - 386.

61. Eyre, T.S., "The mechanisms of wear", Tribology International (April 1978) p. 91.

62. Avery, H.S., "Work hardening in relation to abrasion resistance", Symposium on Materials for the Mining Industry Vail, Colorado (1974) Editor Barr, R.Q.

63. McGregor Tegart, W.J., "Elements of mechanical metallurgy", Macmillan Series in Materials Science, New York (1966) p. 17.

64. Borik, F. and Sponseller, D.L., "Gouging abrasion test for materials used in ore and rock crushing: Part 1 - Description of test", Journal of Materials, JMLSA, Vol. 6, No. 3 (September 1971) p. 586.

65. Brooks, J.W., Loretto, M.H. and Smallman, R.E., "In-situ observations of the formation of martensite in stainless steel", Acta Met., 27 (1979) p. 1829.

66. Lagneborg, R., "The martensite transformation in 18% Cr - 8% Ni steels", Acta Met., 12 (July 1964) p. 828.

67. Honeycombe, R.W.K., "The plastic deformation of metals", (1968).

68. Lecroisey, F. and Pineau, A., "Martensitic transformations induced by plastic deformation in the Fe - Ni - Cr - C system", Metallurgical Transactions, 3 (February 1972) p. 388.

69. Dastur, Y.N. and Leslie, W.C., "The mechanism of rapid work hardening in Hadfield manganese steel", Proceedings 5th Internal Conference on Strength of Metals and Alloys (August 1979), Editors Gerald, V. and Kostorz, G.

APPENDIX A

MICROHARDNESS TRAVERSE DATA

MATERIAL : MILD STEEL
NORMAL LOAD : 68,6 N
TAPER : 5°
ENVIRON: LABORATORY - LOW STRESS

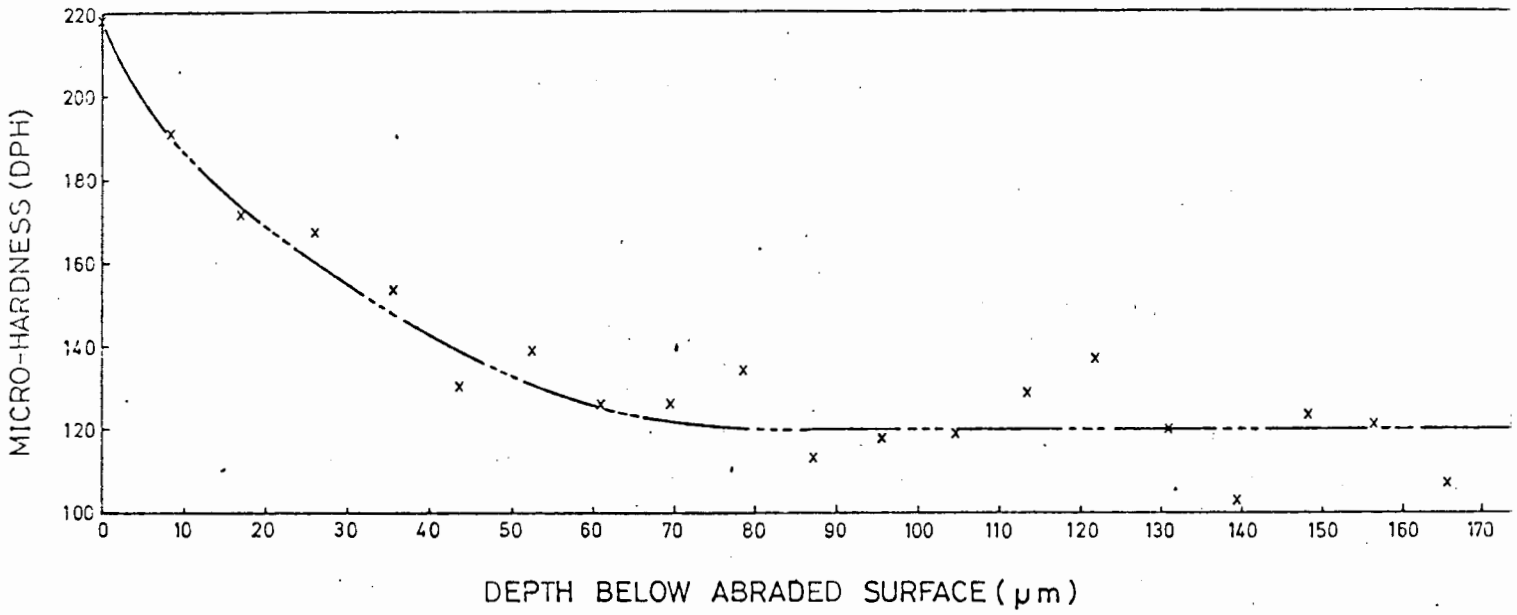

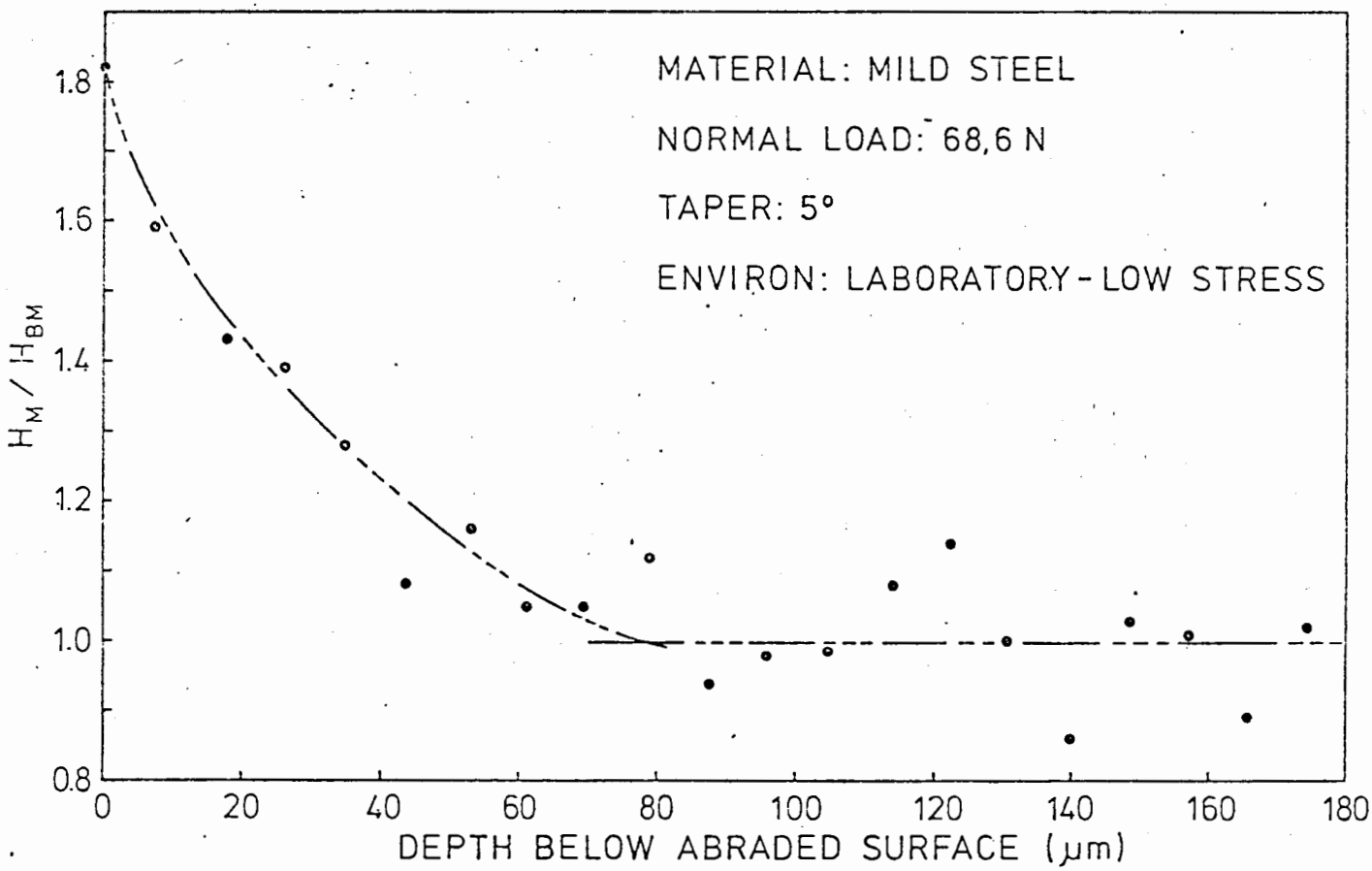

MATERIAL : AISI 304 L
NORMAL LOAD : 68,6 N
TAPER : 2°& 5°
ENVIRON: LABORATORY-LOW STRESS

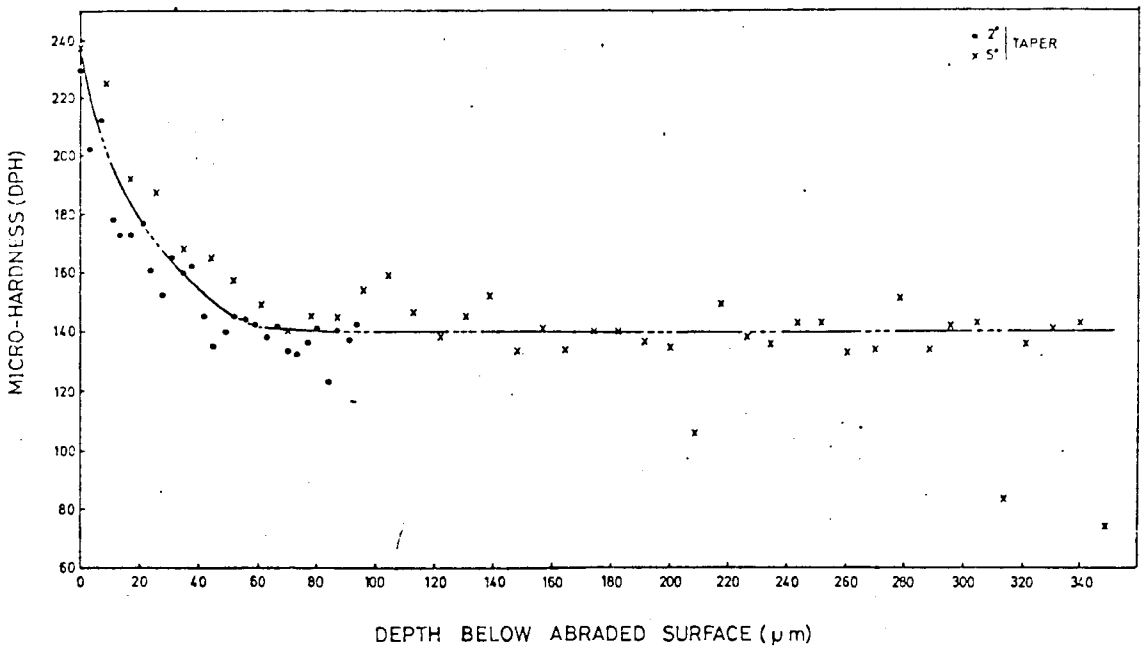

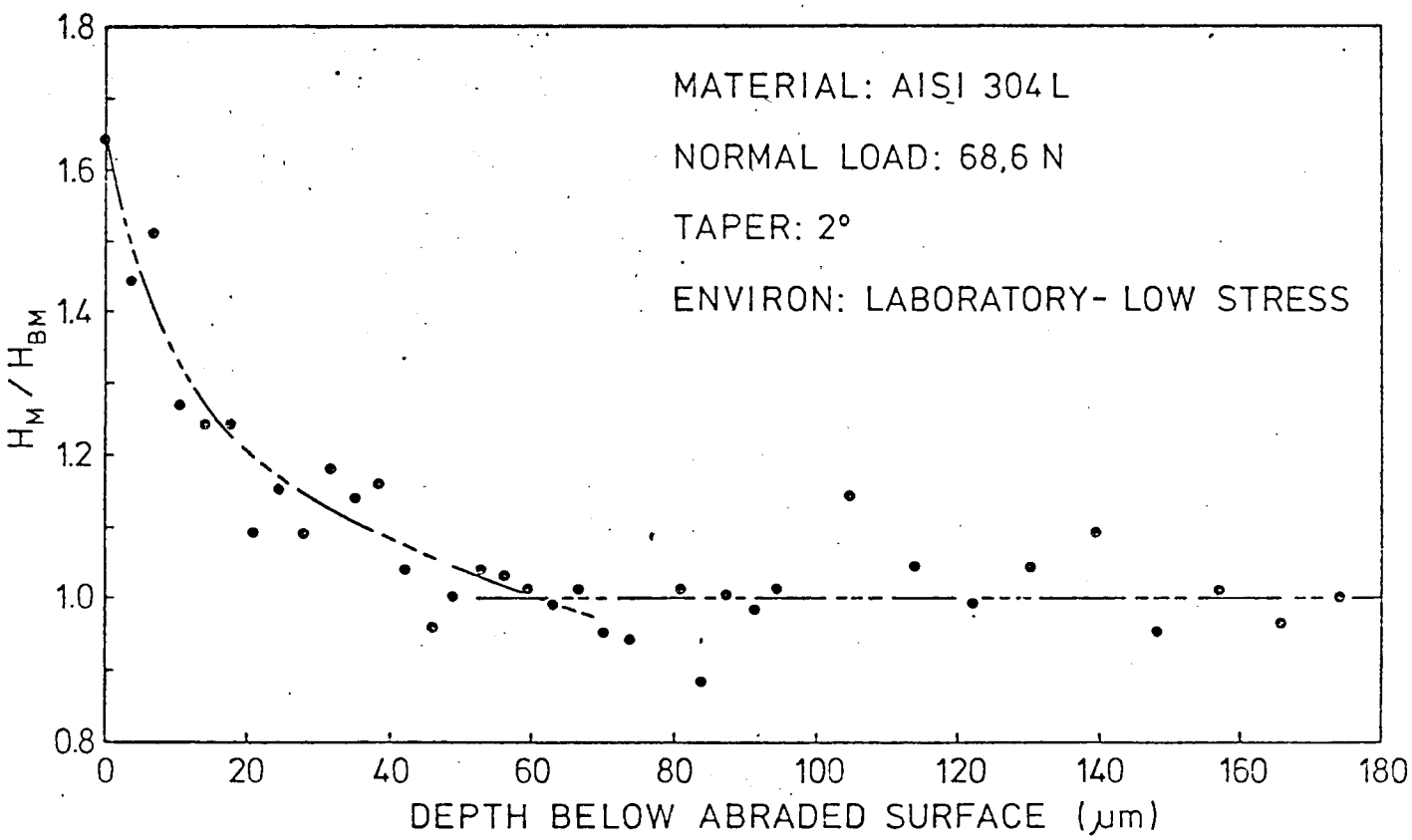

MATERIAL : ABRASALLOY
NORMAL LOAD : 68,6 N
TAPER : 2°
ENVIRON: LABORATORY - LOW STRESS

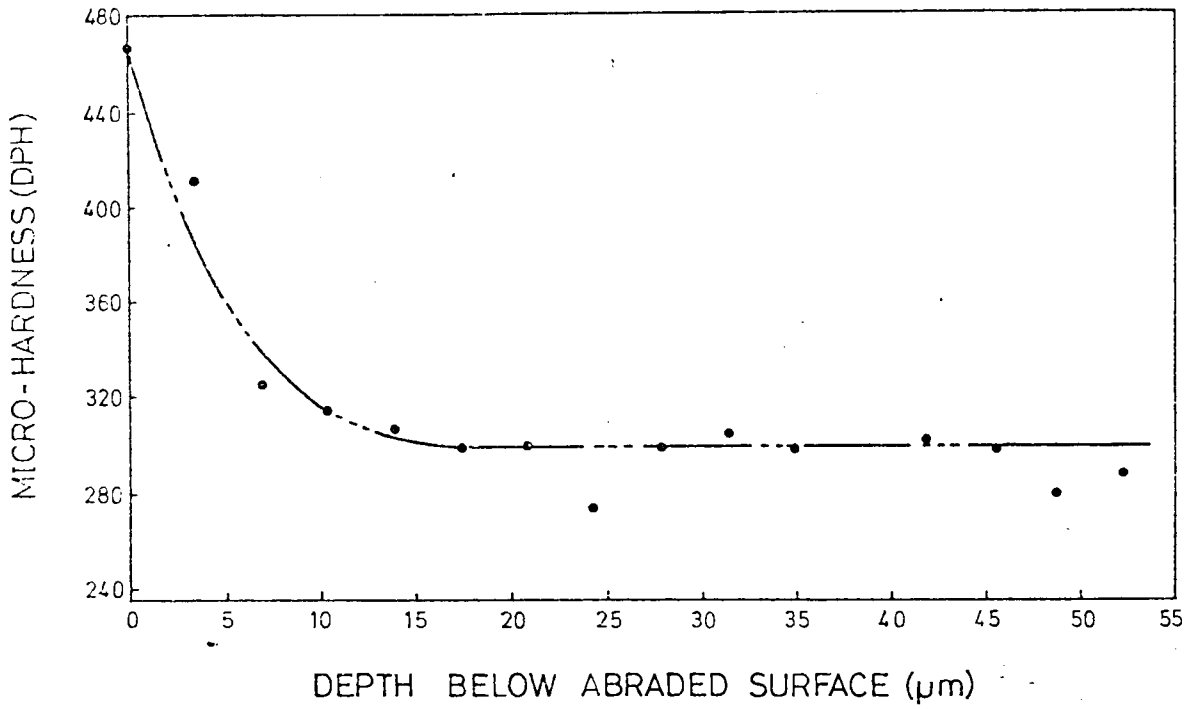

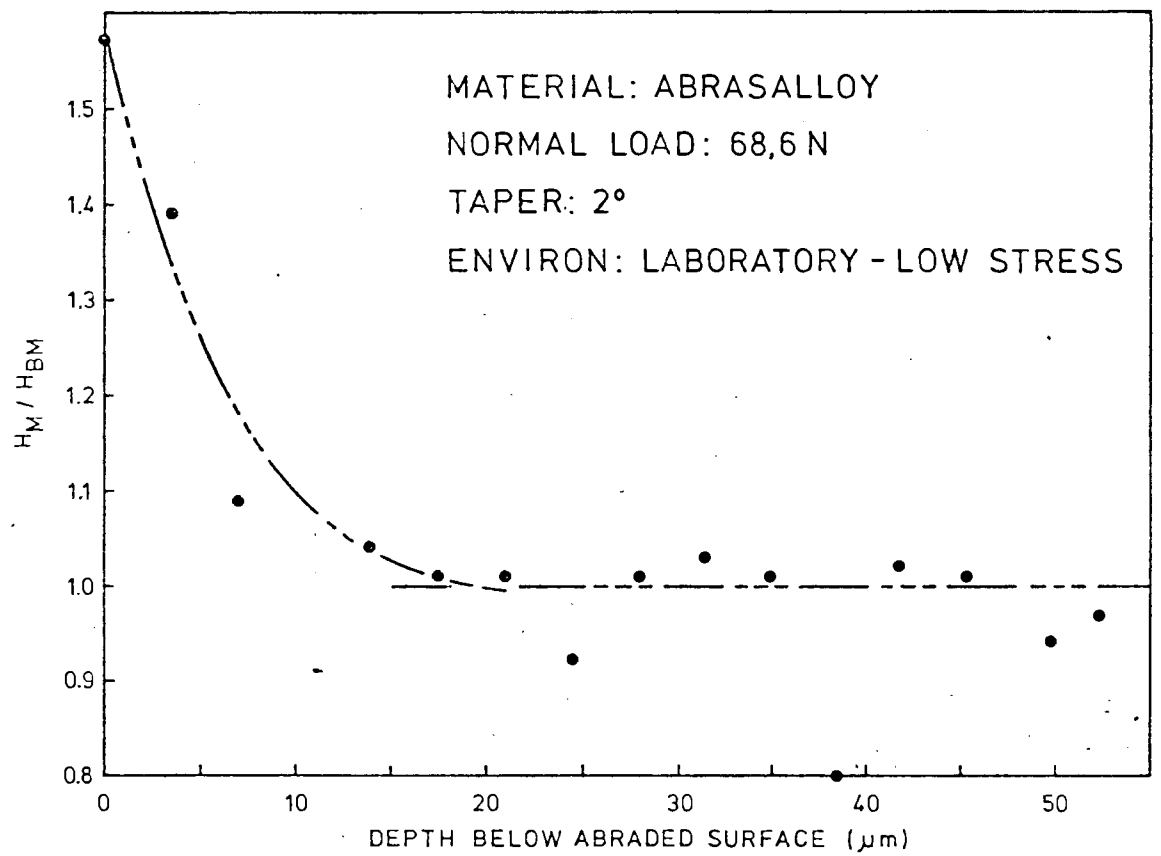

MATERIAL : QUATOUGH
NORMAL LOAD : 68,6 N
TAPER : 2°
ENVIRON: LABORATORY - LOW STRESS

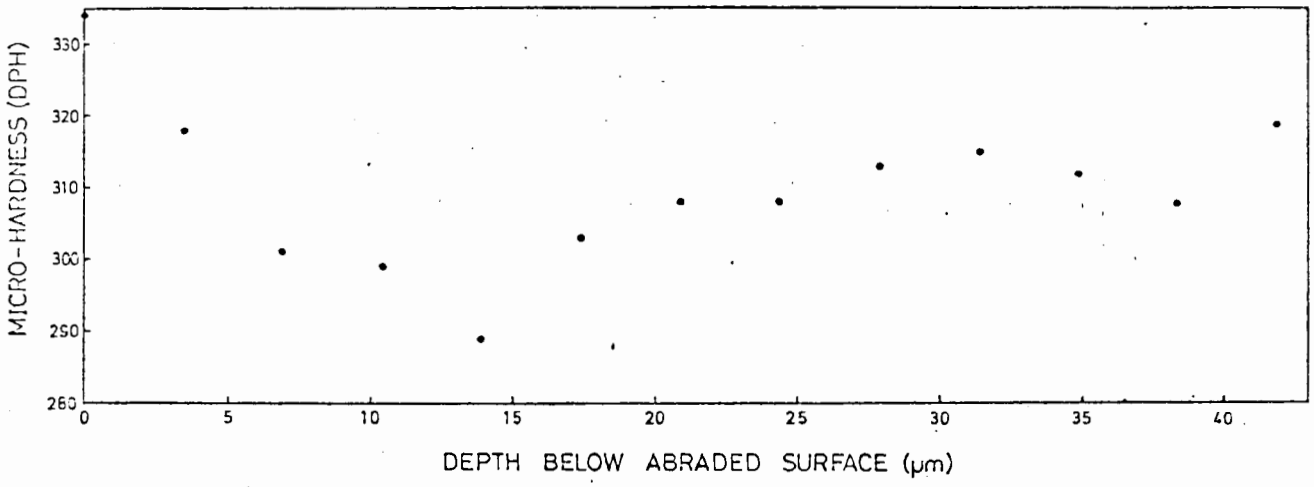

MATERIAL: QUATOUGH
NORMAL LOAD: 68,6 N
TAPER: 2°
ENVIRON: LABORATORY- LOW STRESS

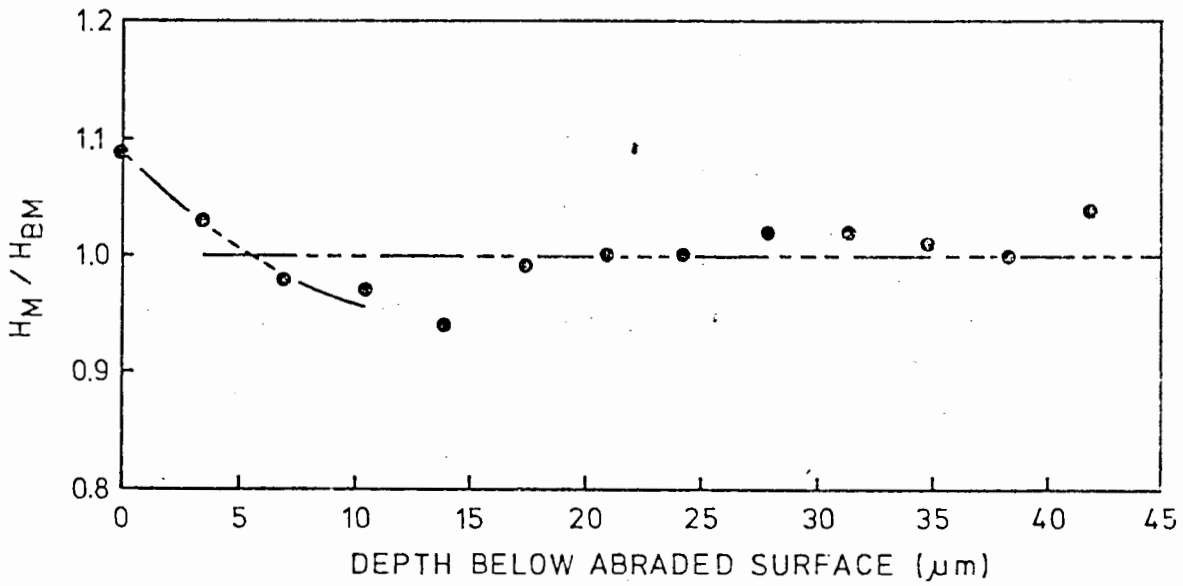

MATERIAL : 3CR12
NORMAL LOAD : 68,6 N
TAPER : 5°
ENVIRON: LABORATORY - LOW STRESS

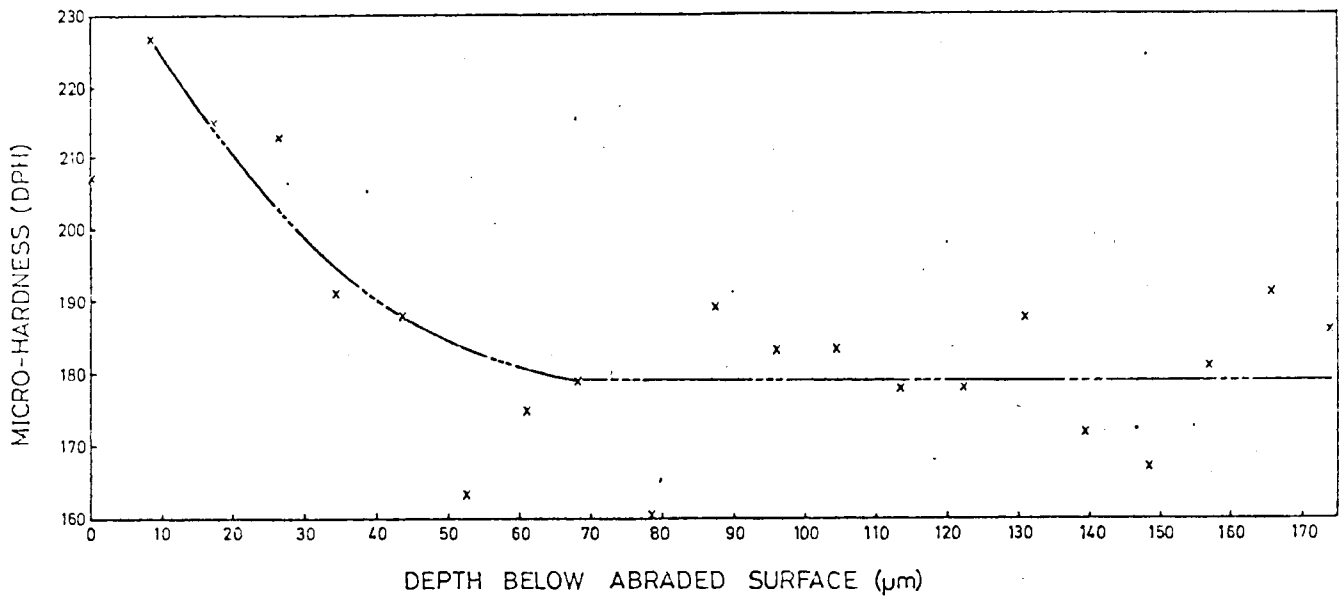

MATERIAL: 3CR12
NORMAL LOAD: 68,6 N
TAPER: 5°
ENVIRON: LABORATORY - LOW STRESS

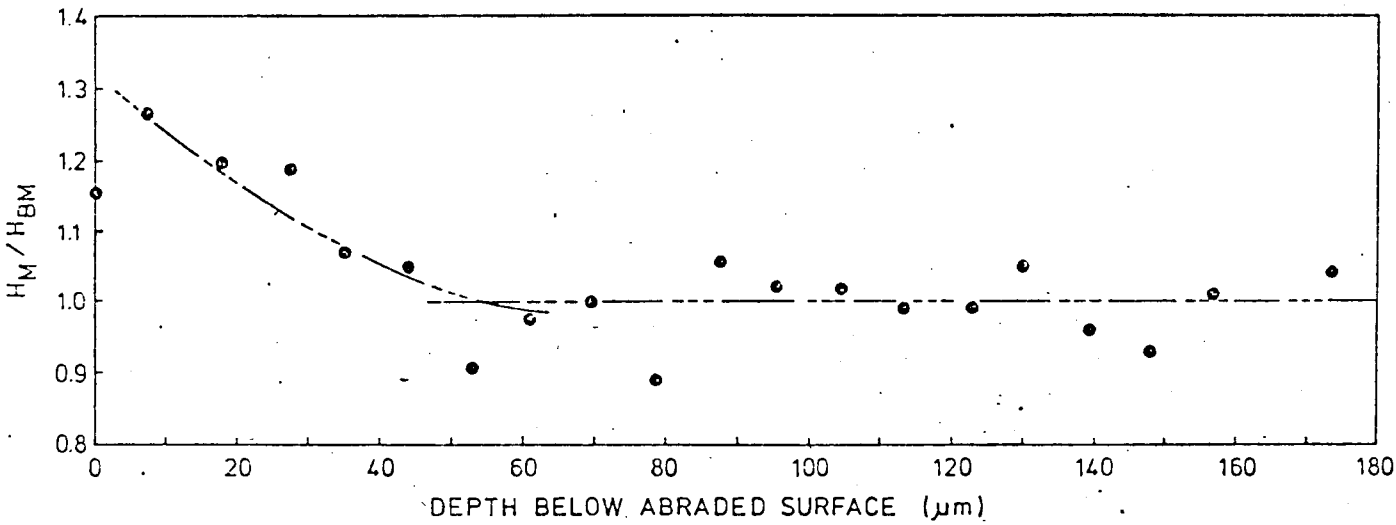

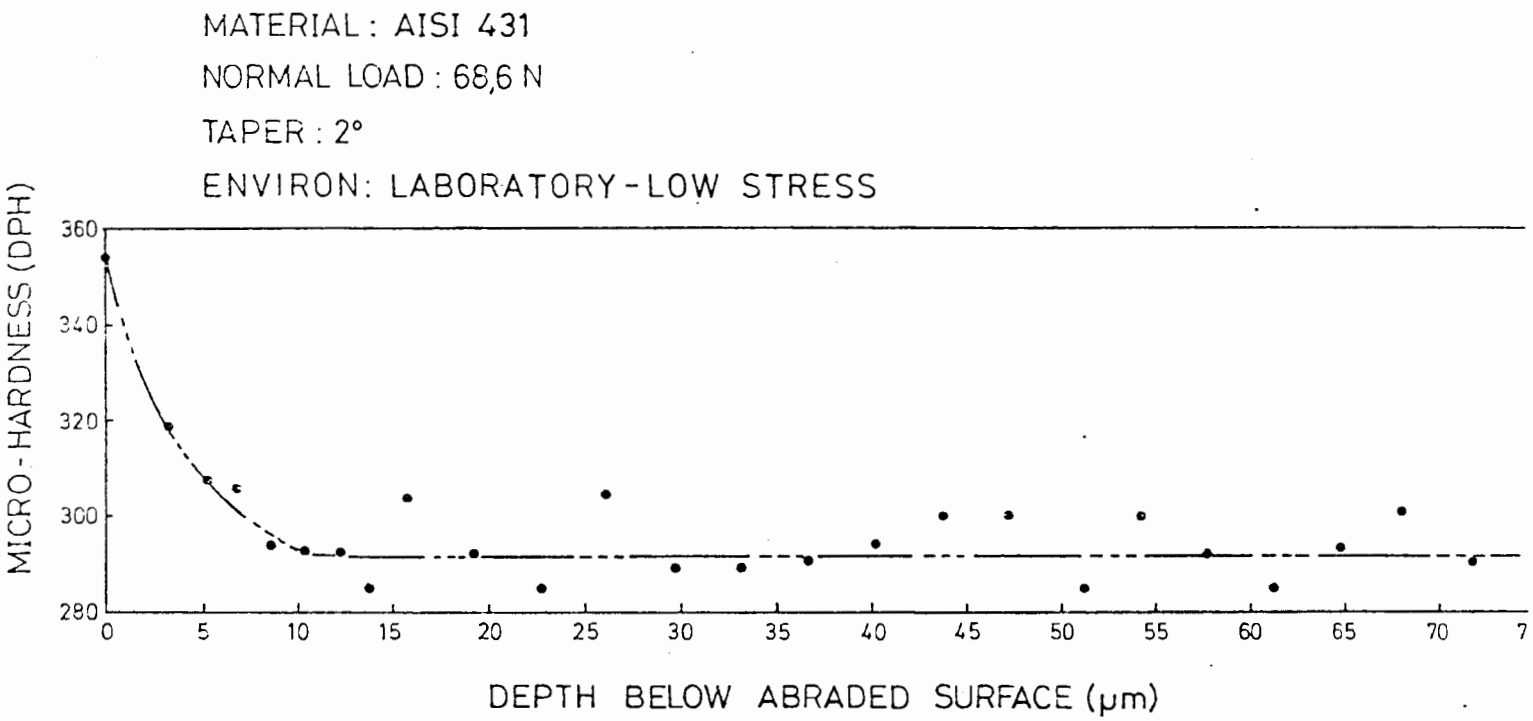
MATERIAL : AISI 431
NORMAL LOAD : 68,6 N
TAPER : 2°
ENVIRON: LABORATORY-LOW STRESS
MICRO-HARDNESS (DPH)
360
340
320
300
280
0
5
10
15
20
25
30
35
40
45
50
55
60
65
70
DEPTH BELOW ABRADED SURFACE (μm)

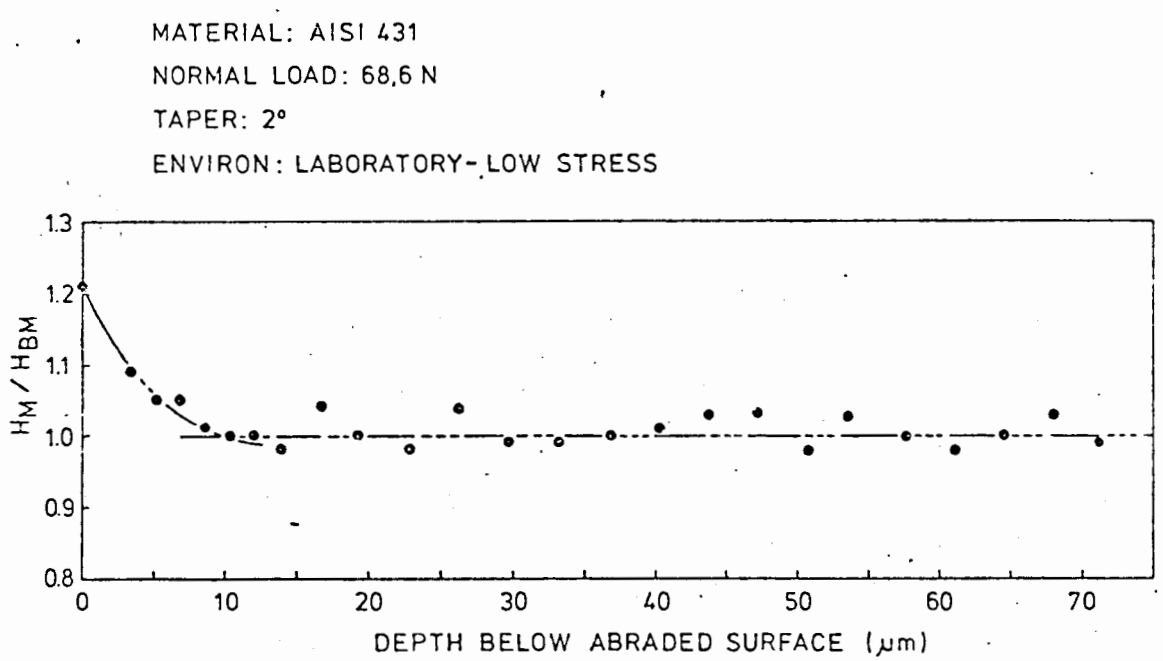
MATERIAL: AISI 431
NORMAL LOAD: 68,6 N
TAPER: 2°
ENVIRON: LABORATORY-LOW STRESS
H_M / H_{BM}
1.3
1.2
1.1
1.0
0.9
0.8
0
10
20
30
40
50
60
70
DEPTH BELOW ABRADED SURFACE (μm)

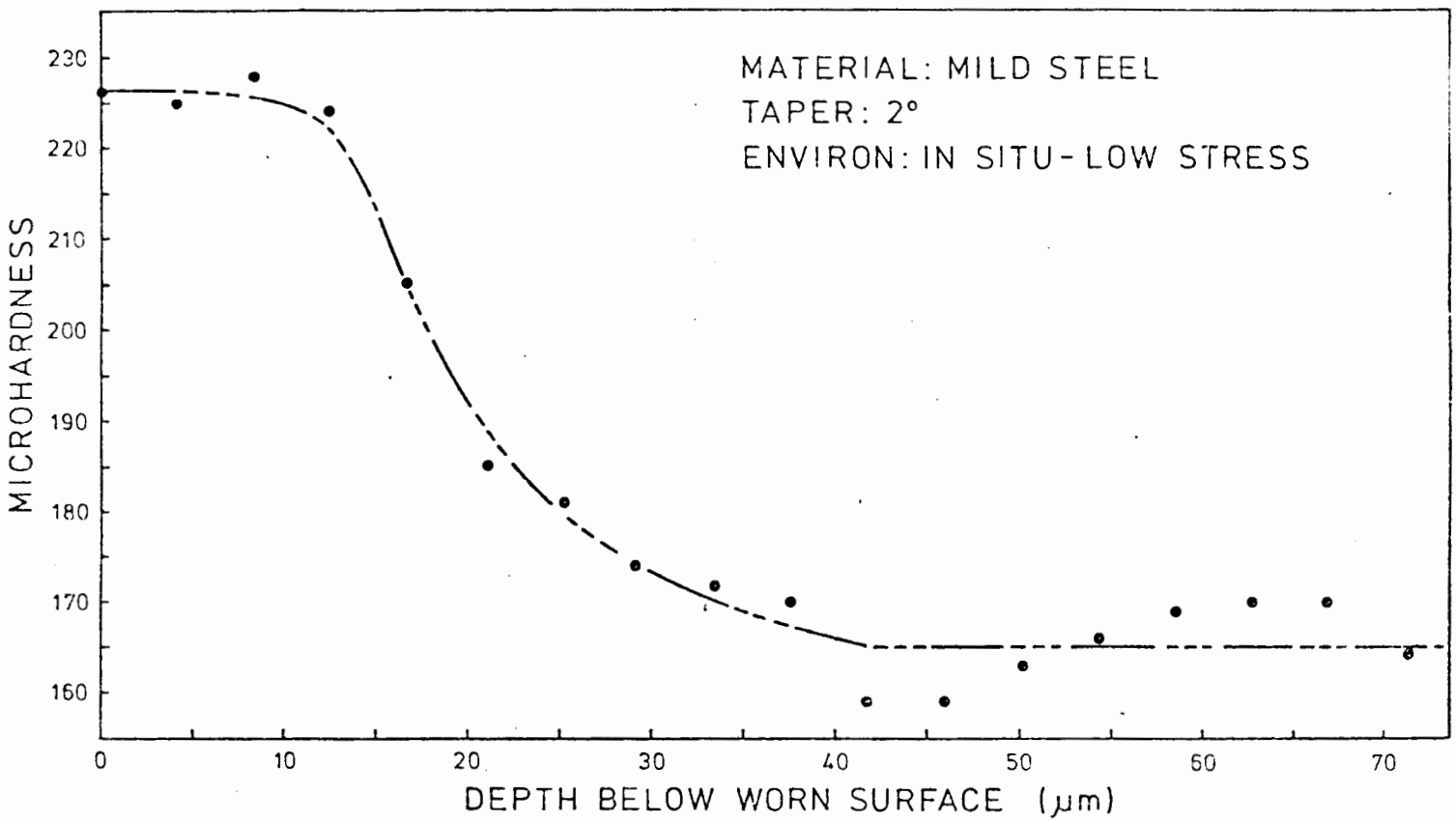
MATERIAL: MILD STEEL
TAPER: 2°
ENVIRON: IN SITU - LOW STRESS
MICROHARDNESS
230
220
210
200
190
180
170
160
0
10
20
30
40
50
60
70
DEPTH BELOW WORN SURFACE (μm)

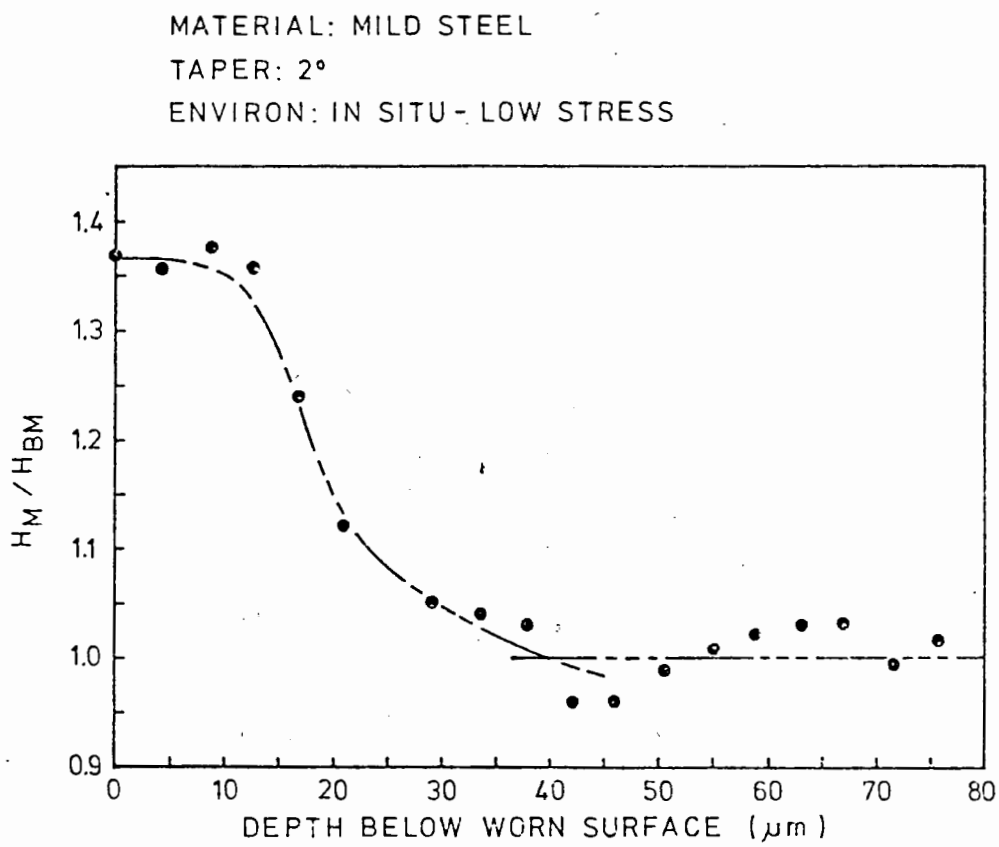
MATERIAL: MILD STEEL
TAPER: 2°
ENVIRON: IN SITU - LOW STRESS
H_M / H_{BM}
1.4
1.3
1.2
1.1
1.0
0.9
0
10
20
30
40
50
60
70
80
DEPTH BELOW WORN SURFACE (μm)

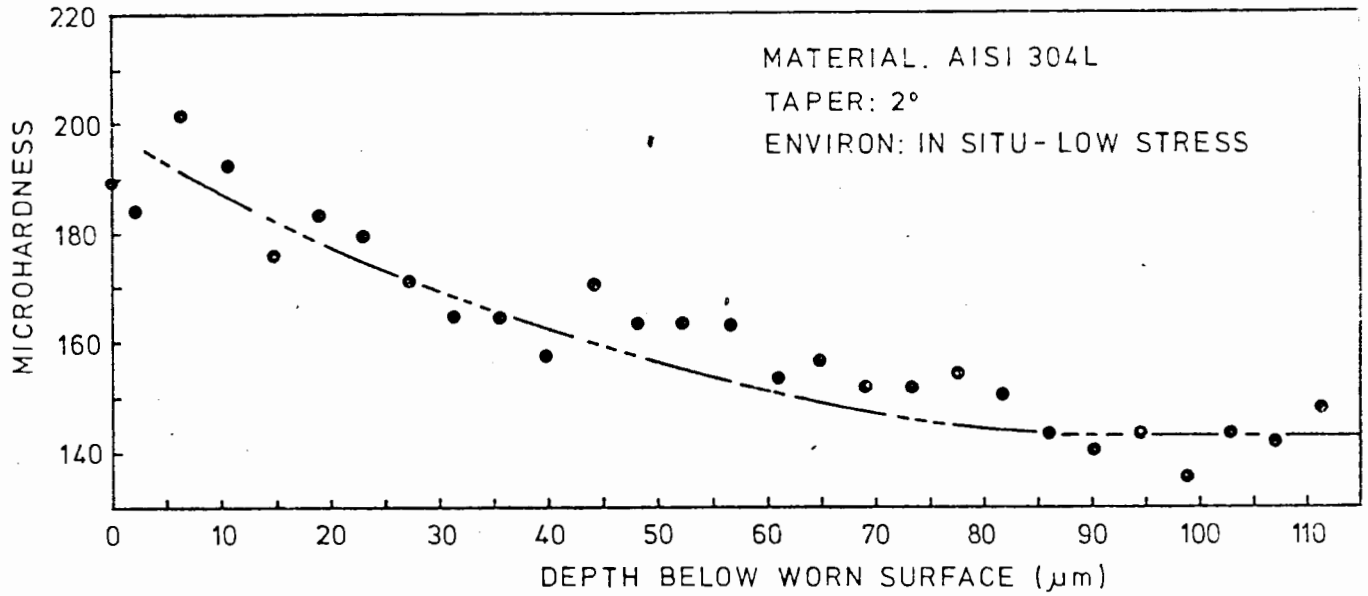

MATERIAL: AISI 304L
TAPER: 2°
ENVIRON: IN SITU - LOW STRESS

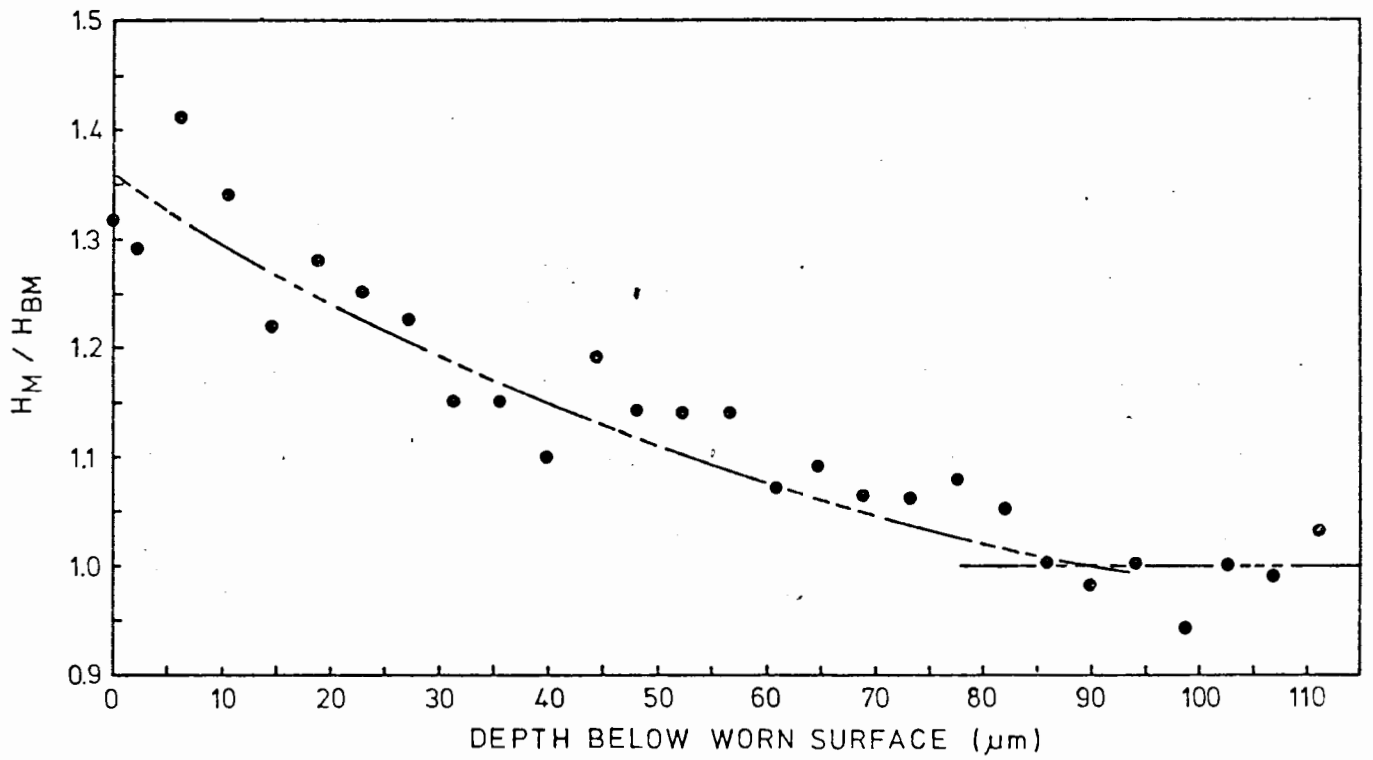

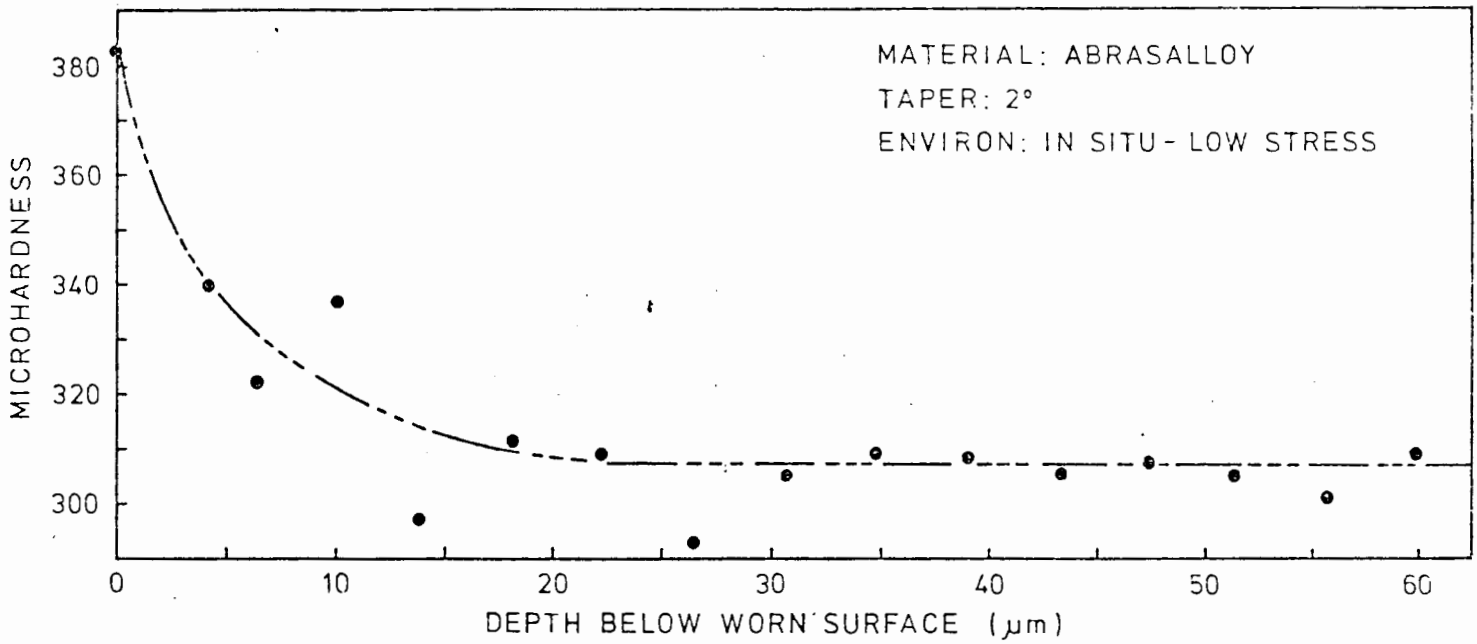
MATERIAL: ABRASALLOY
TAPER: 2°
ENVIRON: IN SITU - LOW STRESS
MICROHARDNESS
380
360
340
320
300
0
10
20
30
40
50
60
DEPTH BELOW WORN SURFACE (μm)

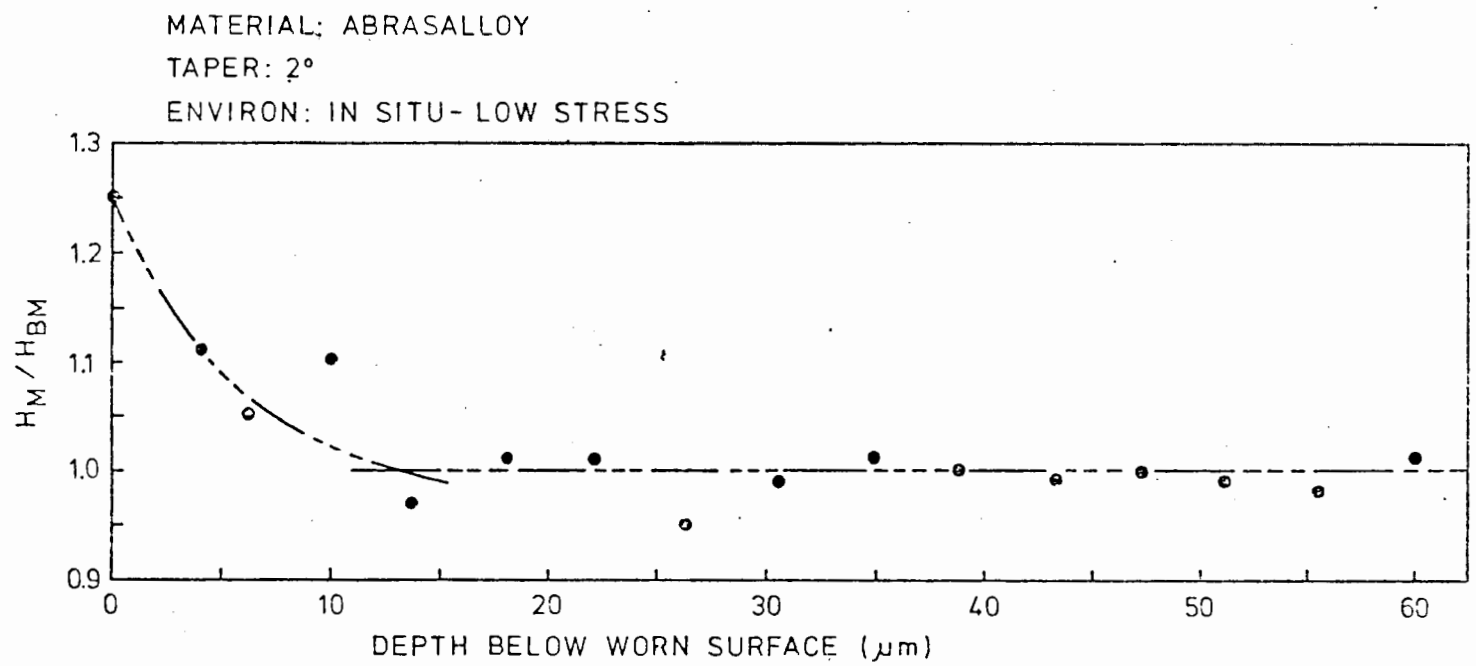
MATERIAL: ABRASALLOY
TAPER: 2°
ENVIRON: IN SITU - LOW STRESS
H_M / H_{BM}
1.3
1.2
1.1
1.0
0.9
0
10
20
30
40
50
60
DEPTH BELOW WORN SURFACE (μm)

MATERIAL: BENOX

TAPER: 2°

ENVIRON: IN SITU - LOW STRESS

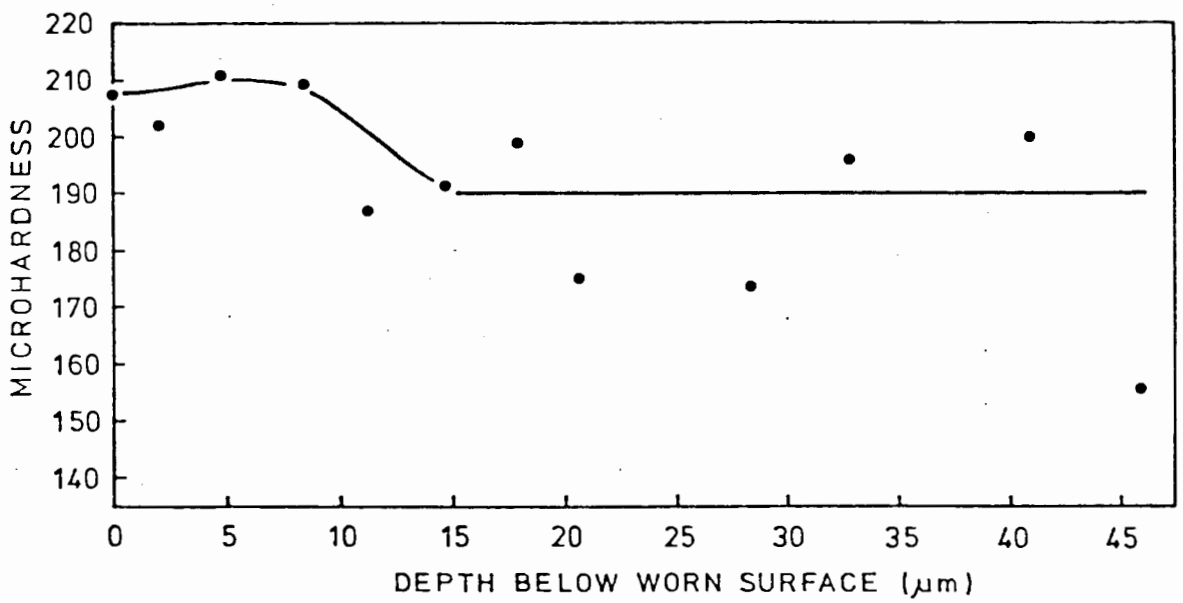

MATERIAL: BENOX

TAPER: 2°

ENVIRON: IN-SITU – LOW STRESS

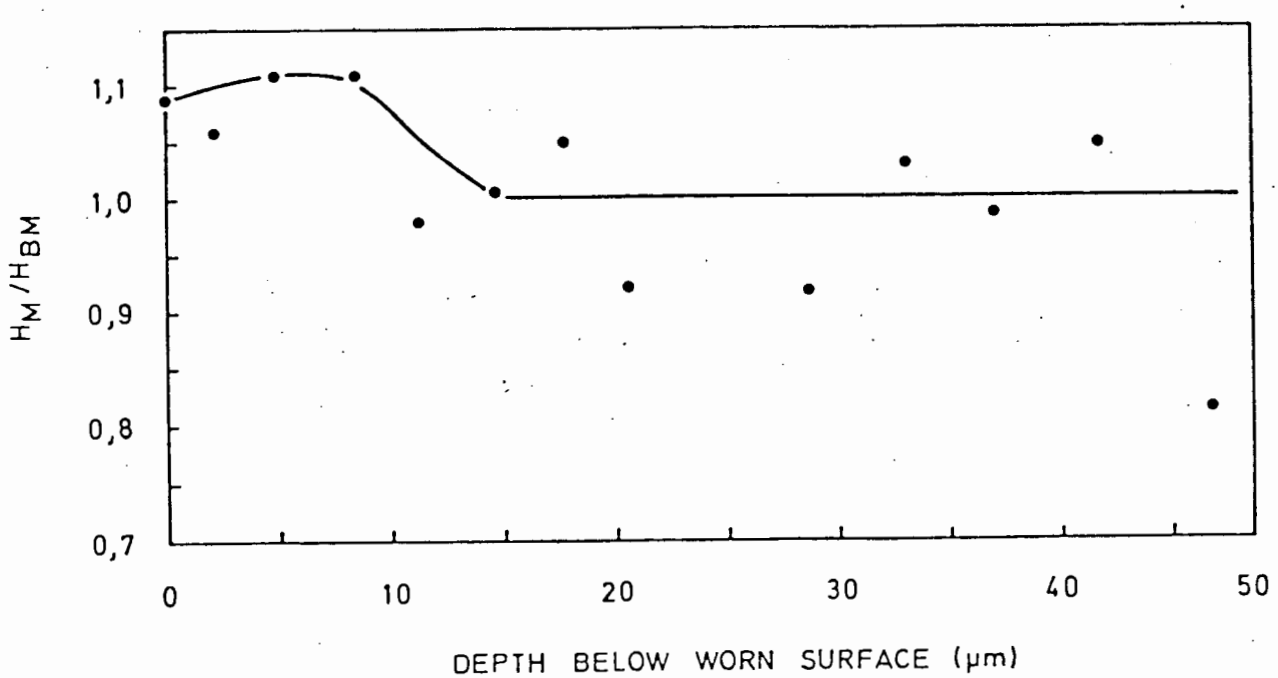

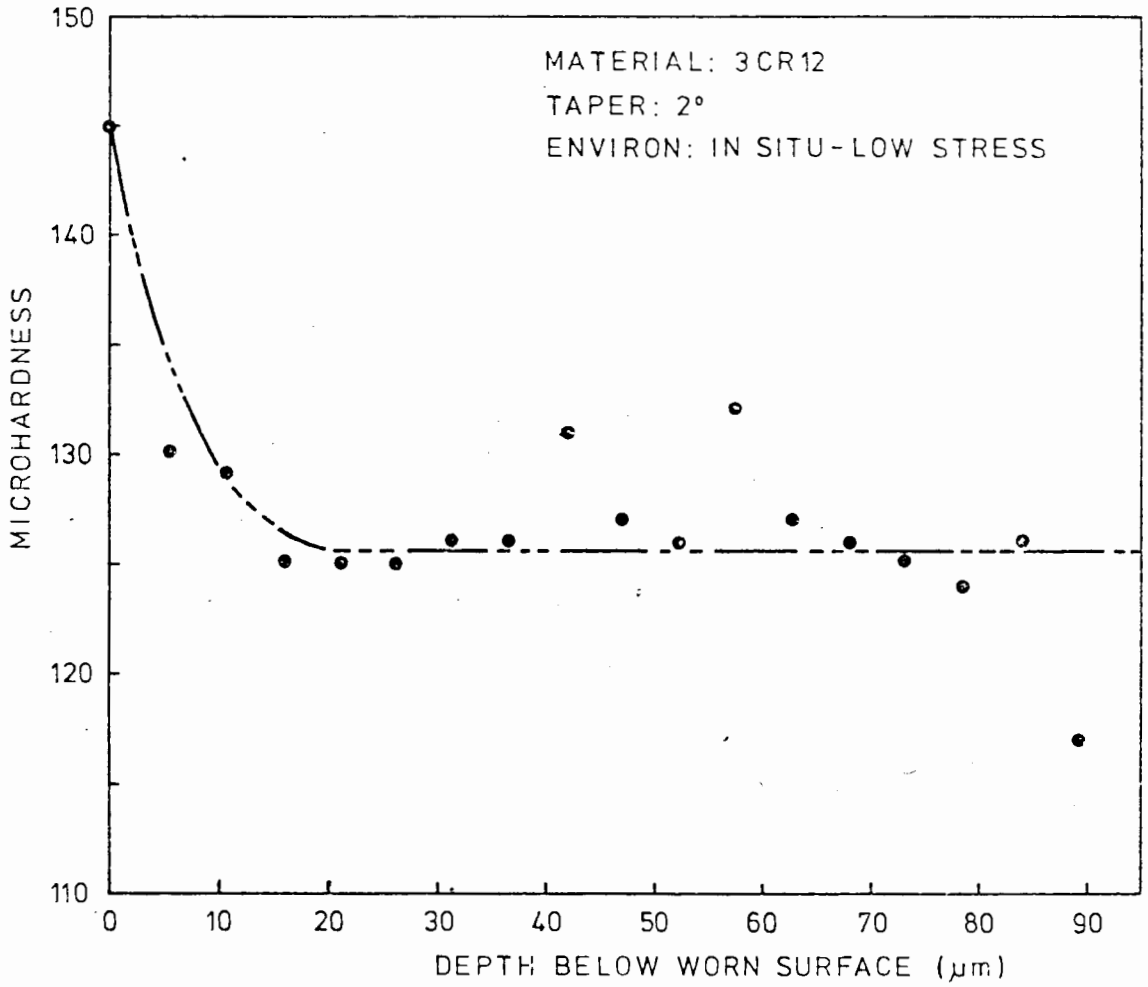
MATERIAL: 3CR12
TAPER: 2°
ENVIRON: IN SITU-LOW STRESS
MICROHARDNESS
150
140
130
120
110
0
10
20
30
40
50
60
70
80
90
DEPTH BELOW WORN SURFACE (μm)

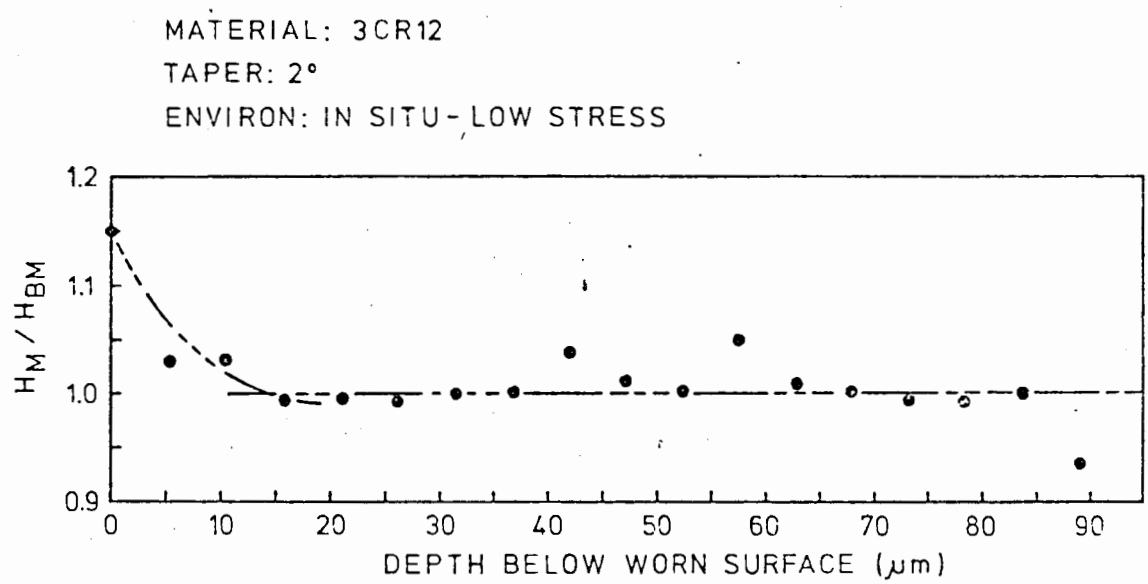
MATERIAL: 3CR12
TAPER: 2°
ENVIRON: IN SITU-LOW STRESS
H_M / H_{BM}
1.2
1.1
1.0
0.9
0
10
20
30
40
50
60
70
80
90
DEPTH BELOW WORN SURFACE (μm)

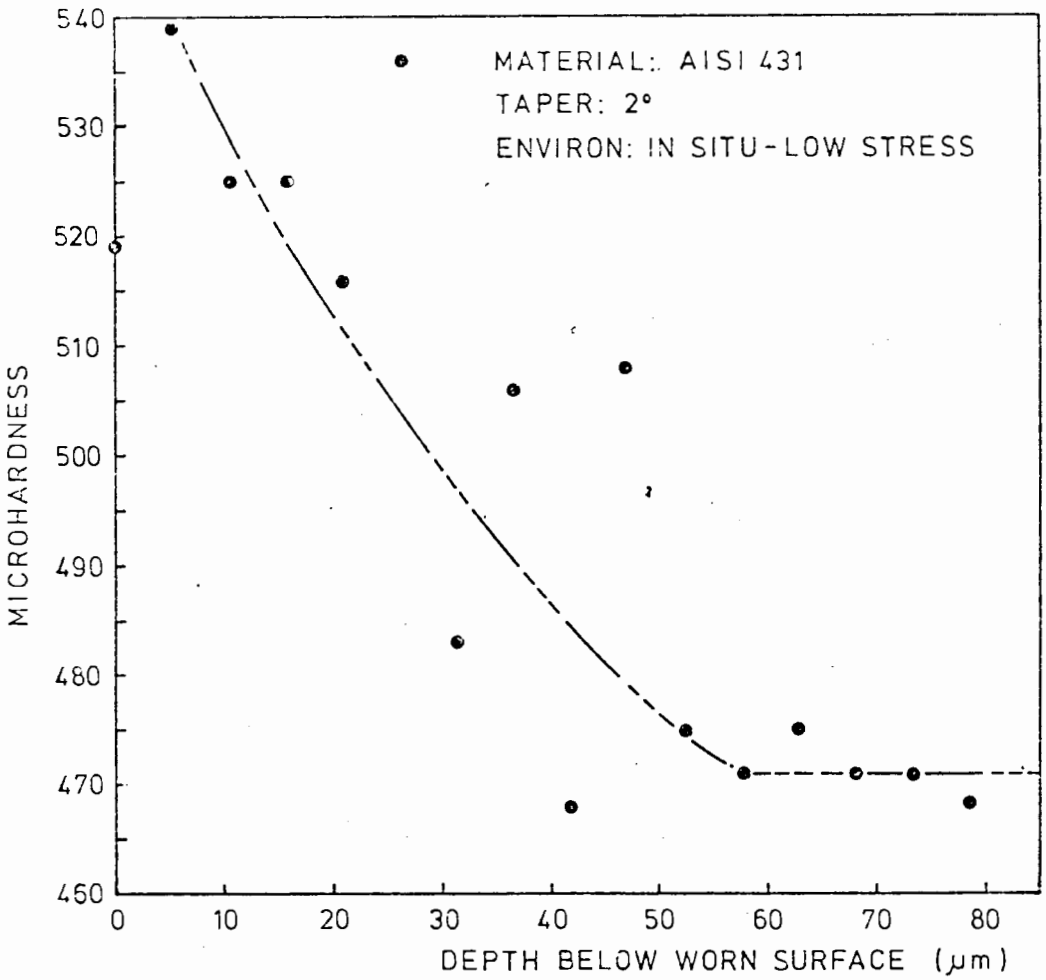
MATERIAL: AISI 431
TAPER: 2°
ENVIRON: IN SITU - LOW STRESS
MICROHARDNESS
540
530
520
510
500
490
480
470
460
0
10
20
30
40
50
60
70
80
DEPTH BELOW WORN SURFACE (μm)

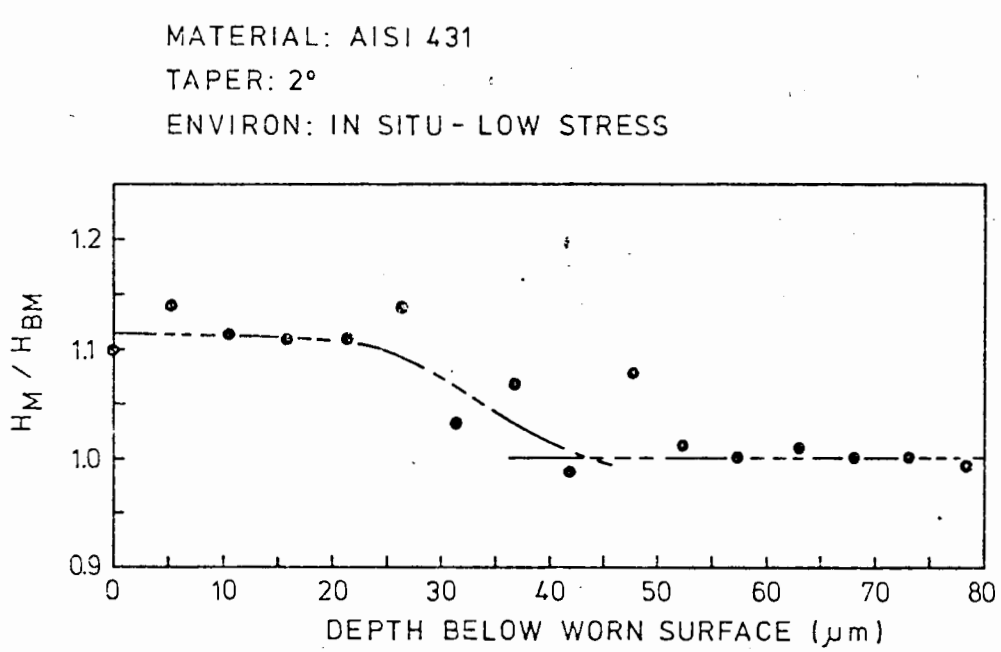
MATERIAL: AISI 431
TAPER: 2°
ENVIRON: IN SITU - LOW STRESS
H_M / H_{BM}
1.2
1.1
1.0
0.9
0
10
20
30
40
50
60
70
80
DEPTH BELOW WORN SURFACE (μm)

MATERIAL: MILD STEEL
TAPER: 2°
ENVIRON: LABORATORY - HIGH STRESS

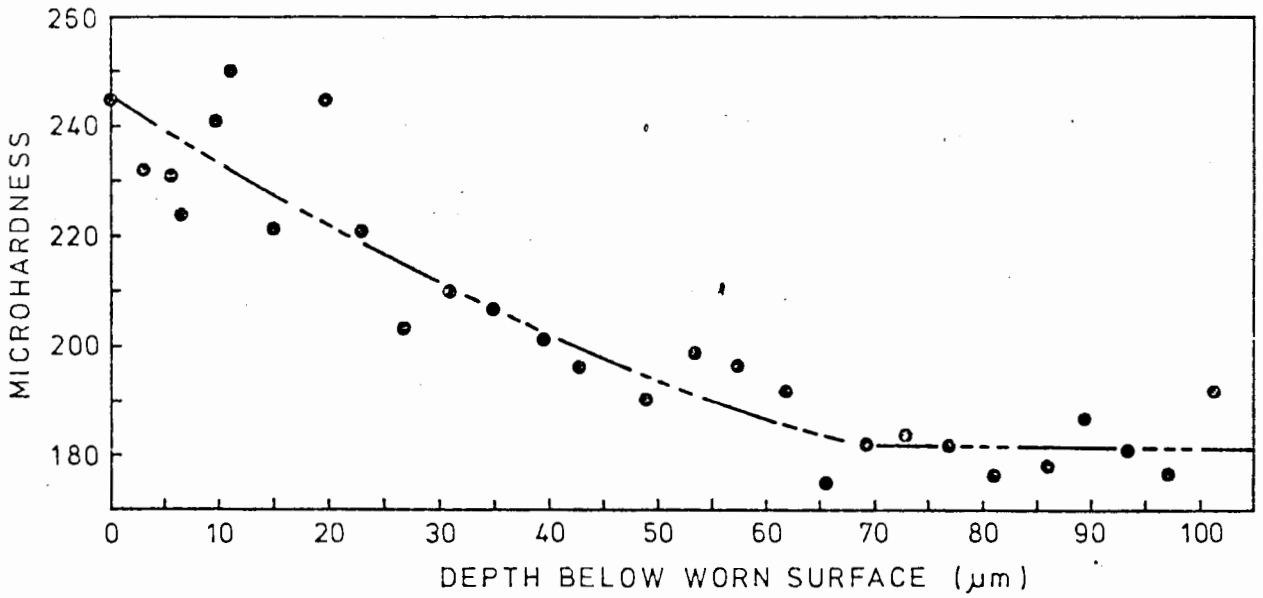

MATERIAL: MILD STEEL
TAPER: 2°
ENVIRON: LABORATORY - HIGH STRESS

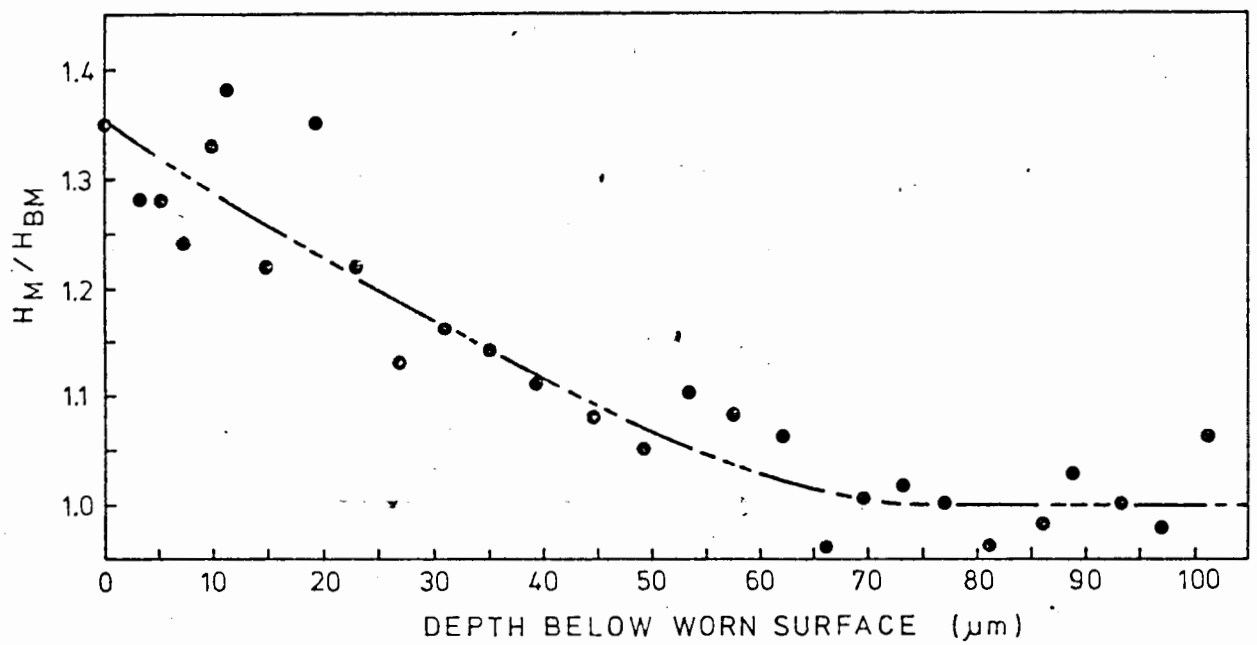

MATERIAL: AISI 304L
TAPER: 2°
ENVIRON: LABORATORY - HIGH STRESS

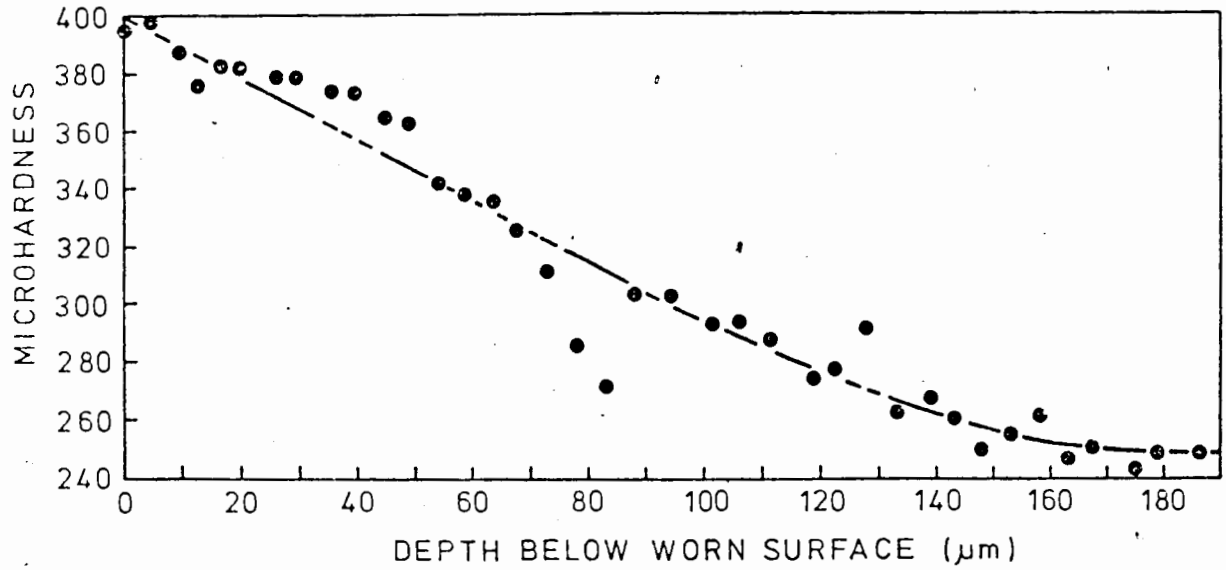

MATERIAL: AISI 304L
TAPER: 2°
ENVIRON: LABORATORY - HIGH STRESS

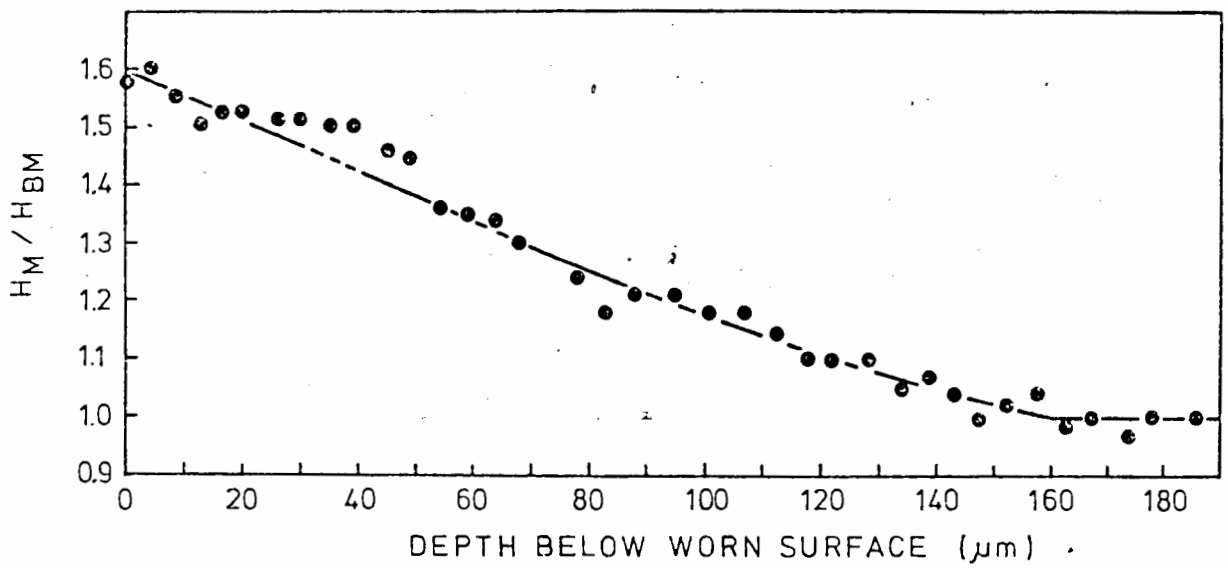

MATERIAL: ABRASALLOY
TAPER: 2°
ENVIRON: LABORATORY - HIGH STRESS

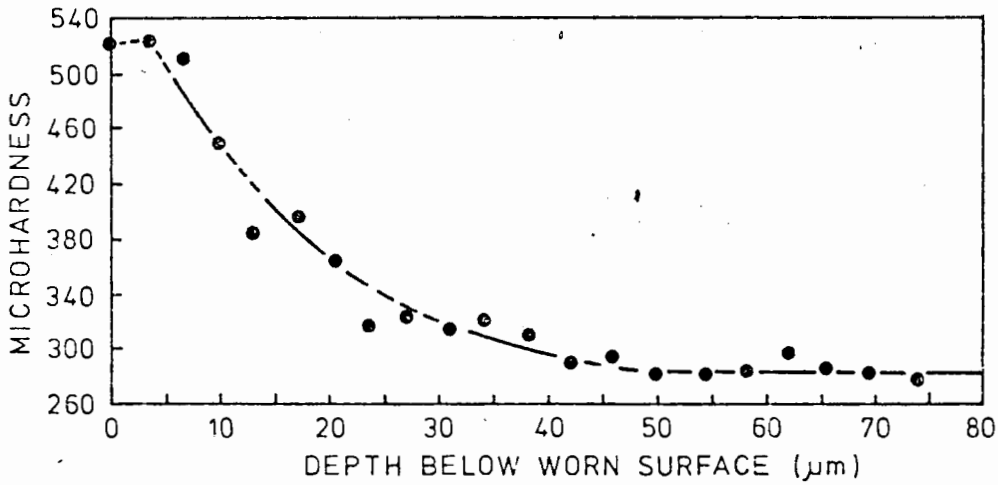

MATERIAL: ABRASALLOY
TAPER: 2°
ENVIRON: LABORATORY - HIGH STRESS

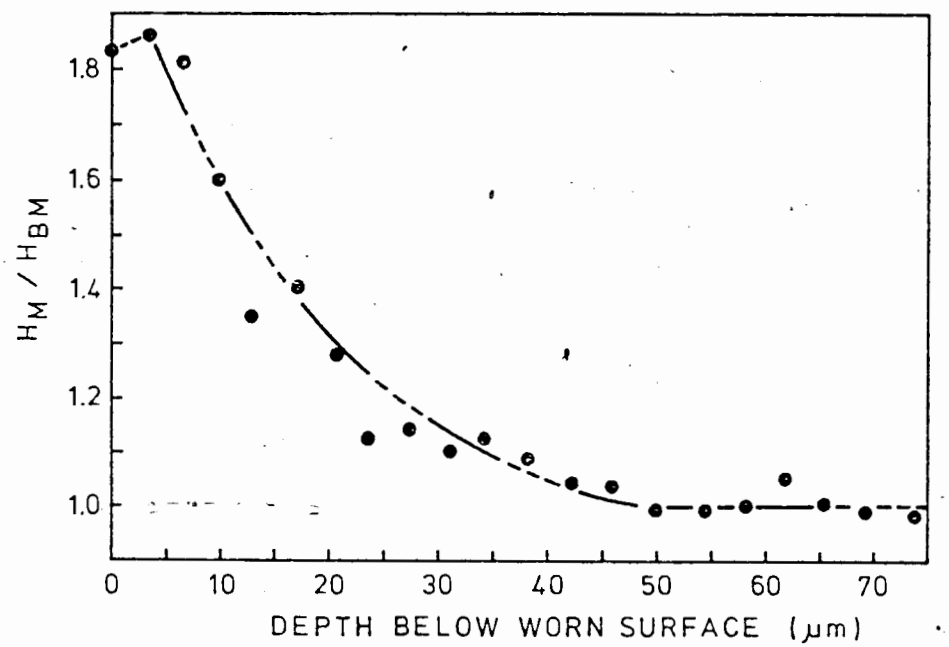

MATERIAL: ROQLAST AH 400
TAPER: 2°
ENVIRON: LABORATORY - HIGH STRESS

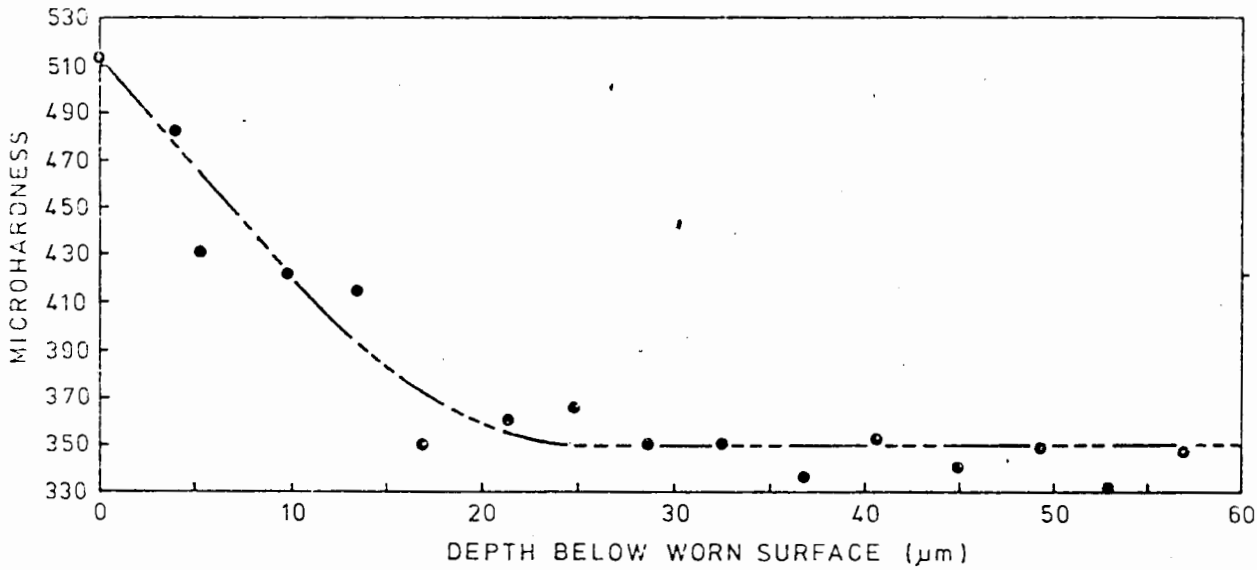

MATERIAL: ROQLAST AH 400
TAPER: 2°
ENVIRON: LABORATORY - HIGH STRESS

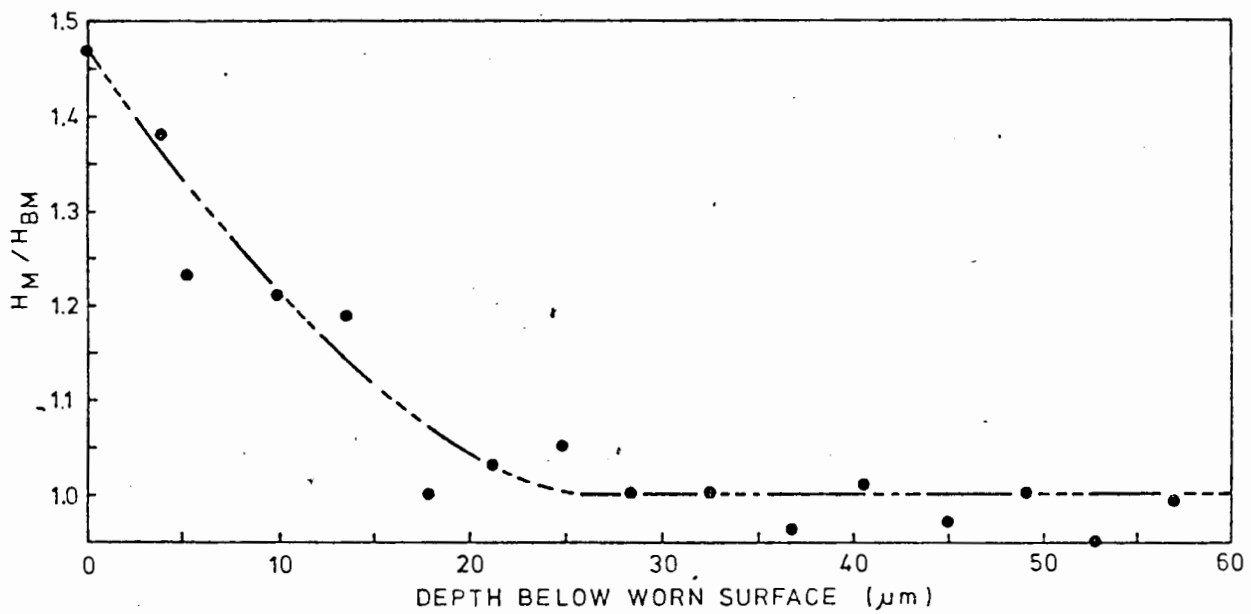

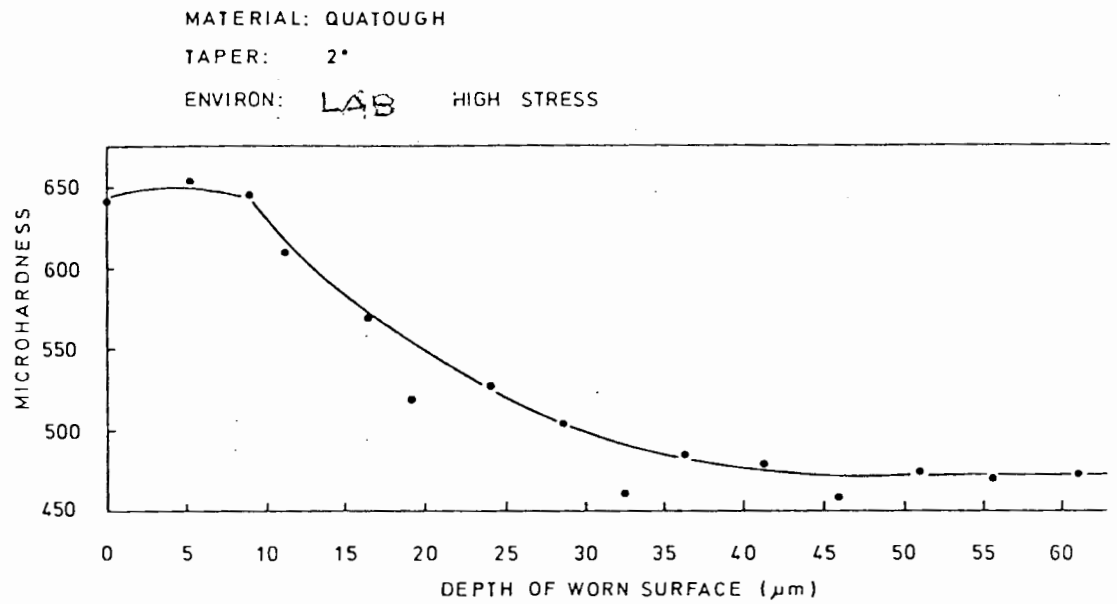
MATERIAL: QUATOUGH
TAPER: 2°
ENVIRON: LAB HIGH STRESS
MICROHARDNESS
650
600
550
500
450
0 5 10 15 20 25 30 35 40 45 50 55 60
DEPTH OF WORN SURFACE (μm)

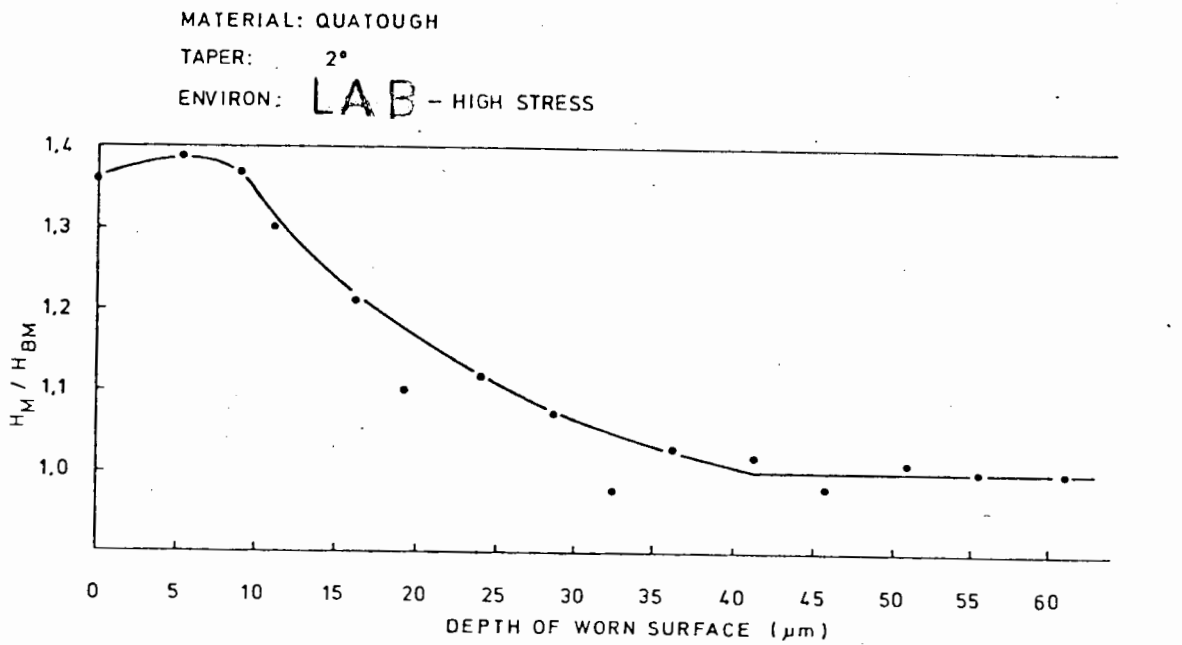
MATERIAL: QUATOUGH
TAPER: 2°
ENVIRON: LAB – HIGH STRESS
H_M / H_{BM}
1,4
1,3
1,2
1,1
1,0
0 5 10 15 20 25 30 35 40 45 50 55 60
DEPTH OF WORN SURFACE (μm)

MATERIAL: MILD STEEL
TAPER: 2°
ENVIRON: IN-SITU – HIGH STRESS

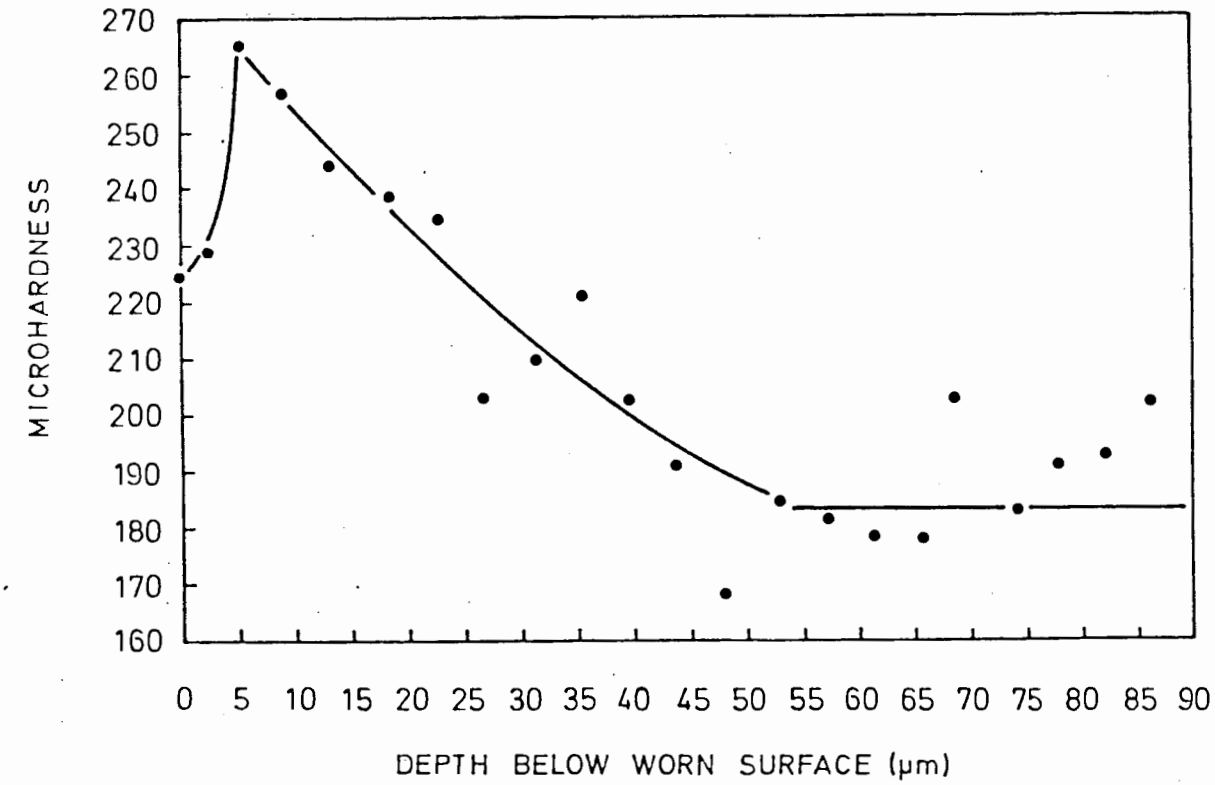

MATERIAL: MILD STEEL
TAPER: 2°
ENVIRON: IN-SITU – HIGH STRESS

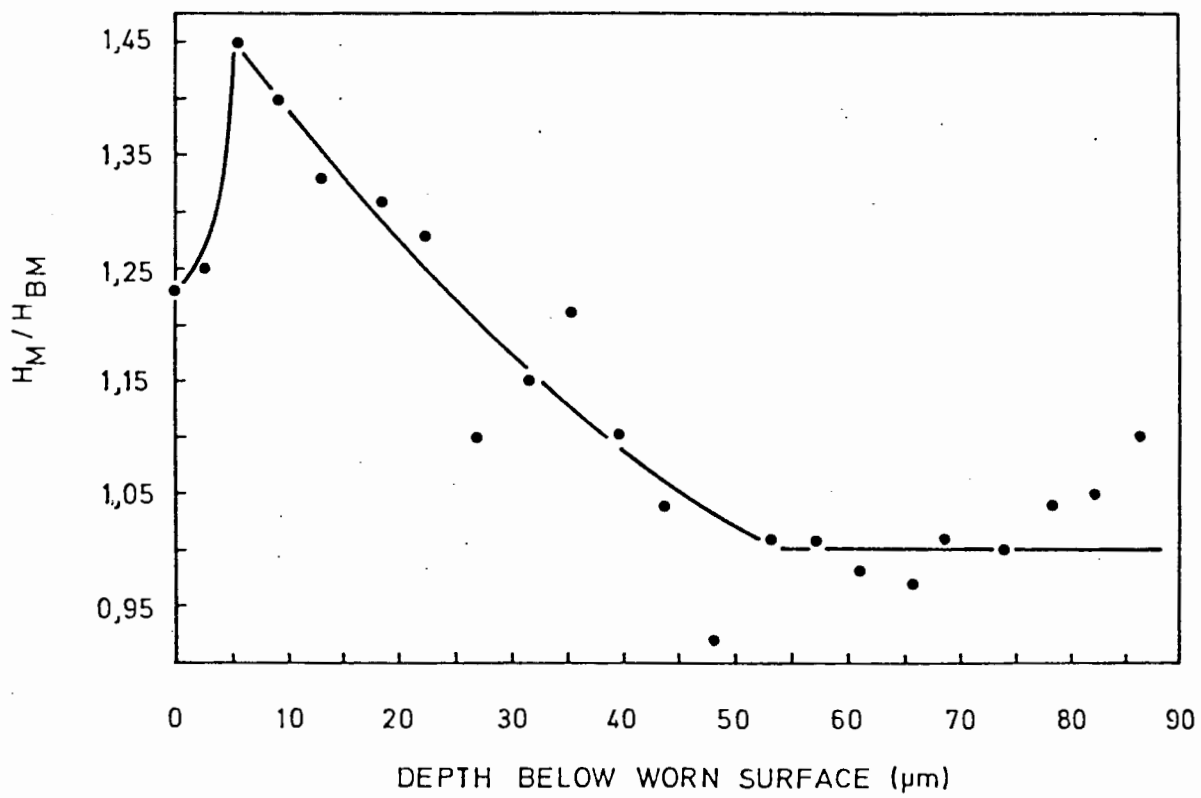

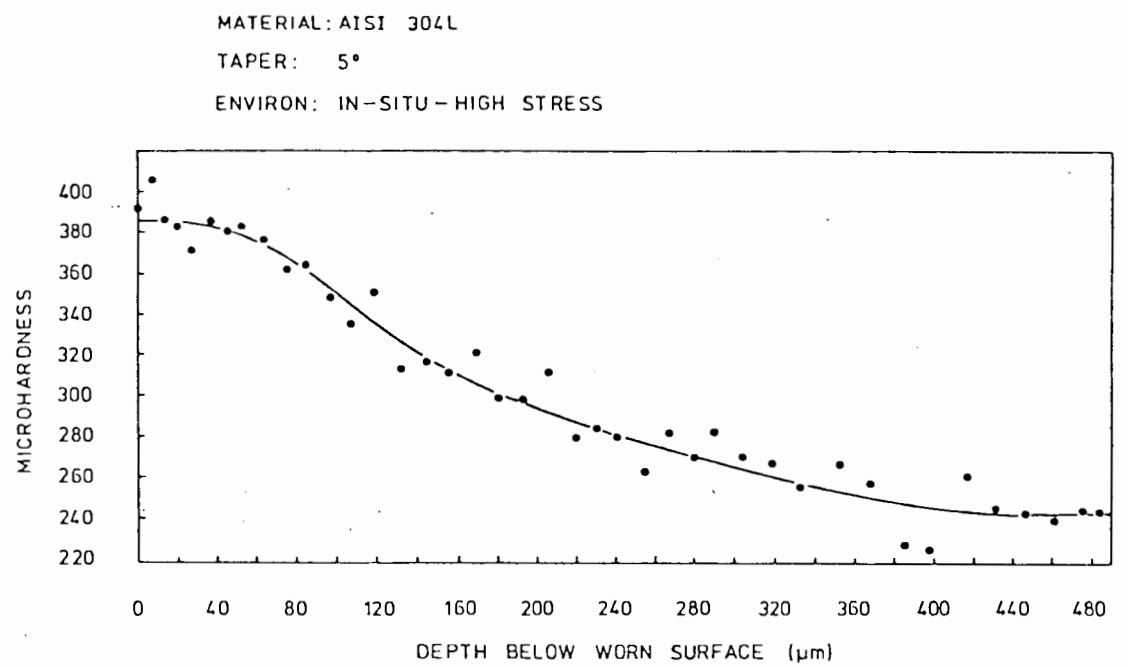
MATERIAL: AISI 304L
TAPER: 5°
ENVIRON: IN-SITU - HIGH STRESS
MICROHARDNESS
400
380
360
340
320
300
280
260
240
220
0
40
80
120
160
200
240
280
320
360
400
440
480
DEPTH BELOW WORN SURFACE (μm)

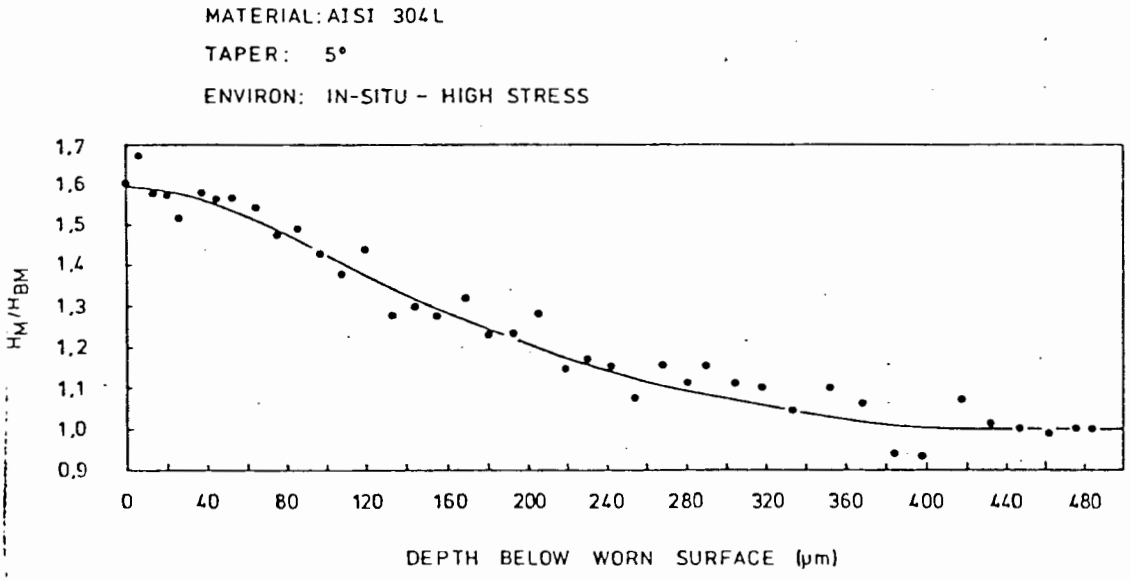
MATERIAL: AISI 304L
TAPER: 5°
ENVIRON: IN-SITU - HIGH STRESS
H_M/H_{BM}
1.7
1.6
1.5
1.4
1.3
1.2
1.1
1.0
0.9
0
40
80
120
160
200
240
280
320
360
400
440
480
DEPTH BELOW WORN SURFACE (μm)

MATERIAL: ABRASALLOY
TAPER: 2°
ENVIRON: IN SITU-HIGH STRESS

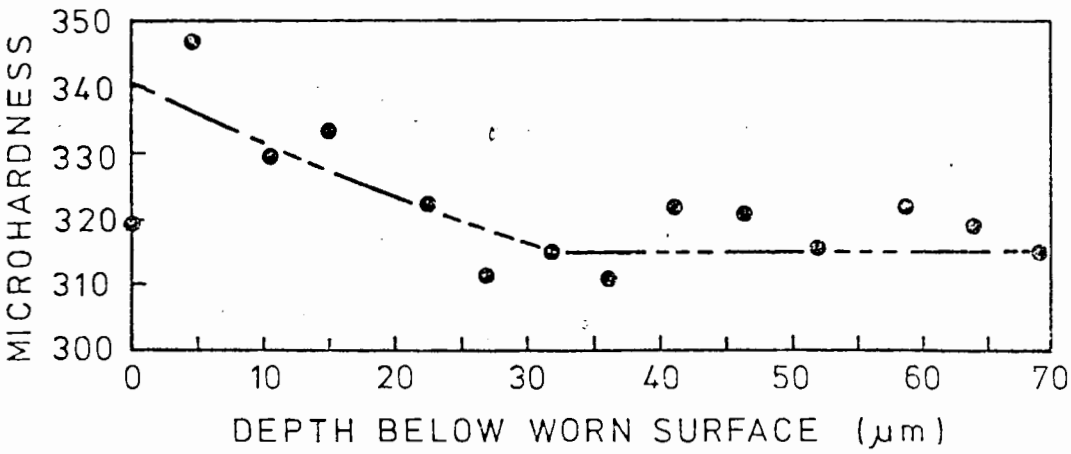

MATERIAL: ABRASALLOY
TAPER: 2°
ENVIRON: IN SITU-HIGH STRESS

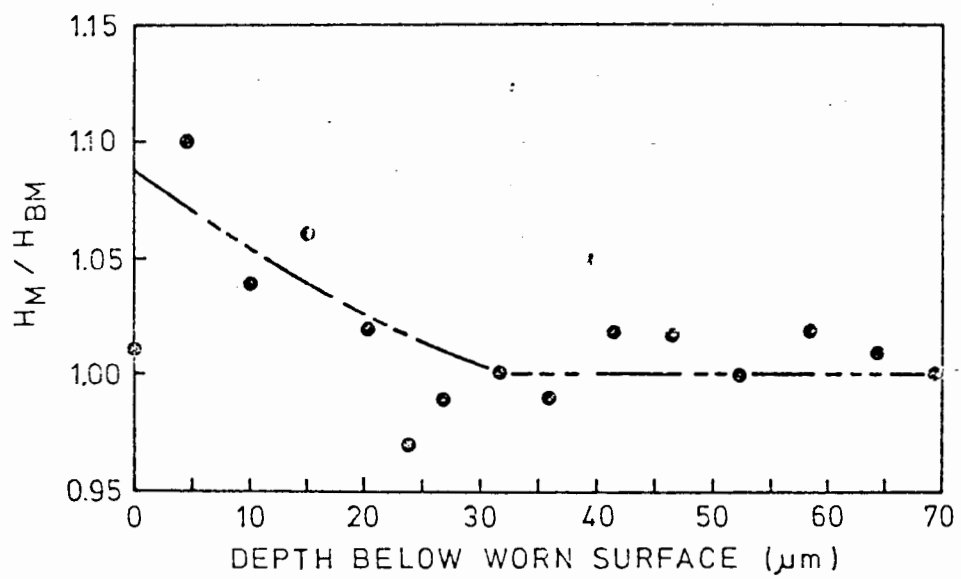

MATERIAL: BENOX
TAPER: 2°
ENVIRON: IN SITU - HIGH STRESS

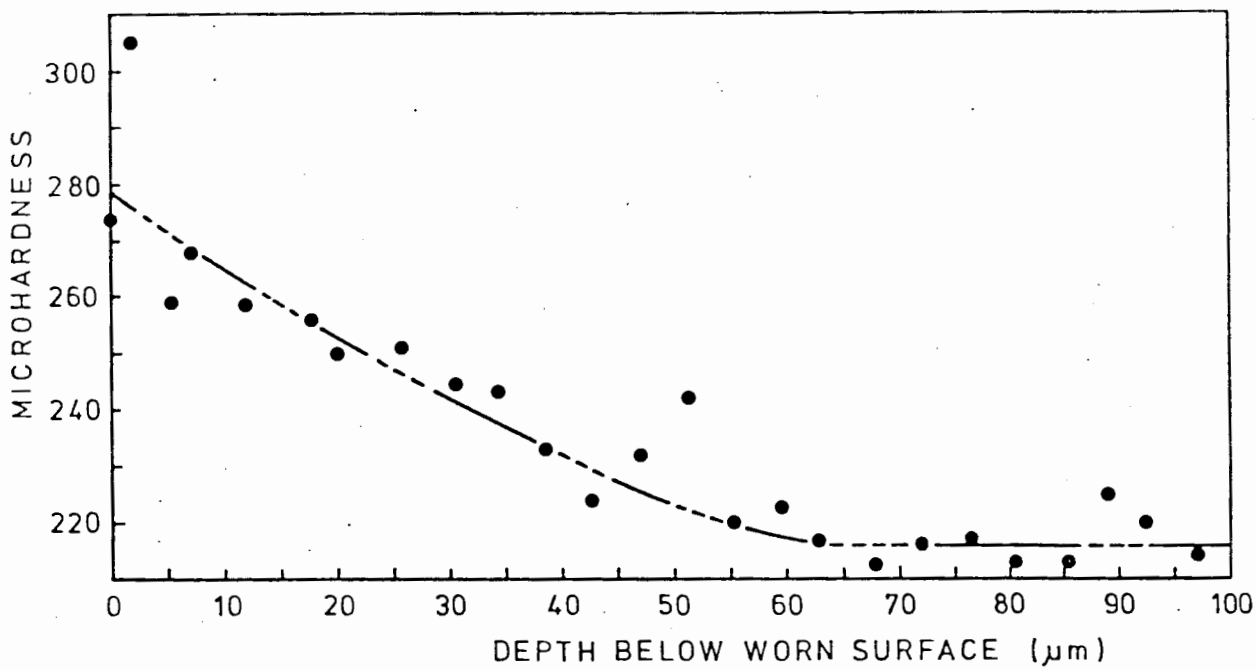

MATERIAL: BENOX
TAPER: 2°
ENVIRON: IN SITU - HIGH STRESS

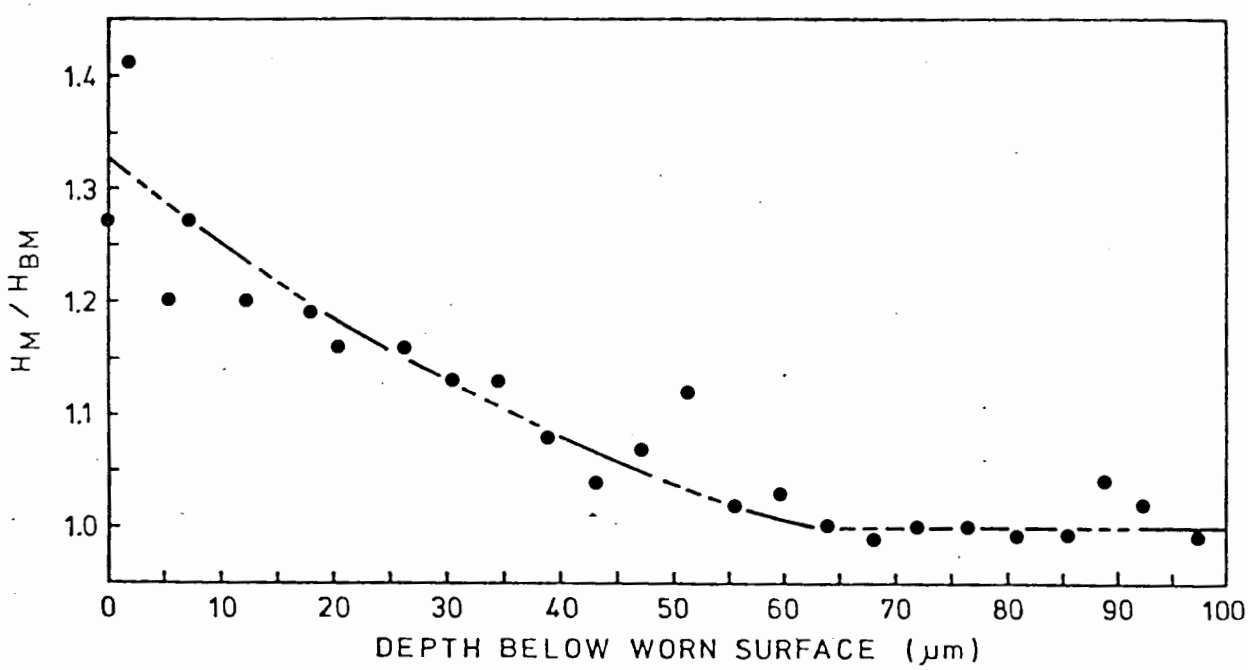

MATERIAL: HADFIELD BW10
TAPER: 2°
ENVIRON: IN SITU - HIGH STRESS

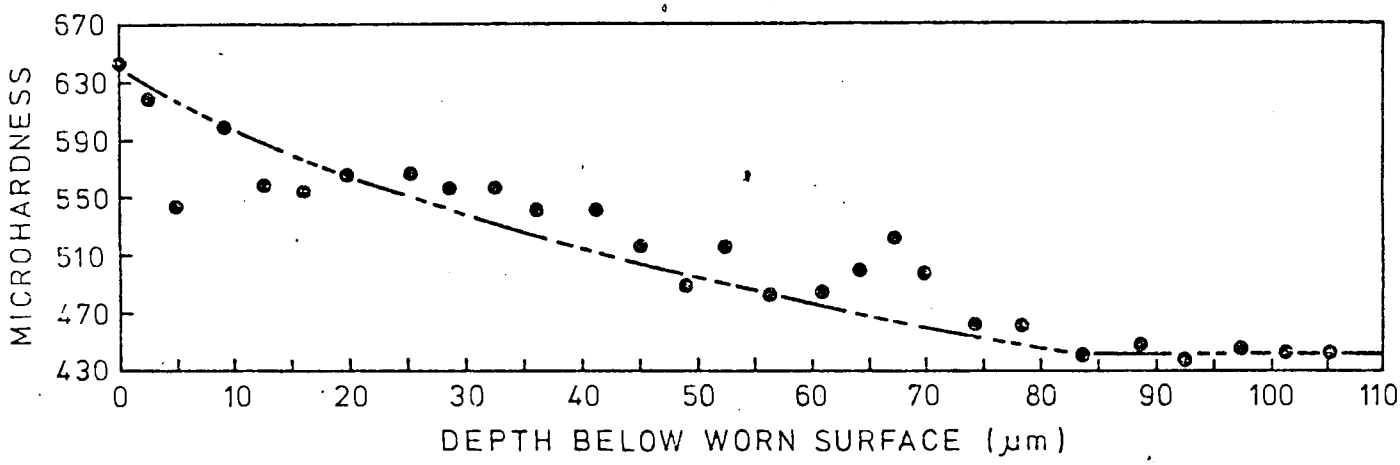

MATERIAL: HADFIELD BW10
TAPER: 2°
ENVIRON: IN SITU - HIGH STRESS